THE COASTAL CIRCULATION MODEL OF BÜYÜK MENDERES RIVER MOUTH AND ADJACENT COASTAL AREAS

A THESIS SUBMITTED TO
THE GRADUATE SCHOOL OF NATURAL AND APPLIED SCIENCES
OF
MIDDLE EAST TECHNICAL UNIVERSITY

BY

MEHMET SEDAT GÖZLET

IN PARTIAL FULFILLMENT OF THE REQUIREMENTS
FOR
THE DEGREE OF MASTER OF SCIENCE
IN
CIVIL ENGINEERING

SEPTEMBER 2019

Approval of the thesis:

THE COASTAL CIRCULATION MODEL OF BÜYÜK MENDERES RIVER MOUTH AND ADJACENT COASTAL AREAS

submitted by **MEHMET SEDAT GÖZLET** in partial fulfillment of the requirements for the degree of **Master of Science in Civil Engineering Department, Middle East Technical University** by,

Prof. Dr. Halil Kalıpçılar
Dean, Graduate School of **Natural and Applied Sciences** _____

Prof. Dr. Ahmet Türer
Head of Department, **Civil Engineering** _____

Assist. Prof. Dr. Gülizar Özyurt Tarakcıoğlu
Supervisor, **Civil Engineering, METU** _____

Assist. Prof. Dr. Cüneyt Baykal
Co-Supervisor, **Civil Engineering, METU** _____

Examining Committee Members:

Prof. Dr. Ahmet Cevdet Yalçıner
Civil Engineering, METU _____

Assist. Prof. Dr. Gülizar Özyurt Tarakcıoğlu
Civil Engineering, METU _____

Assist. Prof. Dr. Cüneyt Baykal
Civil Engineering, METU _____

Prof. Dr. Bülent Akınoğlu
Physics, METU _____

Assist. Prof. Dr. Alp Küçükosmanoğlu
Civil Engineering, Burdur Mehmet Akif Ersoy University _____

Date: 23.09.2019

I hereby declare that all information in this document has been obtained and presented in accordance with academic rules and ethical conduct. I also declare that, as required by these rules and conduct, I have fully cited and referenced all material and results that are not original to this work.

Name, Surname: Mehmet Sedat Gözlet

Signature:

ABSTRACT

THE COASTAL CIRCULATION MODEL OF BÜYÜK MENDERES RIVER MOUTH AND ADJACENT COASTAL AREAS

Gözlet, Mehmet Sedat
Master of Science, Civil Engineering
Supervisor: Assist. Prof. Dr. Gülizar Özyurt Tarakcıoğlu
Co-Supervisor: Assist. Prof. Dr. Cüneyt Baykal

September 2019, 158 pages

In this study; coastal circulation of Buyuk Menders river mouth and the adjacent coastal areas is modeled to determine the current characteristics of the region under river-sea interaction. For this purpose, Finite Volume Coastal Ocean Model (FVCOM) numerical model is setup and run under wind, tide, and river forcing conditions. Current, salinity, temperature data from field measurements are used to validate the performance of the model setup with default parametrization. Significance of each forcing on the overall current system is assessed by modeling each forcing independently and comparing these results with the current measurements. It is seen that tidal forcing has the lowest contribution, as the area is microtidal. Wind and river contributes much significantly however the river effect is seen in the closer regions and under higher river discharge conditions whereas contribution of wind is observed all over the area but with a lag in time. As the default model setup performed satisfactorily, 09 - 20 January – 2016 event that represent maximum river flow, maximum wind speed extreme forcing event is also modeled. As hydrodynamics of river mouths is very complex, longer measurement datasets both for the coastal area and the river characteristics is required to improve the performance of these models. .

Keywords: Circulation Model, FVCOM, Büyük Menderes River

ÖZ

BÜYÜK MENDERES NEHİR AĞZININ VE KIYI ŞERİDİNİN ÇEVRİM MODELİNİN OLUŞTURULMASI

Gözlet, Mehmet Sedat
Yüksek Lisans, İnşaat Mühendisliği
Tez Danışmanı: Dr. Öğr. Üyesi Gülizar Özyurt Tarakcıoğlu
Ortak Tez Danışmanı: Dr. Öğr. Üyesi Cüneyt Baykal

Eylül 2019, 158 sayfa

Bu çalışmada Büyük Menderes nehir ağzı ve çevresindeki kıyı sularının akıntı sistemini anlayabilmek amacıyla su çevrim modeli oluşturulmuştur. Bu amaçla Finite Volume Coastal Ocean Model (FVCOM) sayısal modeli kurulmuş ve gelgit, rüzgar ve nehir girdileri ile çalıştırılmıştır. Alandan toplanan akıntı, tuzluluk ve sıcaklık değerleri model çıktıları ile karşılaştırılarak kurulan model altyapısının performansı değerlendirilmiştir. Modelin ölçümlerle olan karşılaştırması sonucunda sistemi yeteri kadar iyi tanımladığına karar verilmiştir. Ayrıca gelgit, rüzgar ve nehir girdilerinin akıntı düzenindeki etkileri ayrı ayrı da modellenmiştir. Bölgenin mikro gelgit özelliği nedeniyle gelgite bağlı hareketin oldukça az olduğu görülmüştür. Nehir ağzına yakın ve nehrin yüksek debili aktığı zamanlarda akıntı düzeninin nehirden yoğun şekilde etkilendiği gösterilmiştir. Rüzgar ise en çok etkili olan parametredir. Ancak rüzgar etkisi belirli bir zaman farkı ile kendini akıntı sisteminde hissettirmektedir. Model bölgede 09 - 20 Ocak 2016'da gözlenen rüzgar hızı ve nehir debisinin en yüksek olduğu bir zamanı değerlendirmekte de kullanılmıştır. Nehir ağızları hidrodinamik açıdan oldukça karmaşık alanlardır ve su çevrim modeli gibi modellerin daha iyi çalışabilmesi için çok daha uzun süreli ölçümlere ihtiyaç duymaktadır.

.

Anahtar Kelimeler: Su Çevrim Modeli, FVCOM, Büyük Menderes Nehri,

“If there is an amateur reader still left in the world -or anybody who just reads and runs- I ask him or her, with untellable affection and gratitude, to split the dedication of this” thesis in two; my mother and father.

ACKNOWLEDGEMENTS

Foremost, I would like to thank my supervisor, Assist. Prof. Dr. Gülizar Özyurt Tarakcıoğlu, for her guidance, encouragement and support throughout not only this research, but also for the bad days in my life. Furthermore, I would like to thank to my co-supervisor Assist. Prof. Dr. Cüneyt Baykal for his advices, guidance throughout my graduate studies. I would like to express my sincere gratitude to Prof. Dr. Ayşen Ergin, Prof. Dr. Ahmet Cevdet Yalçıner and Dr. Işıkhan Güler, Dr. Doğan Kısacık and Prof. Dr. Ayşegül Askan Gündoğan for their wisdom, inspiration and always smiling faces.Furthermore, I owe many thanks to Prof. Dr. Jaak Monbaliu, Dr. Pierre W. Cazenave and Dr. Michela De Dominicis. With their unconditional helps and great knowledge, not only I could conclude this study, but also they helped me to understand that science cannot be bounded by borders and should be done by their way.

I would like to present special thanks to my dear friend and colleague Abdurrahman Polat for the things he has done for me. Also, I would like to thank Bora Yalçıner for his efforts and support on this study and my dear friends Cem Bingöl, Ghazal Khodkar, Koray Deniz Göral, Can Özsoy, Kadir Karakaş, Emrecan Işık, H. Gökhan Güler, B. Ufuk Şentürk, İlker Çoban, Mert Yaman, Elif Bilir, Begüm Balcı, Baran Kemer, Mert Oytun, Gamze Sümer, Derya Atalay, Serkan Gökmener, Berrak Erdal, Deniz Sınar, Emrah Sezer, Özgür Karadeniz, Yiğit Gencal and Cem Severcan for being in my life, crying and laughing together.

I would like to thank my girlfriend Gizem Akköse for her unexpected and unconditioned love, support, above all her beautiful laughter for all the time we have spent together.

Finally, I would like to thank to my family not giving up on me. Their support and patience for all these years helped me to reach this degree.

TABLE OF CONTENTS

LIST OF FIGURES

FIGURES

CHAPTER 1

INTRODUCTION

"The coastal zone is a zone of transition between the purely terrestrial and purely marine components on Earth's surface. It is widely recognized as being an important element of the biosphere – as a place of diverse natural systems and resources." (Crossland et al. 2005). The subject of the study is a part of west coast of Turkey, where Büyük Menderes discharges into Aegean Sea. This area is named Delta Plain of Büyük Menderes River. As being the western border of the Büyük Menderes Basin, the Büyük Menderes Delta Plain is one of the greatest plains of the country. The basin, reaching up to a total area of 24,976 km^2, it comprises the areas of ten cities, partially: Aydın (%95), Denizli (%70), Uşak (%67) Afyonkarahisar (%23), Muğla (%19), İzmir (%3), Isparta (%1.6), Burdur (%0.6), Kütahya (%1), Manisa (%0.03) (Strategic Environmental Assessment Report 2016). The coastal area of the study, which lays in the borders of Aydın, is an area that contains high agricultural activities and the one of the important lowlands of the country. Other than farming, tourism is the other important income for the local people. Located between Kuşadası and Didim, which are two cities of the Turkish Riviera, the area of interest also includes the Dilek Peninsula – Buyuk Menderes Delta National Park (Strategic Environmental Assessment Report 2016). Fishing is another activity widely done by local people. Therefore both of the water resources (the sea and the river) is very important for the region.

The water quality for river affects not only the quality of the foods or industrial plants, but also the efficiency and unit price of agricultural products. Anything that affects the water quality of the river directly affects the water quality of

the coastal zone. To exemplify this perspective, any pollutant that will be spreading from the river have an influence on the adjacent seaside settlements, the plain and fisheries located at the offshore part of Doğanbey Village (Bekdemir; 2016). Additionally, when the river discharge is low, under right coastal conditions, salinity intrusion to the river is observed. This is another parameter that changes the river water quality. Other than that, the focused area is a delta plain, according to the seasonal changes or extreme conditions, coastal erosion and flooding may take place and stake holders are directly affected. The currents generated by a variety of coastal conditions such as winds are the main driving physics of such changes in the coastline. Therefore, it is important to understand the mechanism of river-sea interaction under different climate conditions. Coastal circulation modeling provides this information by simulating the water circulation under a combination of forcing such as wind, tide, river, waves and groundwater.

The aim of this study is to model the coastal circulation Büyük Menderes Delta coastline focusing the river mouth and the adjacent coastal waters. The coastal circulation model is used to simulate the flow under wind, tide and river forcing using Finite Volume Coastal Ocean Model (FVCOM) numerical model. Field measurements of river flow, wind, current, salinity and temperature are used to validate the model setup. Historical extreme events are also modeled to analyze the circulation pattern of the region under extreme forcing such as maximum river discharge, maximum wind speed, minimum river discharge and very calm conditions (Chen and Beardsley 2011).

Chapter two introduces the literature review on the coastal circulation modeling and a summary on how this review is used in the model setup. FVCOM model is presented in chapter three, highlighting the important points in the model setup. The study area and all the data used in the modeling is discussed in chapter four. Chapter five presents the final model setup and

results of the study are discussed with comparisons to field measurements. Chapter six concludes this thesis with recommendations on future studies.

CHAPTER 2

LITERATURE REVIEW

In this section, some of the most relevant water circulation studies will be summarized in both chronological and contextual means. For that reason, especially the studies about coastal circulation models on a pre-defined domain having similar aspects to Büyük Menderes river mouth and adjacent coastal areas, with the use of parameters like; wind, Coriolis, tide, river forcings have been investigated. The previous research helped to set the limits of the study as well as to determine the significant parameters and dataset quality for a successful application of a water circulation model.

Legović (1991) has implemented a method for fluid interaction "between a coastal basin and the adjacent sea" which has been applied as a case study of the Rijeka bay located on the northeast of the Croatia. As the procedure, exchange percentages have been calculated for the seasons, winter and summer. As a result, the middle of the winter exchange value quadruples the value of midsummer. The study reveals that the direction and the magnitude of water exchange differs for one season to another (Legović 1991).

Davies et al. (1998) built up a 3-D hydrodynamic model in order to model the wind induced currents caused by uniform wind stresses. "The model has a functional approach in the vertical and a finite difference grid in the horizontal. A flow dependent eddy viscosity is used to parameterize vertical mixing of momentum". The outcomes of the simulations show that the incorporation of tidal turbulence indicates that; "the wind induced flow is modified by the non-linear interaction between tidal and wind driven currents arising from the flow dependent eddy viscosity term and bottom friction effects". Due to the topographic and bathymetric varieties in the defined model

area, wind-induced currents behave differently in different positions (Davies et al. 1998).

Pietrzak (2002) has built up a hydrostatic model, in an immersive environment, that puts together “a generalized vertical coordinate system with an efficient implicit solution technique for the free surface”. The model was able to sustain high resolution both at levels of bottom and the surface boundary layers. Smagorinsky Formulation and the vertical κ–ε turbulence model was used for solving horizontal diffusion. For validation purposes, the model has been tested. And the results indicated that the hydrostatic model works good enough for; “simulating shallow nearshore, estuarine flows as well as large-scale geophysical flows” (Pietrzak et al. 2002).

De Castro et al (2000) investigated the circulation behavior caused from the wind-induction between the ria, submerged river valley, of Ferrol -located at the North West of Spain- and the adjacent shelf via the hydrodynamic model: MOHID2000, in 3-D. The calibration of the model was done with real in situ data of wind recordings, furthermore; the data was used for the analysis. “The approach to study the wind effect on water exchange through the ria strait consisted in subtracting the signal calculated with only tidal forcing (Ts) from the one with wind and tidal forcing (WTs)”. The resultant circulation is a proof that the water flowing in direction of wind, along surfaces and layers, causes an opposite current flowing in the counter direction at the layers close to the bottom (DeCastro et al. 2000).

Zheng et al. (2003) studied the domain of Satilla River estuary, in Georgia, for “flooding-drying process over intertidal zone”. As the turbulent closure model, Mellor and Yamada’s level 2.5 model was used with the three-dimensional model. The model operated with tide and river inputs. Moreover, wetting-drying treatment technique was implemented for the sigma coordinate of the estuary model. The consequences of the analysis had a good compliance with the data collected from the site. With the correlation of the results and the data, it can be stated that the study “model provided

a reasonable simulation of the temporal and spatial distributions of the 3-D tidal current and salinity" (Zheng et al. 2003).

Koçyiğit and Koçyiğit (2004) have implemented a model that works in an immersed environment using a semi-implicit time discretization with finite difference method. To include the influence of the vertical acceleration component of internal velocities, and the changes related to bathymetry considered to be comparatively significant physical parameters for the circulation patterns; "the conventional sigma coordinate system and the non-hydrostatic pressure component in the vertical direction" were implemented into the model. To observe the different circulation scenarios, starting from very basic bathymetries to advanced ones, were tested. As examples from the study; from a constant depth bathymetry of a rectangular shape, to Esthwaite Water in Cumbria, a tidal marsh in Lake District National Park in UK, with a complex bathymetry were tested with the model. In the light of the results of the analysis and the comparisons with the analytical solutions and data; it was concluded that bathymetry characteristics has a substantial role over the circulation pattern. As the secondary parameters, directionality and the magnitude of wind speed, and eddy viscosity have effect over the results. (Koçyiğit and Koçyiğit 2004)

A hydrodynamic model was improved by Tsanis et al. (2005), which can be used to analyze the wind driven pollutant transport cases as three-dimensional phenomenon under various environmental conditions. The model was used for wind-induced circulation in closed basins with the three-dimensional governing equations. Control volume method was used for the approximation of the governing equations on the "Arakawa-C staggered grid". The calculations are done including with the Coriolis effect and the main parameters to compute inflows and outflows. For the barotropic pressure condition, a semi-implicit difference scheme was implemented to the model, "the Adams–Bashford scheme for the temporal terms and the weight averaged Donor-cell scheme for the advective terms". Although for the test cases, in which the model has handled the tests, uniform wind speed and one source was used; yet, model can

cope with “non-uniform wind conditions, multiple sources, and nearshore applications”. (Tsanis et al. 2005).

Ulses et al. (2005) used “a high horizontal resolution 3D hydrodynamic model SYMPHONIE to a semi-enclosed bay” located in Western Mediterranean Sea. In this work, the wind-induced “specific circulation patterns” and the “scales of residence times” are described. Generalized wind forcing conditions were implemented the model for the idealized simulations. As inputs, “actual conditions of Rhone river discharges”, and “meteorological forcing is used” in the simulations. Effects of the surroundings were taken into consideration for general circulation. Observation data and model results were complying. (Ulses et al. 2005).

Zhao et al. (2006) have studied Mt. Hope Bay and Narragansett Bay via Finite Volume Coastal Ocean Model (FVCOM) for tidal motion. The model has been tested with, irregular coastline, islands, narrow flumes, and high horizontal resolutions. The accuracy of the results is enough for the “tidal wave” phenomenon in the bays. “It also resolves the strong tidal flushing processes in the narrow channels of the bays” (Zhao et al. 2006).

COHERENS; a three-dimensional hydrodynamic model for shallow waters was developed by Marinov et al. (2006). The model can achieve various kind of operations; coastal and shelf seas, estuaries, lakes, reservoirs, and even, including; “managing oil spills”, “linking eutrophication problems to human activities”. This model has been proved to give good results for “short observations”. The site measurements that are made for currents and water surface elevation for high tide events. Simulations and measurements gave parallel results. The results of the analysis were close enough for the seasonal trends. Furthermore, the simulation results fit the trends of salinity and temperature observations. (Marinov et al. 2006).

De Serio et al. (2007) inspected the hydrodynamic processes in a specific coastal area in the Ionian Sea on the northern side of the Gulf of Taranto which is called Mar Piccolo. In this study, mainly the baroclinic conditions are implemented into the

mathematical model by the field measurements. Princeton Ocean Model (POM) has been chosen for the three-dimensional analysis. Moreover, the analysis brought a solution for the following facts; “a simple tidal wave”, “a homogeneous and stationary wind field”, and “a constant outflow and vertical stratification of temperature and salinity”. For validation purposes, the results of the POM analysis were compared with the velocity data that has been collected with the field surveys. (De Serio et al. 2007).

Levasseur et al. (2007) worked on a model which was a three-dimensional hydrodynamic model to make simulations for water circulations in estuarine systems. This model is using the in Cartesian coordinates equations with a “terrain-following structure”. Also, the model is coupled with a turbulence method of Mellor-Yamada 2.5 turbulence scheme. A fractional-step method has been implemented and the subset of equations are solved with, both; finite volume and finite element methods. At low water for the tidal forcing simulations “a drying and wetting method is used. “Point-source method is used for river inputs. The model was tested in an estuary which is macrotidal, partially mixed, temperate estuary”. Other than that, the model is also tested by the change in the sea surface elevation oscillations and salinity data collected from the domain. (Levassuer et al. 2007).

In 2007, Sankaranarayanan implemented a boundary-fitted hydrodynamic model, three-dimensional model, named BFHDYRO, in a domain at Buzzards Bay, Massachusetts. The aim of the work was to set up a model simulating the effect of the parameters; the wind and tide-induced circulation in the bay. Primarily, wind force is applied over the entire surface of the domain and the tidal force was applied from the open boundary nodes. The model calibration was done with the literature and the data from site surveys. The results of the analysis indicate that the wind is the main driving force of the formation of barotropic residual currents inside the Buzzards Bay. (Sankaranarayanan 2007)

Chen et al. (2008) has focused over the area, the Satilla River Estuary, the tidal flooding and drying process are examined via the Finite Volume Coastal Ocean model

(FVCOM). The FVCOM has been implemented with tidal forcing from the open boundary nodes and river discharge at the upstream end, which has resulted in a solid result for “the tidal flushing in this specific estuarine tidal-creek intertidal salt-marsh complex”. Therefore, the results were acceptable by means of the amplitudes and phases of measurements at mooring sites and, also, along the hydrographic transects that belong to the tidal wave, and salinity data. (Chen et al. 2008).

Liu et al. (2008) has implemented a time-dependent, three-dimensional hydrodynamic numerical model, which is called SELFE, for the Danshuei River adjacent to coastal part of the sea in Taiwan, to analyze the entire estuarine system. The dominating parameters involved in the analysis were; freshwater input from the mainstream and branches in the Danshuei River system, and the tidal elevations along the open boundary nodes. The numerical analysis results were in good compliance with the field measurements. (Liu et al. 2008).

Shore (2009) has implemented a circulation model for Lake Ontario, Canada. In his studies, he has inspected the monthly climatological circulation, ever the domain of Kingston Basin. The consequences of the analysis implied that the model can take up to 3 years to ramp-up from rest for a wind-forced, nearly full enclosed lake model for an analysis duration of 10 years. The result of the model run have parallelization with the current measurements through the inside of the main body of the Lake Ontario (Shore 2009).

Akbaşoğlu (2011), has studied the area of Fethiye Bay, south west of Turkey, by means of wind-induced circulation patterns, water exchange and sediment analysis. The study conducted on a semi-enclosed basin, and via FVCOM. As parameters; Coriolis Force, wind, tide, river and sediment data have been implemented the model as inputs. Moreover, the parameters are handled in different scenarios like; different combinations of various direction, speed and durations of constant wind data, and river forcings and tidal conditions. The model study started using test scenarios, and ripen

with the simulations of water exchange, circulation pattern and sedimental analysis inside Fethiye Bay. (Akbaşoğlu 2011)

In 2012, Jiang and Fissel made some changes on the three-dimensional model, which is called COCIRM-SED, to simulate ocean currents and water levels in a specific area of BC, Canada, starting from southern Discovery Passage to Canoe Pass. The numerical model is based on Reynolds-averaged Navier-Stokes fluid dynamics equations and uses finite difference and volume methods. Depending on the results of the numerical model, probable locations for underwater tidal current turbines can be determined and environmental impacts of those turbines can be predicted. While modeling the case; Coriolis force, tidal force, southern Discovery Passage, and freshwater discharge from Campwell River are all implemented. Several parameters such as; water elevation and current were used for calibration purposes using the available data and measurements. In this way, the model has a higher sensibility. There is a man-made rock dam between Quadra Island and Maude Island, In Canoe Pass. In the first model, underwater tidal current turbines were arranged to be implemented, instead of abolishing the dam. In the second model, this time Coriolis force and tidal forces were included, and again there was a calibration phase in accordance with the measurements and observations. This study has shown that, both models have high resolutions in terms of circulation. For deciding the probable locations for constructing the underwater tidal turbines; the flow patterns that obtained, and the results of analysis can be used for. (Jiang and Fissel 2012)

Pitcher, G. C. et al., modelled the circulation and exchange during the summer months from 2009 to 2011, in succession, for the Saginaw Bay-Lake Huron system. The validation of the model was done with ADCP observations of currents, a Lagrangian drifter test in the Saginaw Bay and the temperature data from the National Data Buoy Center gauges. As a fact, circulation in the Saginaw Bay is shaped by the presence of an anticyclonic gyre which is located at the mouth of the outer bay. New estimations are done for the mean flushing times and residence times for Saginaw Bay. (Pitcher, G. C. et al. 2014)

Sirisup et al., aimed simulating the ocean circulation in the Gulf of Thailand, in their study in 2016. The Gulf of Thailand is composed of complex coastlines and sea bottom topography which may result in complicated ocean currents. For this reason, they have conducted their study with the unstructured grid Finite-Volume Coastal Ocean Model (FVCOM) to overcome the problem of complexity issue with the geometric flexibility capability of FVCOM. For validation purposes, they have used the surface currents data measured by high frequency surface wave radar (HFSWR) from Geo-Informatics and Space Technology Development Agency (GISTDA). Furthermore, it is found that the RMS error proves the model output agrees with the observation well. Other than that, the Empirical Orthogonal Function (EOF) used for investigating the overall characteristic of the simulate currents all together with the measured currents as well. (Sirisup et al. 2016)

Ding and his colleagues used a high-resolution unstructured grid finite volume community ocean model (FVCOM) to inspect the North South China Sea shelf characteristics and dynamical mechanism of seasonal currents. As the dominant forces change, the current characteristics inside the bay varies. To understand the phenomena, the model studies has concentrated on freshwater discharge, wind forcing, tidal rectification, and stratification (Ding et al. 2017).

Yılmaz, used HYDROTAM-3D for modelling the current pattern in Samsun Bay under the parameters of wind, wave and tide. The model has the modules of hydrodynamic, turbulence and transport. Furthermore, the verification has done with the monthly data that collected from the site, regularly. (Yılmaz 2018)

Huang and Li used baroclinic Finite Volume Community Ocean Model (FVCOM) in the Lake Pontchartrain Estuary to model the wind-driven circulations during a period across the board, 16 cold fronts in the system. The aim of the study is to inspect the spatial circulation pattern that is the result of local and remote winds. And the results they have found are; remote wind effect decays through the inside due to bottom friction. Local wind effect tends to generate downwind flows in coastal regions, on

the other hand; upwind flows near the bottom, a result consistent with barotropic wind-driven circulations. (Huang and Li 2019)

This review on literature showed the important points for an ocean circulation model study such as;

- Accurate bathymetry data and its representation in the numerical grid has a substantial role in modeling the circulation pattern
- Wind over the entire surface of domain, water elevation including tidal constituents from the open boundary nodes, Coriolis force and river input (as point source or number of points across very wide rivers) are the external forcing parameters commonly used in the circulation studies
- In situ current measurements, as well as salinity and temperature observations are mainly used for calibration and validation of the circulation models
- Mellor-Yamada 2.5 turbulence scheme is commonly used for turbulence closure method.

CHAPTER 3

METHODOLOGY

This chapter gives information about the methodology of the study focusing on describing the use of the numerical model, FVCOM (Finite-Volume Coastal Oceanographic Model) developed by the University of Massachusetts at Dartmouth and the Woods Hole Oceanographic Institute (UMASSD-WHOI) collective efforts (Chen et al. 2006; and Georgiou 2007). The formulation and capabilities of FVCOM are summarized, together with some of its limitations. The procedure of creating a FVCOM model setup is described. Model calibration and validation approach is discussed.

3.1. Finite-Volume Coastal Oceanographic Model (FVCOM)

FVCOM is an unstructured-grid, finite-volume, three-dimensional, primitive equation, coastal ocean circulation numerical model, developed by the University of Massachusetts at Dartmouth and the Woods Hole Oceanographic Institute (UMASSD-WHOI) collective efforts (Chen et al. 2006; and Georgiou 2007). It has been designed to simulate time-dependent variation in water levels, currents, temperature, salinity, tracers, cohesive and non-cohesive sediments and waves in a variety of marine and freshwater systems.

3.1.1. The Governing Equations

The governing equations that has been used include the following: momentum, continuity, temperature, salinity, and density equations.

The governing equations (from 3.1 to 3.7) that has been used include the following: momentum, continuity, temperature, salinity, and density equations.

Momentum:

$$\frac{\partial u}{\partial t} + u\frac{\partial u}{\partial x} + v\frac{\partial u}{\partial y} + w\frac{\partial u}{\partial z} - f\mathrm{v} = -\frac{1}{\rho_0}\frac{\partial P}{\partial x} + \frac{\partial}{\partial z}\left(K_m\frac{\partial u}{\partial z}\right) + F_u \tag{3.1}$$

$$\frac{\partial u}{\partial t} + u\frac{\partial u}{\partial x} + v\frac{\partial u}{\partial y} + w\frac{\partial u}{\partial z} + f\mathrm{u} = -\frac{1}{\rho_0}\frac{\partial P}{\partial x} + \frac{\partial}{\partial z}\left(K_m\frac{\partial u}{\partial z}\right) + F_u \tag{3.2}$$

$$\frac{\partial P}{\partial z} = -\rho\mathrm{g} \tag{3.3}$$

Continuity:

$$\frac{\partial u}{\partial x} + \frac{\partial v}{\partial y} + \frac{\partial w}{\partial z} = 0 \tag{3.4}$$

Temperature:

$$\frac{\partial T}{\partial t} + u\frac{\partial T}{\partial x} + v\frac{\partial T}{\partial y} + w\frac{\partial T}{\partial z} = \frac{\partial}{\partial z}\left(K_h\frac{\partial T}{\partial z}\right) + F_T \tag{3.5}$$

Salinity:

$$\frac{\partial S}{\partial t} + u\frac{\partial S}{\partial x} + v\frac{\partial S}{\partial y} + w\frac{\partial S}{\partial z} = \frac{\partial}{\partial z}\left(K_h\frac{\partial T}{\partial z}\right) + F_S \tag{3.6}$$

Density:

$$\rho = \rho(T, S) \tag{3.7}$$

Variables used in these equations:

(x, y, z) – east, north, and vertical axes in Cartesian coordinates

(u, v, w) – velocity components in the x, y, and z directions

(F_u, F_v) – horizontal momentum diffusivity terms the x and y directions

F_T – horizontal thermal diffusion term

F_S – horizontal salt diffusion term

K_m – vertical eddy viscosity coefficient

ρ – density

P – pressure

T – temperature

S – salinity

f – Coriolis parameter

These equations are closed mathematically using the Mellor-Yamada level-2.5 turbulence closure model (Mellor and Yamada 1982). This model approximates mixing due to turbulence based on length scale of the boundary layer. FVCOM makes use of a simplification by (Galperin et al. 1988) which removes a slight inconsistency in scaling analysis so that S_m and S_h depend only on G_h. The equations for Galperin's simplification of MY-2.5 are:

$$K_m = q/S_m \tag{3.8}$$

$$S_m = \frac{0.4275 - 3.354G_h}{(1 - 34.676G_h)(1 - 6.127G_h)} \tag{3.9}$$

$$S_h = \frac{0.494}{(1 - 34.676G_h)} \tag{3.10}$$

$$G_h = \frac{l^2 \mathrm{g}}{q^2 \rho_0} \rho_z \tag{3.11}$$

F_u and F_v represent the terms for horizontal momentum diffusion in the x and y direction. F_r and F_s represent the terms for thermal and salinity diffusion. These terms are of the form:

$$F_u \approx \frac{\partial}{\partial x}\left[2A_m H \frac{\partial u}{\partial x}\right] + \frac{\partial}{\partial y}\left[A_m H \left(\frac{\partial u}{\partial y} + \frac{\partial v}{\partial x}\right)\right] \tag{3.12}$$

$$F_v \approx \frac{\partial}{\partial x}\left[A_m H\left(\frac{\partial u}{\partial y}+\frac{\partial v}{\partial x}\right)\right]+\frac{\partial}{\partial y}\left[2A_m H\frac{\partial u}{\partial y}\right] \tag{3.13}$$

$$F_T \approx \left[\frac{\partial}{\partial x}\left(A_h H\frac{\partial}{\partial x}\right)+\frac{\partial}{\partial y}\left(A_h H\frac{\partial}{\partial y}\right)\right]T \tag{3.14}$$

$$F_S \approx \left[\frac{\partial}{\partial x}\left(A_h H\frac{\partial}{\partial x}\right)+\frac{\partial}{\partial y}\left(A_h H\frac{\partial}{\partial y}\right)\right]S \tag{3.15}$$

H is the bottom depth, where it is relative to z=0. The horizontal momentum and thermal diffusion coefficients are denoted as Am and Ah. These coefficients can be set constant or use the Smagorinsky eddy parameterization method (Smagorinsky 1963). The Smagorinsky method defines the formula (3.16) for horizontal momentum diffusion coefficient as:

$$A_m = 0.5C\Omega^u\sqrt{\left(\frac{\partial u}{\partial x}\right)^2+0.5\left(\frac{\partial v}{\partial x}+\frac{\partial u}{\partial y}\right)^2+\left(\frac{\partial v}{\partial y}\right)^2} \tag{3.16}$$

Where *C* is constant and Ω^{u} is the area of the individual momentum control element. Am varies with the model resolution, decreasing as the grid size is reduced.

For temperature and salinity, a similar formula (3.17) is used:

$$A_h = \frac{0.5C\Omega^{\zeta}}{P_r}\sqrt{\left(\frac{\partial u}{\partial x}\right)^2+0.5\left(\frac{\partial v}{\partial x}+\frac{\partial u}{\partial y}\right)^2+\left(\frac{\partial v}{\partial y}\right)^2} \tag{3.17}$$

Where *C* is constant and Ω^{ζ} is the area of the individual tracer control element, and P_r is the Prandtl number. A_h is proportional to the area of the individual tracer control element and the horizontal gradient of the tracer concentration.

With regard to Mellor and Blumberg (1985), and Chen et al., (2006) the reducing made by the equations is equivalent to the postulation that horizontal diffusion

happens only collateral to the sigma-layers since oscillating velocities and length scales are orthogonal to the bottom boundary have to approach to zero. Nonetheless, this simplification could prompt extra mixing on sloping bottoms due to the sigma-transformation (Mellor and Blumberg, 1985).

3.2. Composition of the Unstructured Grid and Computational Time Step

The horizontal mathematical computational domain is divided into several nonoverlapping unstructured triangular cells. The triangular unstructured-grid approach of FVCOM has some advantages compared to a structured-grid model. A triangular grid can provide an accurate representation of the coastline especially for complex regions where a triangular mesh can represent the irregularities of the coastline by using high resolution. The unstructured approach of FVCOM enables adjustment of the grid resolution in regions with a high interest with respect to e.g. the bathymetry. On the other hand, in outer domains the resolution can become very coarse. This way, the number of the nodes and the triangles are kept small, thus the costs of the computations are low, too. Structured-grid models do not have the capability to change the grid resolution over one computational domain with just one model setup. Therefore, a nesting approach must be chosen for structured-grid model, which will increase the computing time.

Below, the figure 3.1 indicates the unstructured triangular cells which involve of three nodes; a center of mass, and three sides. “The Momentum Control Element (MCE)” is the zone delimited with the green lines. “The Tracer Control Element (TCE)” is the field bounded by the red lines.

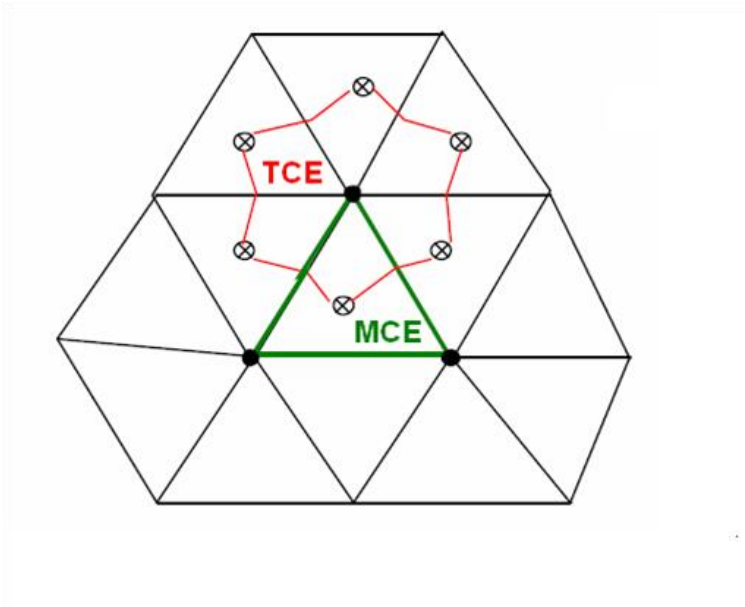

Figure 3.1. Conceptional Unstructured Triangular Cell (Chen et al. 2006a)

In FVCOM not all variables are calculated or placed at the same positions. Tracers as e.g. temperature, salinity or surface elevation are calculated on each node while the velocities are calculated at the center of a triangle (Figure 3.1). The separation has to be done due to numerical restrictions to eliminate the numerical errors in the calculated results (Versteeg and Malalasekera 2007). The scalar variables at each node are calculated by the net flux through the sections linked to the center of the triangles and the mid-point of the adjacent sides in the surrounding triangle (tracer control element or TCE). The velocities at the centroids are determined using the net flux through the three sides of this triangle (momentum control element or MCE).

A sigma-level coordinate system is used in the vertical direction to finest fit the bottom boundary in the model to the bathymetry. The sigma layers are distributed uniformly at different depths of the model (Walter et al. 2007). All model variables are calculated on the mid-level of the layers, except the vertical velocity u, which is calculated on the layer surfaces. Different structures of the sigma layers can be used, but in this thesis, an equidistant structure was chosen.

For computational efficiency, FVCOM employs a mode-split model with an external 2D mode and an internal 3D mode. The time step depends on the chosen grid size. The time step utilized in the external mode of FVCOM is limited by the Courant-Friedrich Levy (CFL) benchmark as:

$$\Delta t_E \leq \frac{\Delta \mathrm{L}}{\sqrt{gD}} \tag{3.18}$$

In which, the external mode time step is represented as 〖Δt〗_E, the numerical computation length scale ΔL, which is the edge has the minimum length of a characteristic or single triangular grid unit, and "the local depth" is D. The limiting value of time step for the internal mode is:

$$\Delta t_I \leq \frac{\Delta \mathrm{L}}{C_I} \tag{3.19}$$

where, C_I is the maximum phase speed of internal gravity waves. Since C_I is usually smaller than $\sqrt{gD}$, it is usually suggested that ratio between internal and external time step (I_{split});

$$\mathrm{I_{split}} = \Delta t_I \leq 10 \Delta t_E \tag{3.20}$$

3.3. The Turbulent Closure Models

3.3.1. The Horizontal Closure Treatment

Smagorinsky (1963) suggested this method to model horizontal diffusion. As opposed to utilizing a constant horizontal diffusivity, which is the other option as a closure treatment; the Smagorinsky approach is based on the horizontal velocity gradient. In this thesis, Smagorinsky approach is used (see the Section 3.1.1)

3.3.2. The Vertical closure treatment

Parameterization of the vertical eddy viscosity K_m, and vertical thermal diffusivity K_h which is possible by using, (i) constant diffusivities, (ii) the method proposed by Mellor and Yamada in 1982, and (iii) the k- ε approach. In this thesis, Mellor-Yamada Level 25 Scheme which is the default turbulence closure method of FVCOM is used.

3.4. Boundary Treatment and External Forcing

3.4.1. Wall or Solid Boundary Conditions

The original approach of FVCOM calculates the velocity in a cell adjacent to a solid boundary such as coastline using the same method as interior cells and then adjusts it so that the component normal to the wall is zero. This approach can introduce errors if the coastline is highly irregular or coastal angle is rapidly changing. Therefore, FVCOM handles this issue by introducing `ghost cells` depending on the number of sides of boundary cell being part of the coastline (Figure 3.2).

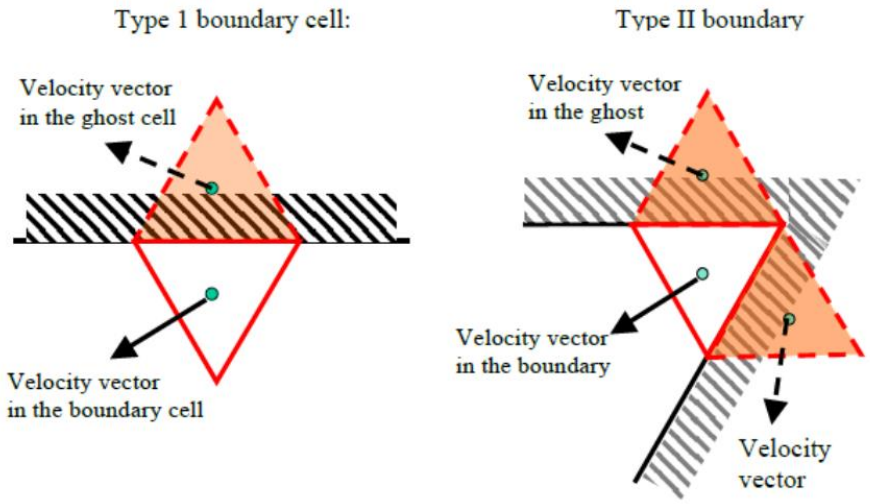

Figure 3.2. Boundary Treatment Types (Chen et al. 2006a)

Although ghost cell treatment might increase the performance of model for irregular coastlines, in the case where the boundary edge is normal to the dominant flow direction, the ghost cell boundary condition leads to a reflection of energy, which can generate high frequency internal waves that require a reduction in time step. Additionally, Type II boundary condition is suggested to be avoided in general. For this thesis, ghost cell treatment is activated.

3.4.2. Open Boundaries

One of the difficulties in applying an ocean model to a coastal region is how to specify a proper open boundary condition that allows the momentum or mass to be radiated out of or flow into the computational domain. FVCOM introduces five open boundary conditions such that user can either apply a predetermined surface elevation (e.g. water level measurements including tidal constituents) or user can select from various types of radiation open boundary conditions. In this thesis, a predetermined surface elevation was defined at every node of the open boundary based on mareograph measurements for the region.

3.4.3. External Forcings

External physical forcings driving FVCOM include the surface wind stress, heat flux, precipitation/evaporation, tides, river discharges, and groundwater flux. In this thesis, surface wind, tides and river discharge are applied as external forcings.

Users can define wind either as wind stress or wind speed and apply it with a constant uniform forcing or with time-dependent, spatially non-uniform forcing fields specified from observational data or from the output of a meteorological model or a combination of both. In this thesis, wind data is applied as wind speed at 10 m and with time-dependent spatially uniform forcing field.

Tide is applied as a component of water surface elevation time series data taken from the closest mareograph station at every node of the open boundary. To explain it briefly, open boundary nodes are defined as the source points for this process. The absolute water elevation for each node is defined with an interval of one hour throughout for the analysis duration to simulation. The software interpolates the water heights for each predefined external time step.

FVCOM uses two methods for including the discharge of fresh water from the coastal solid boundary. The first is to inject the water into the tracer control element (TCE) like a point source and the second is to input the water into the momentum control element (MCE) like a line source. In each of these methods, the salinity, temperature and discharge values can be either specified or calculated through the tracer equation. In this thesis, the data related to river forcing is applied by using tracer control element.

3.5. Model Calibration and Validation

Calibration involves adjusting certain empirical parameters of a model with the aim of fitting the model output to real data. This process succeeds if the model is able to reproduce observed variability in the processes of interest to an acceptable level of accuracy (Moriasi et al. 2007). After model is calibrated, another run is performed for a different set of real data to validate the model. However, a good calibration study depends on the quality and completeness of real data (measurements) for the site. Calibration should evaluate the model performance both qualitatively and quantitatively. The qualitative evaluation is made on the correctness and plausibility of the physical model behavior and requires expert knowledge to judge. On the other hand, the quantitative evaluation can be made with statistical error metrics such as mean absolute error (MAE) or standard regression techniques commonly used to evaluate the linear relationship between modeled data and observations such as correlation coefficient (R).

As the data that included for the statistical computations, only the measured data and the corresponding model results have taken into consideration in the computations. That means, the ramp-up part of the analysis results is not included in the statistical analysis since the ramp-up duration is selected such that this data and field data did not overlap. To visualize, the results of all the analysis can be seen in the following section.

3.6. The Flowchart of the FVCOM Application

FVCOM is written in Fortran 90 with MPI parallelization and runs on a LINUX platform. Alternatively, there exists a modified version of Plymouth Marine Laboratory, UK. The model does not have a built-in graphical user interface therefore, all the input data and model setup have to be provided as text and NetCDF files. Visualization of the model results also requires use of another software such as VisIt®, MATLAB® or Tecplot®. Therefore, the installation, pre-processing and post-processing of model requirements (input/output/setup) make up the major part of the model implementation.

In Figure 3.3, the flow chart is given showing the simulation process starting from zero to the latest step, visualization.

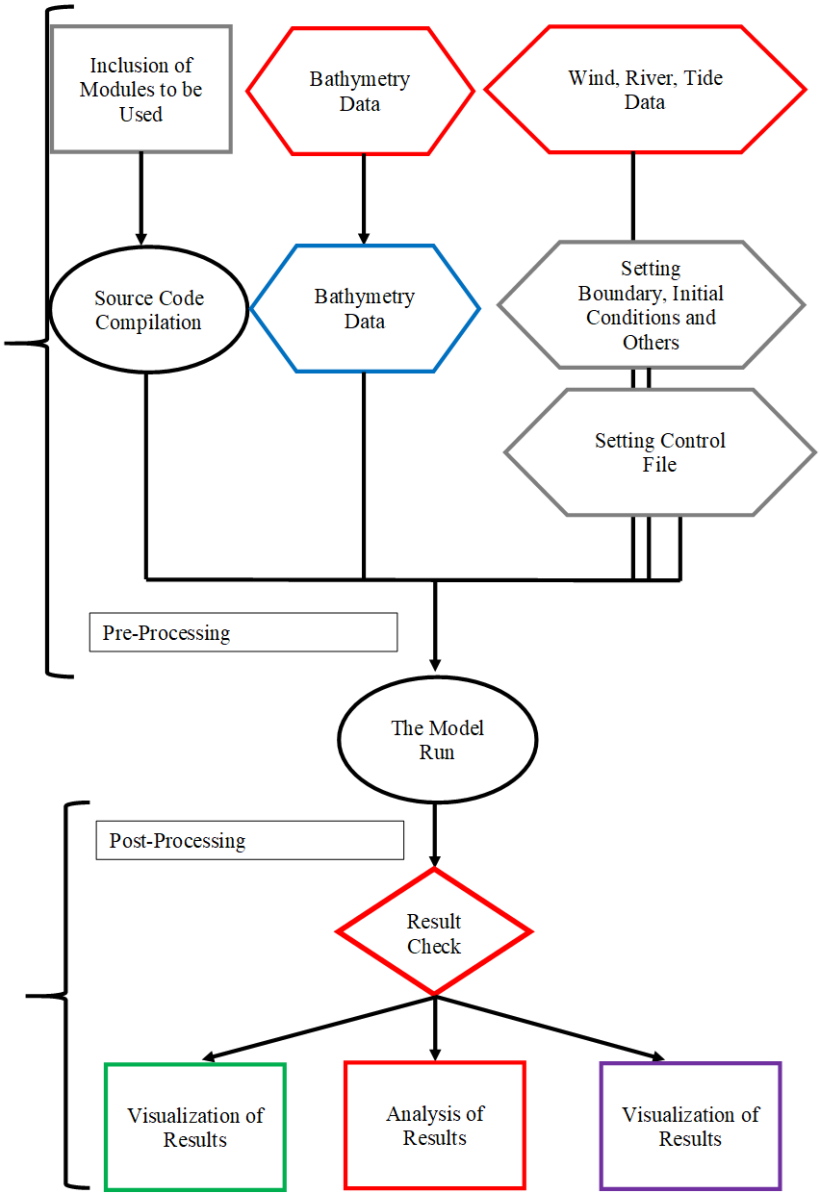

Figure 3.3. Flowchart for the Analysis. The colors belong to the processes of the software: Excel and txt – grey, MATLAB – red, VisIt – green, Tecplot – purple.

CHAPTER 4

THE CASE STUDY AND THE DATA SET

4.1. The Study Area

The study area is a part of west coast of Turkey, where Büyük Menderes river meets Aegean Sea located on the western part of Söke which lies between Dilek Peninsula National Park and, one of the cities of the Turkish Riviera, Didim. Furthermore, the zone has an approximate border which is the Greek Island, Agathonisi. The coordinates of the domain lie between points: 37.40° - 37.65° North and 26.90° – 27.25° East. The bay is located at the west of Turkey and has a coast connecting Kuşadası and Didim which are the two important touristic sites of Aegean District in Turkey. The position of the site is nearly the middle of Aegean Sea in terms of latitude (Figure 4.1). Although secondary to the nearby centers of tourism on the coast, Söke is a common visiting place for tourists, including visitors to the nearby historical site of Priene.

Söke shows typical Eastern Mediterranean climate characteristics. Summers are hot and dry, while winters are warm and rainy. On the average, the warmest month is August while the coolest month is February. Moreover, the months January, February, March, November, and December have a high chance of precipitation. The average annual rainfall is over 1000 mm which is above Turkey's average.

Figure 4.1. The Location of the Area (Retrieved from Google Earth, August 2019)

The areas morphological characteristics are mainly shaped by Büyük Menderes River pouring freshwater and sediment in the bay. There exist three main channels reaching the bay. The first one is the main branch of Büyük Menderes. The second one is the secondary channel of Menderes, which is brought to Lake Bafa, within the scope of *Latmos Project* before pouring Aegean Sea. Finally, the smallest and the third discharge source is the irrigation discharge channel through the middle of the Söke Plain.

In the northeastern part of the study area, just below the southern part of the Dilek Peninsula, there exists a lagoon which is used as fishery. This natural fishery has been affected by morphodynamical changes. Also, that dynamic process affects the erosion and accretion trends on the coastline. The northern part of the area has a steeper characteristic arising from the mountain of the national park which relatively causes a formation of high-sloped cliff. Furthermore, the deepest part of the basin is located at north-western part of it. At the south west, the island Agathonisi is situated. The island represents a natural border for study area. The south border of the study area is the headland of Didim.

The coastline being highly active geomorphologically means that it is important to understand the hydrodynamics of the area. The existing economic activities of fishery, agriculture and tourism along this area enhances the importance of such knowledge since modeling of shoreline movements and water quality of the region would be important for management of the region. Modeling the water circulation of the bay would provide information on the current characteristics and water properties (temperature and salinity) which are input parameters of many sediment and ecological models.

The circulation model of the area is studied by using FVCOM version 4.1 (Chen & Beardsley 2013). Datasets used in the model runs are explained in detail in this chapter.

4.1.1. The Bathymetry

The bathymetry data have been retrieved from two different sources; the first one is the TUBITAK Project of Kısacık et al. and the second one is The European Marine Observation and Data Network – EMODnet (https://www.emodnet-bathymetry.eu/). Furthermore, the coastline has been created based on the EMODnet data with an approximation that excludes the lagoon which is located at the north western part of the bay.

To give a detailed information about the bathymetry construction and merging; in the scope of the project, the bathymetry close to river mouth, that is to say, the area stays under the station points, measured by the DT101 Multibeam Profiling Sonar with a spatial resolution of 72 x 72 meters. The measurement area was about 11 km^2, see the Figure 4.2. Additionally, the EMODnet data was used for the rest of the computational domain which has a resolution of 115 x 115 meters. The area between these points were subject to a smoothing operation via MATLAB. The reason behind this merging process is that the TUBITAK project data has a higher resolution.

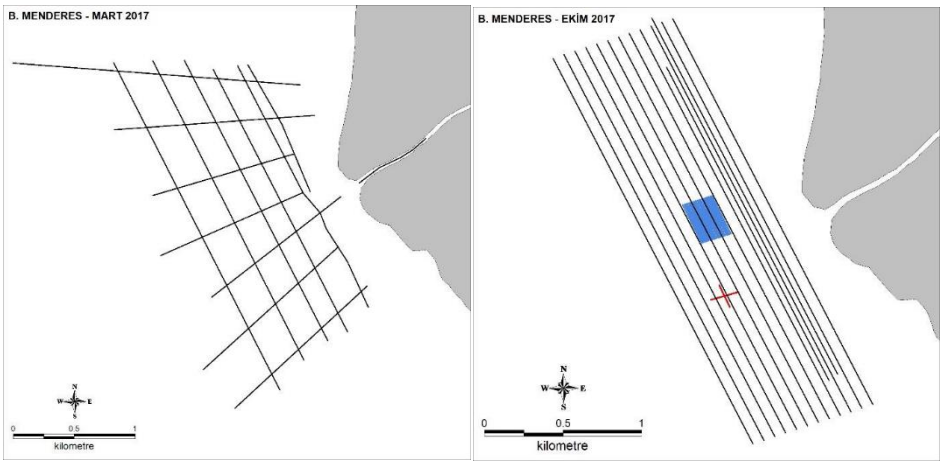

Figure 4.2. Measurement Points for Multibeam Profiling Sonar (Kisacik et al. 2017)

The validation part of the bathymetry is an important step as accurate bathymetry provides higher performance of numerical model. Therefore, the depth of the model bathymetry is compared to the depths of stations used in the field survey. This comparison can be seen in Table 4.1. Using this comparison, the grid is smoothed manually and the stations for validation are located accordingly for the model runs. Other than that, while merging sea reference levels have taken into consideration, mean sea level for each data set has been chosen as common level.

Other than the changes mentioned above, an additional manipulation on the bathymetry of the model has been made at the mouth of the river. The coastline taken from EMODnet database and the real case do not coincide for this specific area, so a channel like structure has been created with a depth of 2.25meters and span of ~200 meters. All the three cases of bathymetry can be seen in Figure 4.3, 4.4, and 4.5. Both the artificial channel and the merged zone can be seen at the Figure 4.5, below.

Table 4.1. *Comparison of the data sets by means of difference in percent.*

	Longitude	Latitude	In-situ Data	Depth(m)	Absolute Difference (m)	Absolute Difference (%)	Depth(m)	Absolute Difference (m)	Absolute Difference (%)
BMN01	27.17414	37.54345	4.50	3.24	1.26	38.89	0.18	3.06	94.44
BMRCM1	27.15883	37.53218	7.20	7.15	0.05	0.70	9.25	2.10	29.37
BMRCM2	27.16411	37.53630	2.70	2.95	0.25	8.47	4.25	1.30	44.07
BM2	27.16645	37.53849	1.60	1.71	0.11	6.43	3.01	1.30	76.02
BM3	27.16531	37.53763	1.50	1.26	0.24	19.05	2.01	0.75	59.52
BM4	27.16153	37.53427	5.20	4.85	0.35	7.22	6.09	1.24	25.57
BM10	27.16064	37.52849	8.00	8.03	0.03	0.37	8.25	0.22	2.74
BM11	27.16257	37.53209	5.30	5.40	0.10	1.85	6.03	0.63	11.67
BM12	27.16531	37.53404	3.50	3.54	0.04	1.13	4.27	0.73	20.62
BM13	27.16905	37.53002	3.70	3.95	0.25	6.33	3.72	0.23	5.82
BM14	27.16537	37.52665	6.80	6.88	0.08	1.16	4.87	2.01	29.22
BM19	27.15736	37.53634	6.00	6.04	0.04	0.66	7.43	1.39	23.01
BM20	27.15986	37.53746	4.90	4.74	0.16	3.38	6.42	1.68	35.44
BM23	27.15569	37.54064	8.00	7.85	0.15	1.91	9.64	1.79	22.80
BM24	27.15989	37.54183	3.40	3.96	0.56	14.14	4.48	0.52	13.13
BM25	27.16294	37.54592	2.30	2.90	0.60	20.69	2.52	0.38	13.10
BM26	27.15563	37.54546	8.10	8.79	0.69	7.85	8	0.79	8.99
BM29	27.14971	37.55007	12.90	12.77	0.13	1.02	10.14	2.63	20.60
BM30	27.15949	37.54937	5.60	5.70	0.10	1.75	4.03	1.67	29.30
				Σ(%)	7.53			Σ(%)	26.17

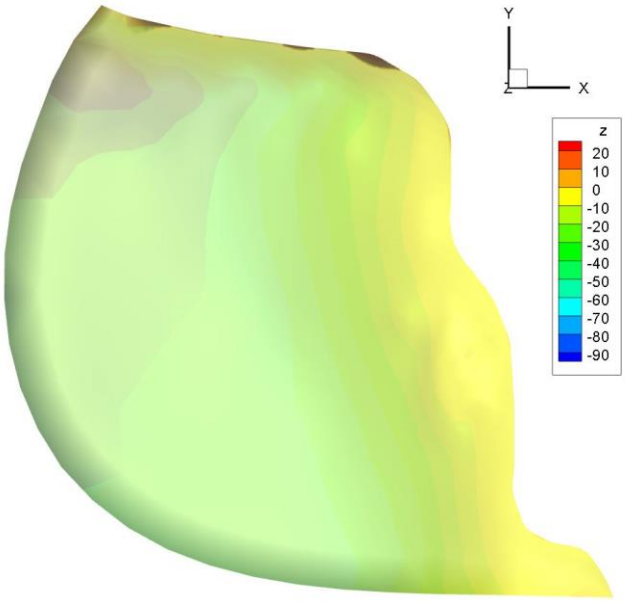

Figure 4.3. The Computational Domain Retrieved from GEBCO Data Set

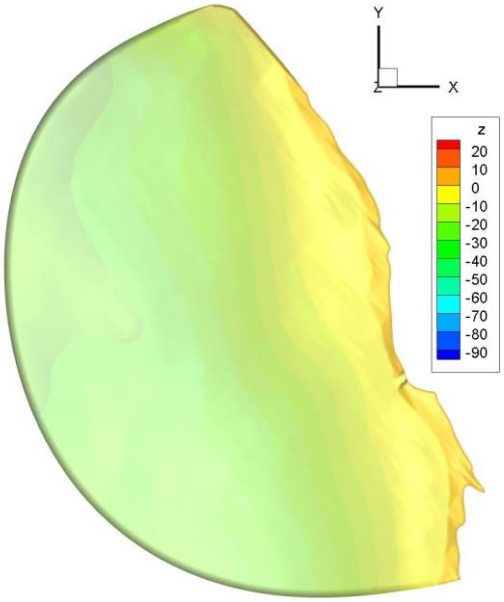

Figure 4.4. The Computational Domain Retrieved from EMODnet Data Set

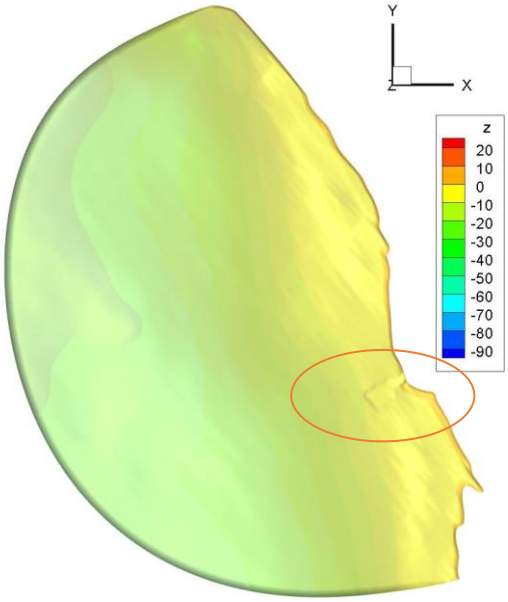

Figure 4.5. The Computational Domain Combined from EMODnet & TUBITAK Study Data Sets

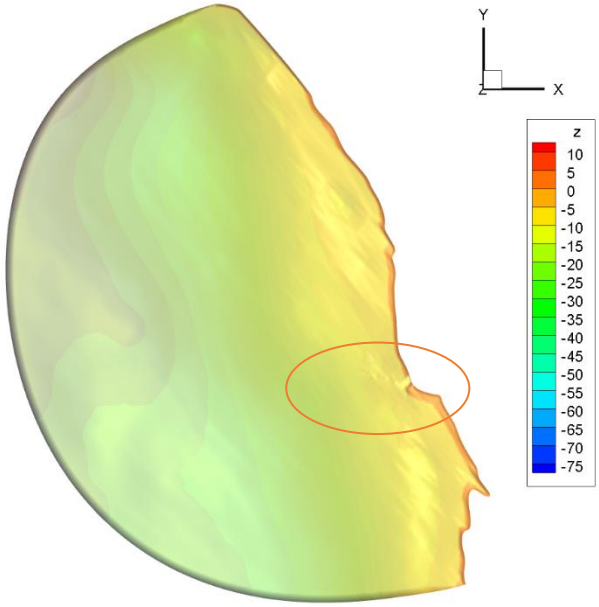

Figure 4.6. The Smoothed Version of the Computational Domain

The computational domain shown in the Figure 4.5 was smoothed to see the differences between those domains in computational manners. At below, it can be seen the difference between these two bathymetric set-ups:

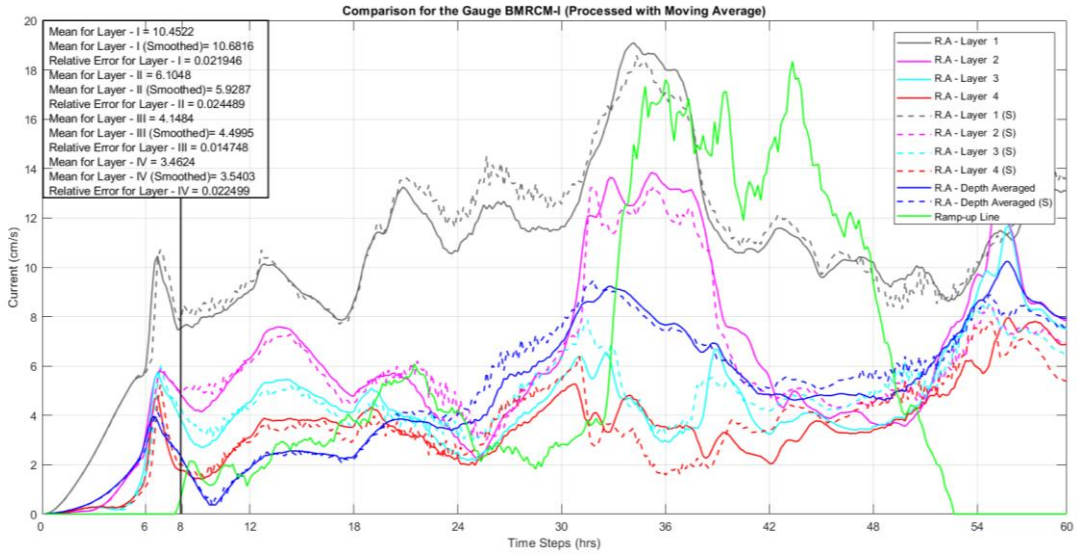

Figure 4.7. Result Comparison for the Merged and the Smoothed Computational Domains at BMRCM-I Station

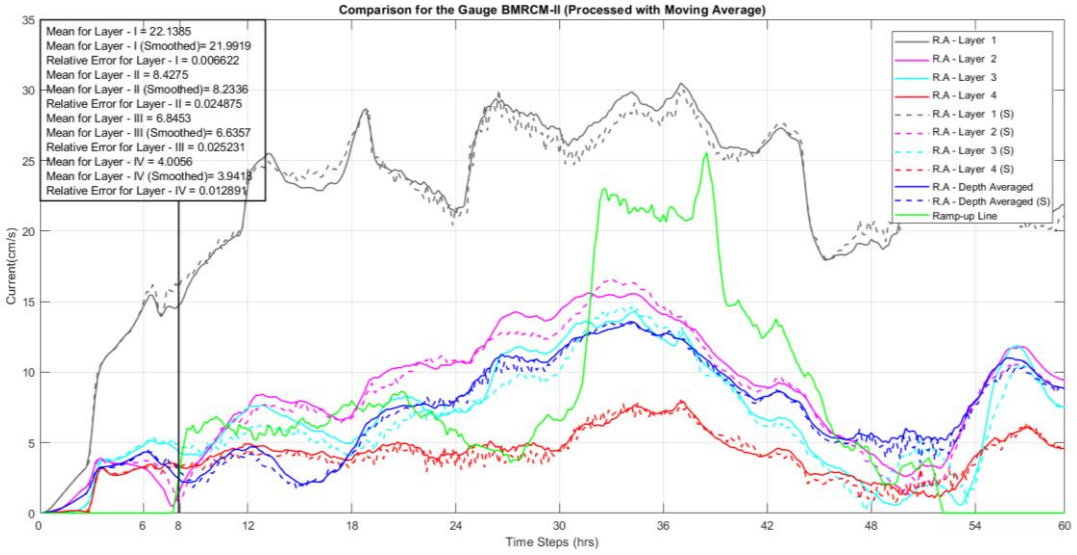

Figure 4.8. Result Comparison for the Merged and the Smoothed Computational Domains at BMRCM-II Station

From the Figures 4.7 and 4.8, it can be understood that the smoothed version of the bathymetry has an effect on the analysis results up to ~2.5% at maximum, ~1.86% on average.

Other than that, a coarser mesh has been produced over the computational domain. At the offshore; 1000 meters, and at the coastline; 250 meters elements were used and the same transition ratio, which was kept as same as the all bathymetric meshing process, applied on this computational domain also. On the other hand, in this domain the nodes do not coincide with the station points as it was overlapped in regular computational domain. So that, the nearest nodes have been selected for the BMRCM-I & BMRCM-II points. The result can be seen on the Figures 4.9 and 4.10 below.

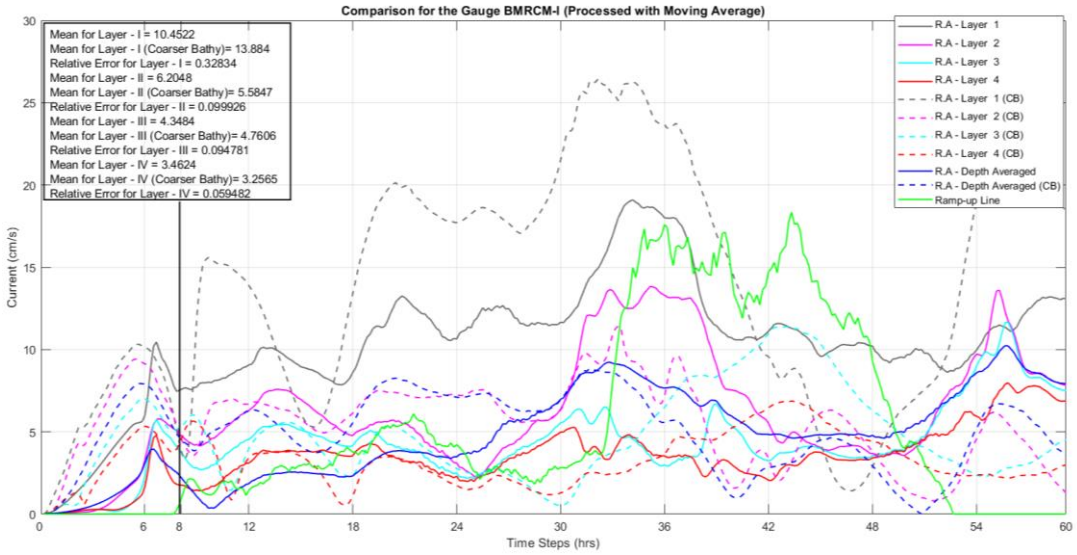

Figure 4.9. Result Comparison for the Merged and the Coarser Computational Domains at BMRCM-I Station

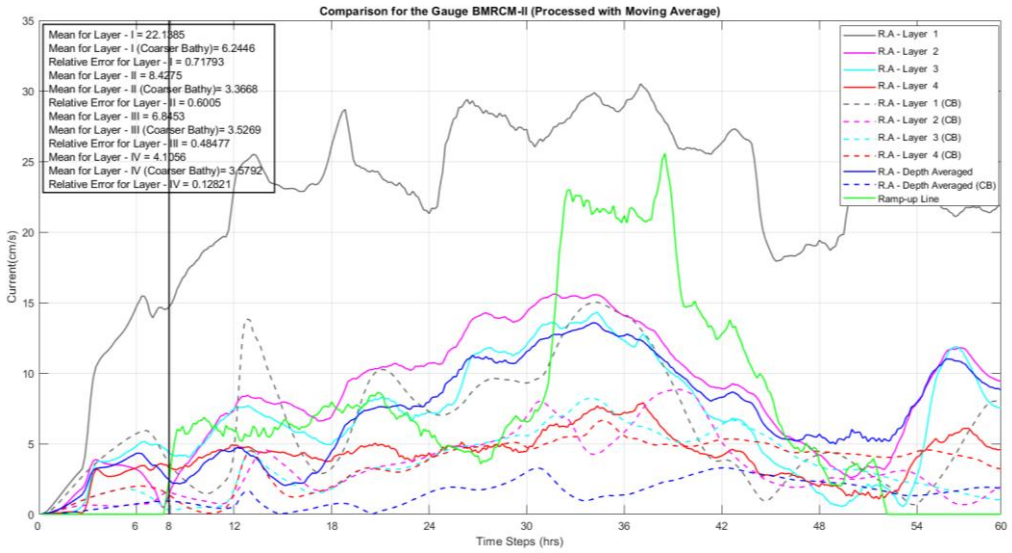

Figure 4.10. Result Comparison for the Merged and the Coarser Computational Domains at BMRCM-II Station

As it can be seen clearly that, for the station BMRCM-I, the coarser bathymetry gives different results changing in an interval between 6% to 32%. The uppermost layer overshoots the result, and the rest of the layers gives the results that stays under the merged bathymetry. On the other hand, for the second station, BMRCM-II, all of the layers undershoot both the measurement result and the merged bathymetry results, ranging in a scale 13% to 71%. As the result, the coarse bathymetry is even further from the measurement results.

4.2. Current, Salinity and Temperature Data

Measurements of current, salinity and temperature around the river mouth was performed as a part of TUBITAK research project no: 115Y722 named *"Evaluation of Short Term Bedforms at River-Sea Interaction Areas: Gediz and B. Menderes Cases"*. In 2017, three field trips were organized by Dr. Kısacık and his team in 12-13 March, 23-24 May and 18-19 October. The collected raw data was provided by Dr. Dogan Kısacık from Dokuz Eylül University and the data is also presented in the final

report of the project (Kısacık et al., 2018). The measurement station names, depths, and locations are tabulated in Table 4.2 and shown in Figure 4.6.

Table 4.2. *The Locations, Depths and Names of the Stations used for data collection*

No	X	Y	Depth(m)	Station Name
1	27.1708	37.5415	2.25	'BM-1'
2	27.1665	37.5385	2.25	'BM-2'
3	27.1653	37.5376	2.5	'BM-3'
4	27.1615	37.5343	4.86	'BM-4'
5	27.1629	37.5367	3.36	'BM-5'
6	27.1566	37.5304	11.19	'BM-6'
7	27.1602	37.5420	5.96	'BM-7'
8	27.1616	37.5389	5.72	BM-8'
9	27.1606	37.5285	7.89	BM-10'
10	27.1626	37.5321	6.16	BM-11'
11	27.1653	37.5340	4.16	BM-12'
12	27.1691	37.5300	3.54	BM-13'
13	27.1654	37.5266	4.98	BM-14'
14	27.1574	37.5363	8	BM-19'
15	27.1599	37.5375	6.2	BM-20'
16	27.1557	37.5406	9.41	BM-23'
17	27.1599	37.5418	6.34	BM-24'
18	27.1629	37.5459	2.46	'BM-25'
19	27.1556	37.5455	8.06	BM-26'
20	27.1497	37.5501	9.25	BM-29'
21	27.1595	37.5494	4.16	BM-30'
22	27.1741	37.5434	2.25	'BMN-1'
23	27.1706	37.5413	2.25	BMN-2'
24	27.1728	37.5425	2.25	BMN-3'
25	27.1588	37.5322	8.9	BMRCM-1'
26	27.1641	37.5363	2.96	BMRCM-2'
27	27.1676	37.5270	3.77	14-M'
28	27.1666	37.5303	3.51	BMS-1'
29	27.1651	37.5331	3.32	BMS-2'
30	27.1647	37.5331	4.18	BMS-3'
31	27.1636	37.5360	4.55	BMS-4'
32	27.1629	37.5367	4.7	BMS-5'
33	27.1602	37.5420	5.7	BMS-7'

Figure 4.11. The Locations of Measurement Stations

4.2.1.1. Current

The current data has been collected with "Seaguard RCM" device. For the current measurement process, the instrument has been fixed to bottom of the sea. In this way the device records the direction and magnitude of the current at the very near by point to the bed within intervals of 5-10 minutes continuously. Time resolution for this data is 10 minutes and, also, absolute speed and directionality are recorded.

The expeditions held within the domain that is close to the river mouth followed two different paths by the means of current. The first one is long-shore which was in March 2017 and the two others in the direction of cross-shore in May and October 2017.

The locations of the stations that current have been measured can be seen in following figures (Figure 4.12).

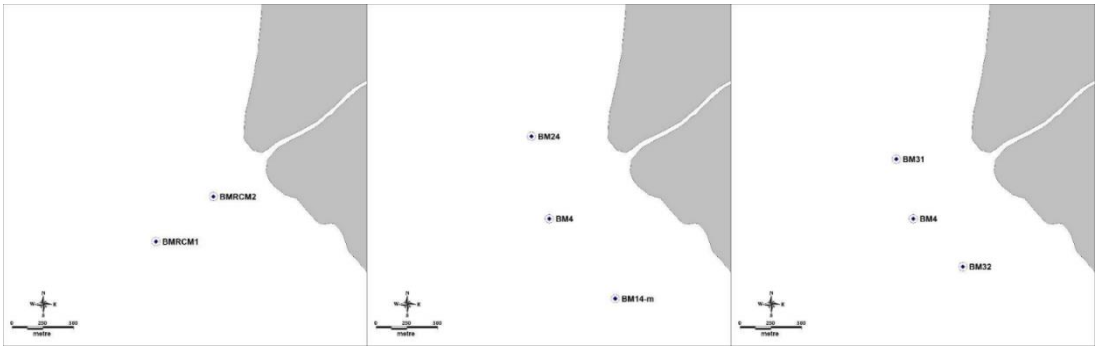

Figure 4.12. The Locations of Stations – March, May and October Measurements

4.2.1.2. Salinity and Temperature

The salinity and temperature data have been collected with "RBR 620 CTD" instrument. The surveying is conducted in the following way: the device sunk into the water from a ship, in the meantime, the instrument records temperature, conductivity and acoustic velocity within a time resolution of 6 seconds through the water column. The locations of the stations that current have been measured can be seen in Figure 4.13.

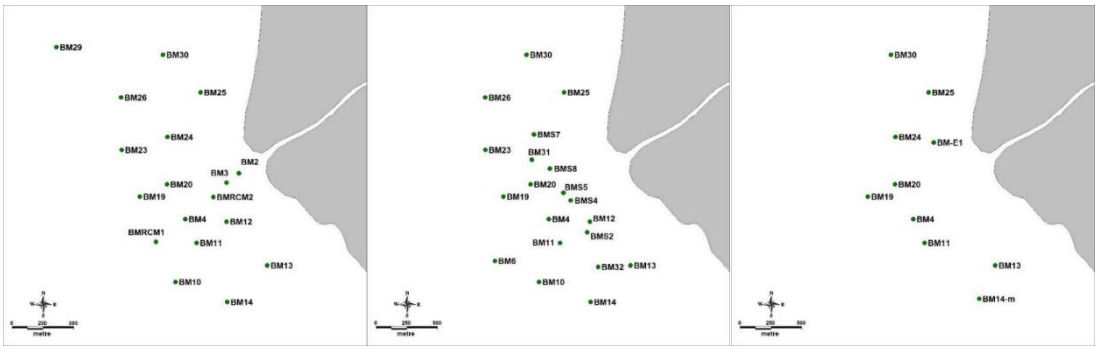

Figure 4.13. The Locations of Stations – March Measurements

4.3. River Discharge

The river discharge data have been gathered from two different sources, The TUBITAK Report and The State Hydraulic Works (DSI). In the scope of the TUBITAK project, the river current velocity data have been collected with an instrument that is named Valeport Model 106 Current Meter. The device was set to record the current data in each 10 seconds. The location of the data collection is given in Figure 4.14.

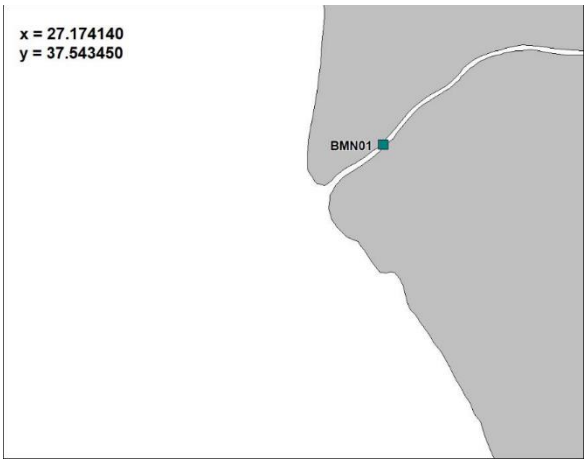

Figure 4.14. The Locations for River Discharge Station

However, this data collection was not continuous therefore there are some gaps within the duration of expeditions. It can be seen in Figure 4.15-4.17, for the first expedition day in March, the device was activated on 9:40 and stopped at 16:00. On the second day, data measurement took place between 9:15 and 18:20. For 48 hours of surveying, data availability is limited with 17 hours, 25 minutes. In May, this total surveying time is in total of 13 hours and 30 minutes. In October, there is no measurement for the river.

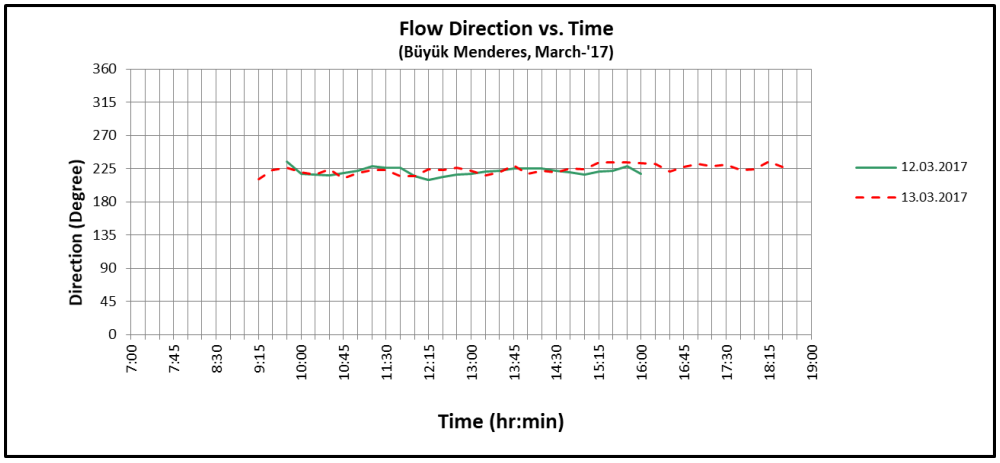

Figure 4.15. The Graph for Flow Direction vs. Time for March – '17

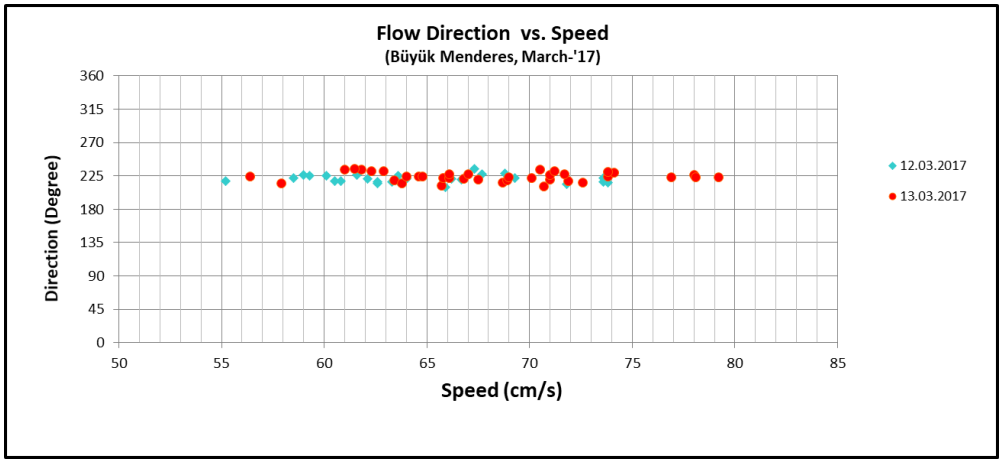

Figure 4.16. The Graph for Flow Direction vs. Speed for March – '17

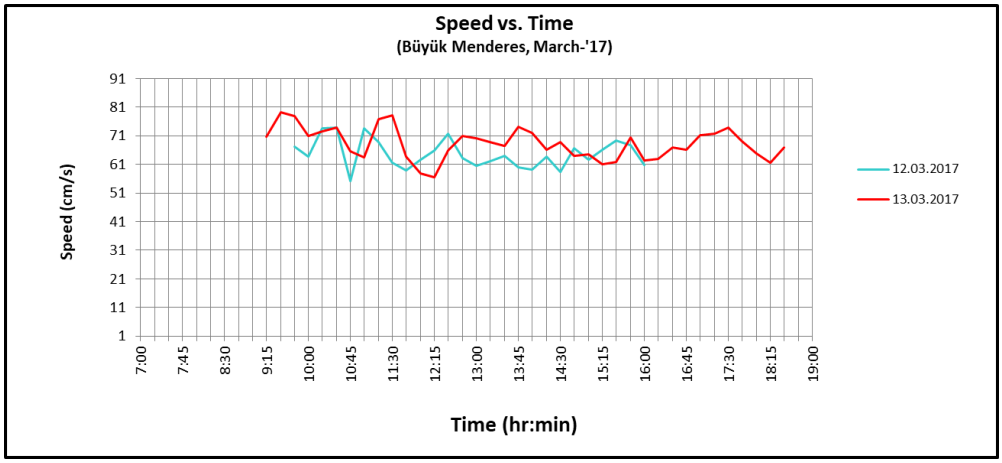

Figure 4.17. The Graph for Speed vs. Time for March – '17

To complete the measurements up to two days of data, average of the measurements is used. For the first half of the first day, the average of the measurements from the first day is used. The same value is used to complete the dataset for the same day (i.e. until 24:00 of March 12. Then until the start of the actual measurements of second day, the average of the measurements of second day is used. Similar to the first day, this same value is used to complete the data set until the end of day 2, March 13. The final dataset is shown in Figure 4.18.

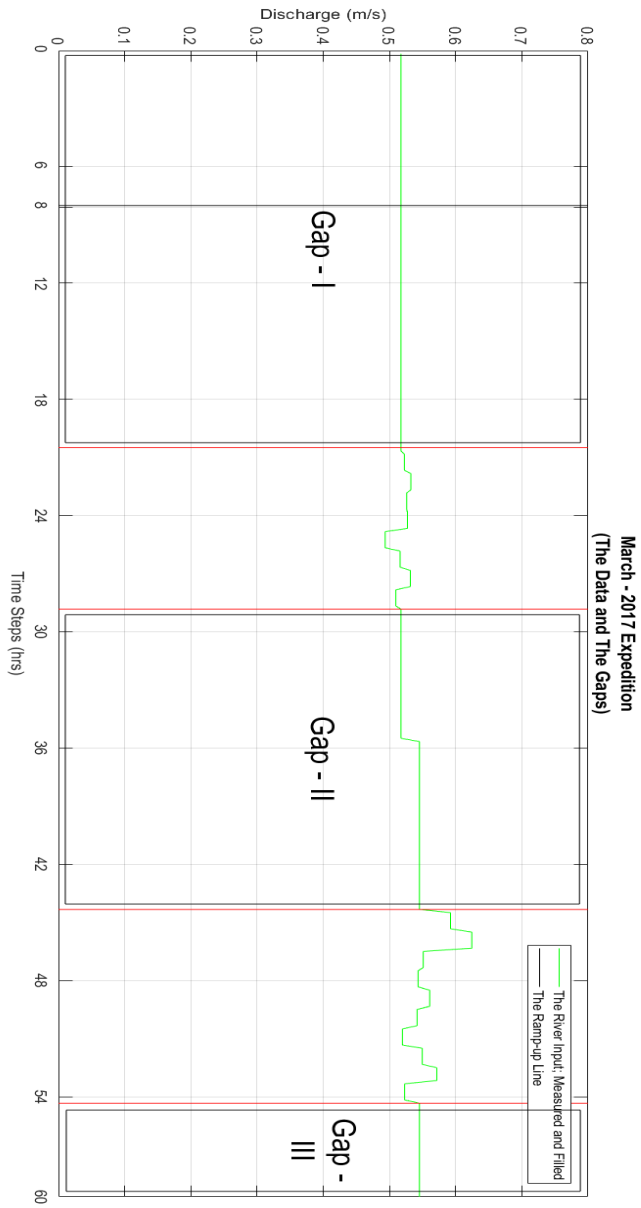

Figure 4.18. The Data and The Gaps for the Site Survey of March – ‘17

Another problem with these measurements is due to the location of the measurement. This location is prone to sea water intrusion which is reflected in the data from May 2017. Contrary to March 2017 where the direction of the flow is uniform and to the sea throughout the duration of the measurements (Figure 4.14), flow direction in May 2017 changes from the sea to the sea (Figure 4.19, 4.20 and 4.21). Especially in the first day of expedition in May, the direction of the river flow varies between the directions 200° and 45°. That shift indicates that sea water arrives, with the help of wind stress, at least until to the point where the river current values are measured. The distance to the measurement station from the river entrance is approximately 750m. This is a highly probable observation as the local farmers claim that that intrusion reaches up to 18-20 kilometers for the dry seasons.

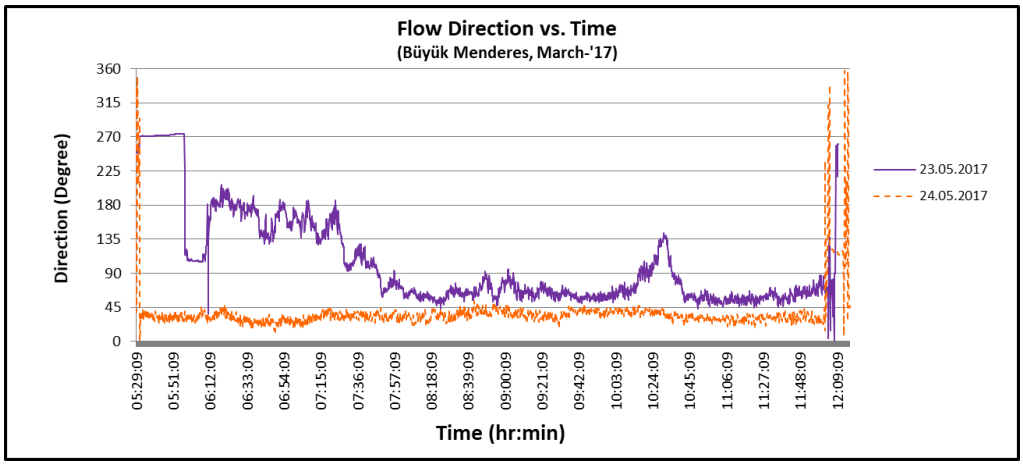

Figure 4.19. The Graph for Flow Direction vs. Time for May – '17

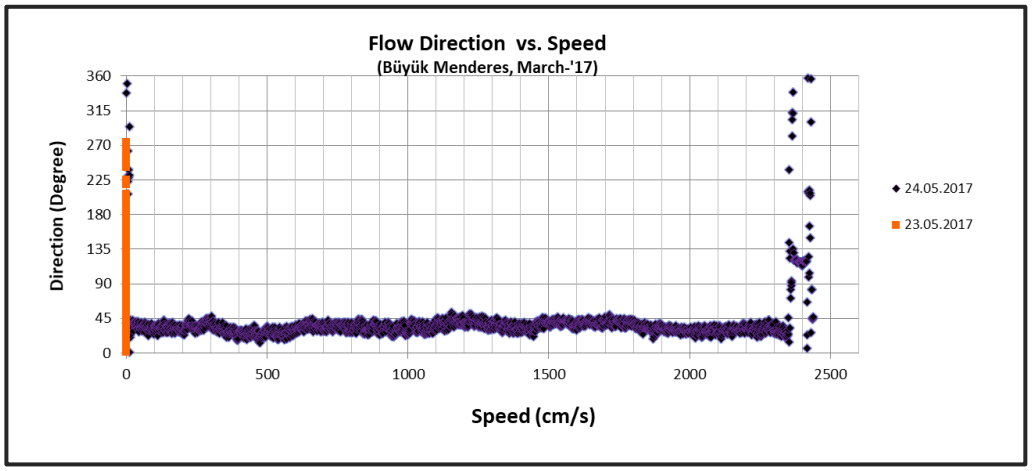

Figure 4.20. The Graph for Flow Direction vs. Speed for May – '17

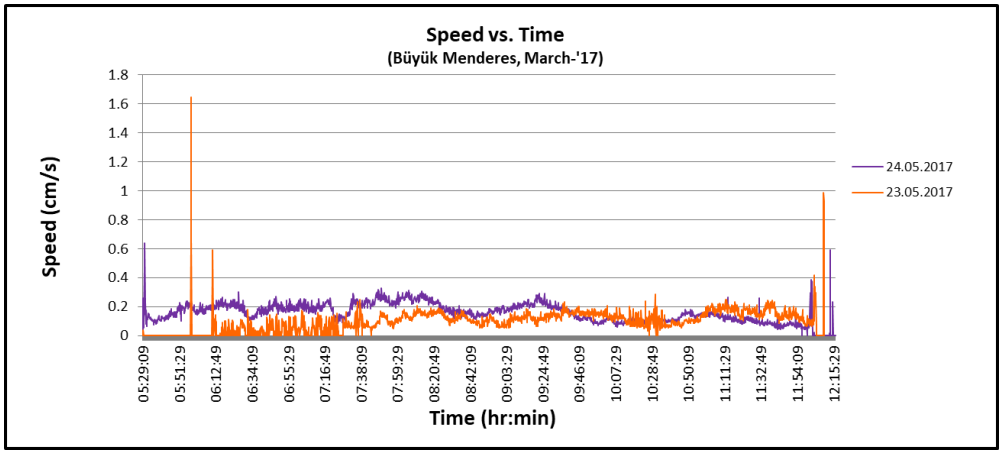

Figure 4.21. The Graph for Speed vs. Time for March – '17

However, because of this observation the river current data cannot be used as river discharge value in the model runs. Only for March case, the measured river velocity is used as model input. For the rest of the cases, another dataset is required for river discharge data. Therefore, a DSI station located close to river mouth is selected. To analyze the general trend of river discharge throughout a year, available river data measured daily from this DSI station is assessed for the years of 2011, 2012, 2013, 2014, 2015 and 2016. Although there are other DSI stations with longer datasets, these stations are far away from the river mouth and cannot represent the flow conditions at

the coastal area. Monthly average discharge values are calculated from the daily discharge data for every year. Average of monthly data is calculated to determine the wet and dry seasons for the river flow. Figure 4.22 shows the minimum, average and maximum river discharge values for each month for the period of 2011-2016. Similar graphs of every year are presented at Appendix.

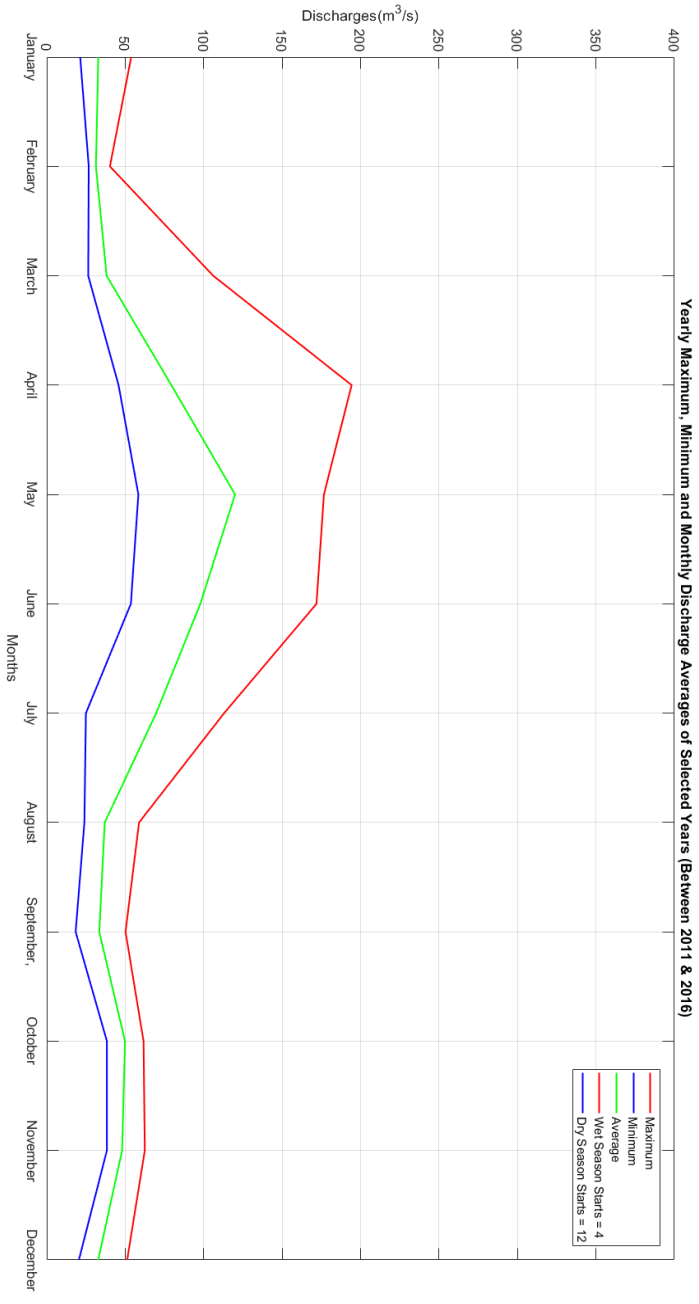

Figure 4.22. The Discharge Averages of Selected Year of Büyük Menderes

Figure 4.22 shows that from March to July, the river discharge is very high but from August to February, flow rates drop significantly. However, when other graphs are considered, it is seen that flow rates can change significantly from year to year.

4.3.1.1. Wind

In the scope of the TUBITAK Project - 115Y722, two observation stations were installed on the site. The stations collected data with a time resolution of hourly averaged. The receptor of the instrument is placed at the height of 10 meters and recorded the data continuously. The first station was established at the river mouth but after a storm it was damaged and then relocated in a fishery named “Taşucu”. The fishery is a secured place and located at the south-east corner of the domain. Both of the locations can be seen in the Figure 4.23.

Figure 4.23. The Locations of the Wind Recording Stations: The Former and the New

On the other hand, even though the station relocated, it has not recorded the data properly on the days that the main model is established. Either the direction, the magnitude or both of them were absent from the dataset. As the result, another data

source was required to model the cases. In the Final Report of TUBITAK Project, ECMWF (European Centre for Medium-Range Weather Forecasts) and CFSR data sets have been crosschecked with the measurements for a duration of six months. This report states that CFSR dataset represents the wind conditions of the region adequately. Therefore, the CFSR data was used for hourly and time-averaged inputs of the model runs and to analyze the wind climate of the region. The location of the CFSR data points can be seen from Figure 4.24. Since there exits only one coordinate at the study region, the data from this point is used as time-dependent but spatially uniform input in the models.

Figure 4.24. CFSR Data Location for Wind

4.3.1.2. Wind Climate of the Region

For cases of March, May and October 2017 expeditions, CFSR data is not processed at all. But we wanted to analyze the representativeness of the wind conditions during these expeditions with respect to the wind climate of the region. Therefore, a wind climate study including long term and extreme value statistics is performed using CFSR data between 1979-2018.

The general characteristics of wind climate is shown using annual, seasonal and monthly wind roses. These wind roses depict the frequency, direction and magnitude of winds for the region for the specified period. Figure 4.25 shows the annual wind rose.

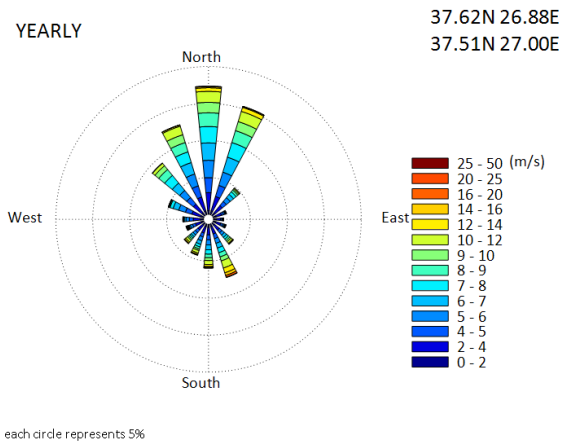

Figure 4.25. Annual Wind Rose using 40 Year Long Data

The main direction of the wind blowing throughout all the observation years is from the northern directions, shown as Figure 4.25. More than 17% of the winds come from the North. Other main wind directions are neighbors of the dominant direction; NNE and WNE. These two dominant wind directions constitute about 15 % and 8 % of the winds for all year distribution, consequently. The wind speeds up to 10m/s are commonly observed from northern and southern directions.

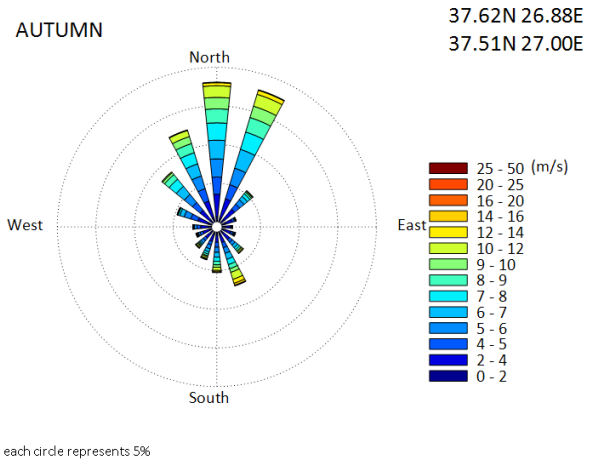

Figure 4.26. Wind Rose for the Fall Season

For the fall season, the main direction of the wind blowing throughout all the observation years is from the north and north of northeast directions (Figure 4.26). More than 17% of the winds come from those two directions. The NNW is the tertiary main wind has a frequency about 13 % of the winds blowing for all year distribution. The wind speeds up to 10m/s are commonly observed.

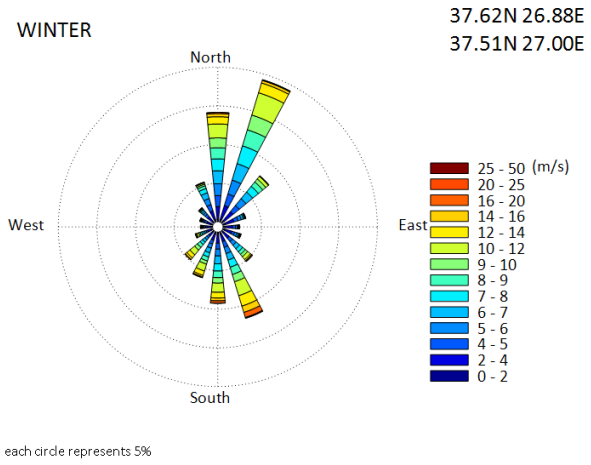

Figure 4.27. Wind Rose for the Winter Season

In the winter season, the main direction is the NNE, with a frequency approximately 20% of the winds come from that direction (Figure 4.27). Secondary and tertiary directions are the N and SSE in return. The N direction has a higher frequency, on the other hand, the SSE direction is important with respect to its magnitude. These two dominant wind directions constitute round about 15 % and 12 % of the winds for all year distribution. The magnitude of wind speeds increases to 20 m/s which shows that storms can be frequently observed in this region.

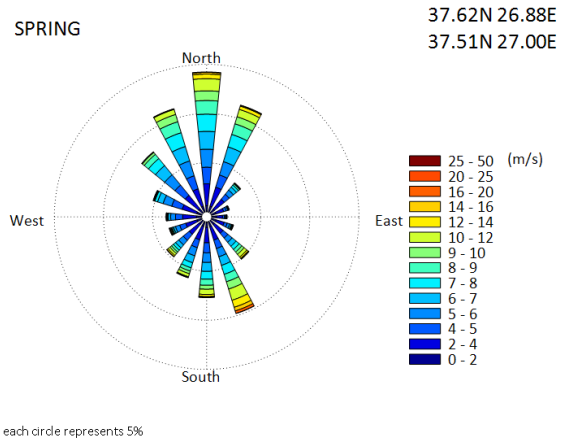

Figure 4.28. Wind Rose for the Spring Season

The main direction of the wind blowing during spring is from the northern directions (Figure 4.28). Around 18% of the winds come from the north direction. Other main wind directions are neighbors of the dominant direction; NNE and WNE. The first of these two dominant wind directions constitute about 12 and 11 % of the winds for all year distribution, consequently. Furthermore, there exists a fourth strong wind, blowing from the SSE direction which has a strong magnitude and a frequency about 10% of all seasonal data.

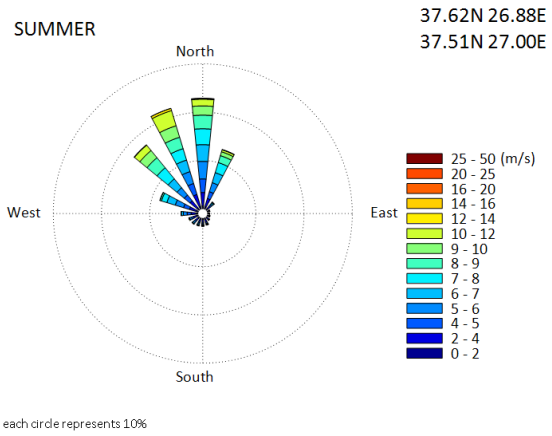

Figure 4.29. Wind Rose for the Summer Season

In the summer season, relatively low magnitude winds are observed, that, again, mainly blowing from the northern directions (Figure 4.29). Around than 20% of the winds come from the N, NNW, and NW directions which are sorted with respect to their occurrence frequency. The monthly wind roses are given in the section Appendix.

Long Term Statistics of Wind Data

The long term wind statistics has been carried out for each direction by plotting the cumulative number of occurrences of wind velocity ($U_{ave,\ 10)}$ classes, divided equally 0.4 m/s in this case for 16 directions for 40 years of data, on to a semi-log graphical paper ($U_{ave,\ 10}$ on normal, and $Q(>U_{ave,\ 10})$ on logarithmic scales). The cumulative exceedance probability of $U_{ave,\ 10}$ is:

$$Q(>U_{ave,10})=\exp[(U_{ave,10}-B)/A] \tag{4.1}$$

Where A and B are the distribution parameters, slope and intercept of the fitted curve respectively. The cumulative exceedance probabilities of hourly average wind velocity Q (>$U_{ave,\ 10}$), results are tabulated in the Table 4.3.

Table 4.3. The Wind Analysis for Cardinal Directions

Hours	Cardinal Directions															
	N	NNE	NE	ENE	E	ESE	SE	SSE	S	SSW	SW	WSW	W	WNW	NW	NNW
1	17.45	17.07	13.32	10.38	9.01	10.12	16.2	21.22	18.69	17.03	17.97	15.2	12.05	13.03	12.88	15.61
5	14.54	14.2	10.52	7.58	6.5	7.63	12.68	17.23	14.99	13.44	13.9	11.36	9.07	10.16	10.65	12.85
10	13.29	12.96	9.31	6.38	5.41	6.56	11.16	15.51	13.4	11.9	12.14	9.7	7.79	8.92	9.68	11.66
20	12.03	11.73	8.11	5.17	4.33	5.48	9.64	13.79	11.8	10.35	10.39	8.05	6.51	7.69	8.72	10.48
50	10.38	10.09	6.51	3.58	2.9	4.06	7.64	11.51	9.7	8.31	8.07	5.86	4.81	6.05	7.45	8.9
100	9.12	8.85	5.31	2.38	1.81	2.99	6.12	9.79	8.1	6.77	6.32	4.21	3.53	4.81	6.48	7.71

As it can be seen from the Table 4.3 above, northern and southern directions are the dominant wind directions for the wind conditions (10 hours per year). For the yearly average wind speeds, the analysis results are in harmony with the wind roses.

Extreme Wind Statistics

In the extreme wind statistics, the best fitting distributions among Gumbel and Weibull are applied using annual maxima method. The non-directional extreme wind statistics used all directional sectors' maximas together as shown in Table 4.4. Figure 4.30 shows the result of extreme wind statistics and indicate that wind speed of 25m/s has a return period of 50 years. This event was already observed during the 40 year of dataset (2016 data) therefore it is selected as a case study event to model the circulation of bay under such extreme wind conditions.

Table 4.4. *Non-Directional Long-Term Analysis of CFSR Data*

##### Non-Directional #####			
Peak Over Treshold is 0.00 m/s			
Best Distribution Is Old Gumbel with 37.000000 points!			
Second Best Distribution Is IS Weibull k=2.0 with 36.000000 points!			
Third Best Distribution Is New Gumbel with 35.000000 points!			
###############			
1979	18.98	1	SSE
1980	21.31	1	SSE
1981	21.05	1	SSE
1982	20.28	1	SSE
1983	17.97	1	N
1984	21.88	1	SSE
1985	20.41	1	SSE
1986	19.3	1	SSE
1987	20.45	1	SSE
1988	23.27	1	SSE
1989	18.57	1	NNE
1990	19.3	1	NNW
1991	21.06	1	SSE
1992	17.33	1	N
1993	20.78	1	S
1994	18.8	1	SSE
1995	19.81	1	SSE
1996	19.92	1	SSE
1997	18.08	1	SSE
1998	17.24	1	S
1999	19	1	SSE
2000	18.32	1	SSW
2001	21.47	1	SSW
2002	16.85	1	SSW
2003	20.11	1	NNW
2004	23.39	1	NNW
2005	22.04	1	SSE
2006	19.32	1	SSE
2007	19.94	1	SW
2008	20.94	1	NNE
2009	21.31	1	SSE
2010	21.51	1	SSE
2011	22.3	1	SSE
2012	23.19	1	S
2013	21.64	1	SSE
2014	19.24	1	SSE
2015	21.58	1	SSE
2016	25.95	1	SSE
2017	22.16	1	S
2018	19.91	1	NW

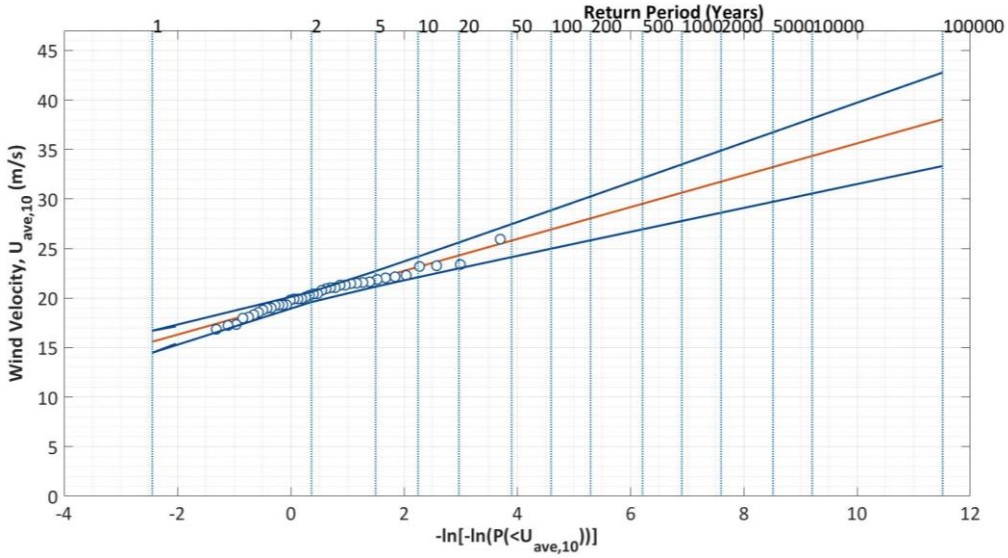

Figure 4.30. Return Period Analysis for Wind Data

4.3.1.3. Tide

Tide data was obtained from the Intergovernmental Oceanographic Commission of UNESCO (IOC-UNESCO) database. Since, there exists no station at Didim, the closest stations that are located in Bodrum and Fethiye, have taken into account. The proximity can be seen from Figure 4.31.

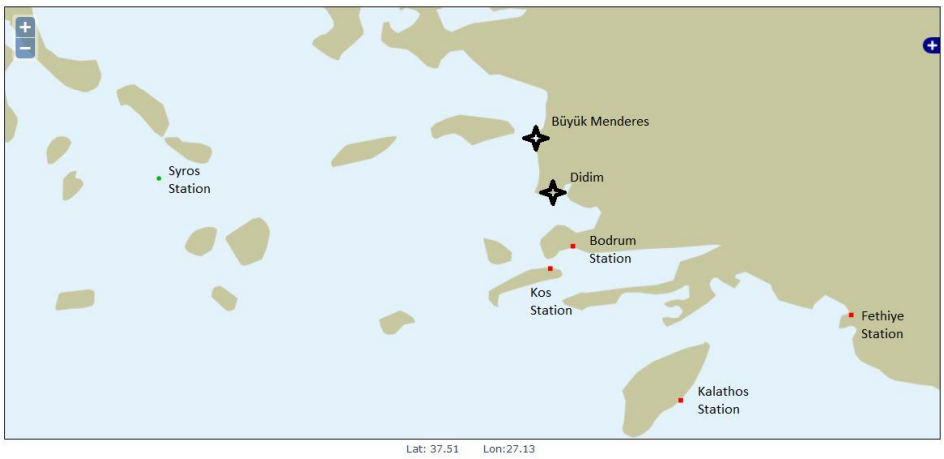

Figure 4.31. The Location and Proximity of Tidal Observation Stations: Bodrum and Fethiye

These stations are connected to General Command of Mapping and Kandilli Observatory and Earthquake Research Institute. The data from Bodrum station shared on the web ends on 26.11.2017 - 04:46 but this is not a problem since all the cases modeled in this study took before this date. This data is sea level data not purely tide data. However, for most of the case studies the dominant component of the signal is the tidal constituents therefore we applied the actual sea level data at the open boundary nodes to represent the tidal forcing that could be observed.

The modeling of the days of expeditions and the additional cases were conducted with the data from Bodrum and Fethiye stations, consequently as presented below. Data for March and May expedition days are given in Figure 4.32. The sea level observation belongs to 11&12&13 March – 2017, it varies between 0.10 cm and 0.10 cm. The sea level observation belongs to 22&23&24 May – 2017, it varies between 0.08 cm and -0.065 cm.

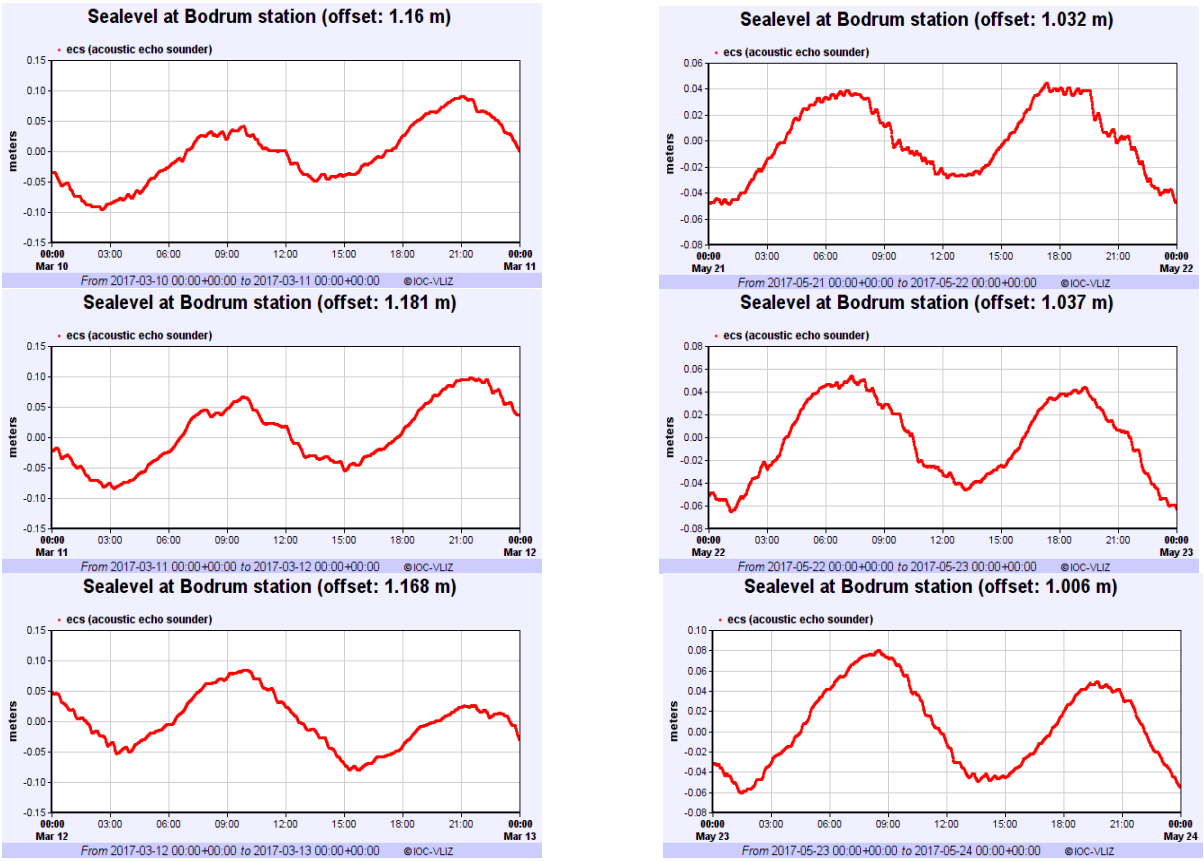

Figure 4.32. Relative Sea Level – March ’17 (left) and May ’17 (right)

The sea level observation belongs to 17&18&19 October – 2017 is given in Figure 4.33, it varies between 0.08 cm and -0.08 cm.

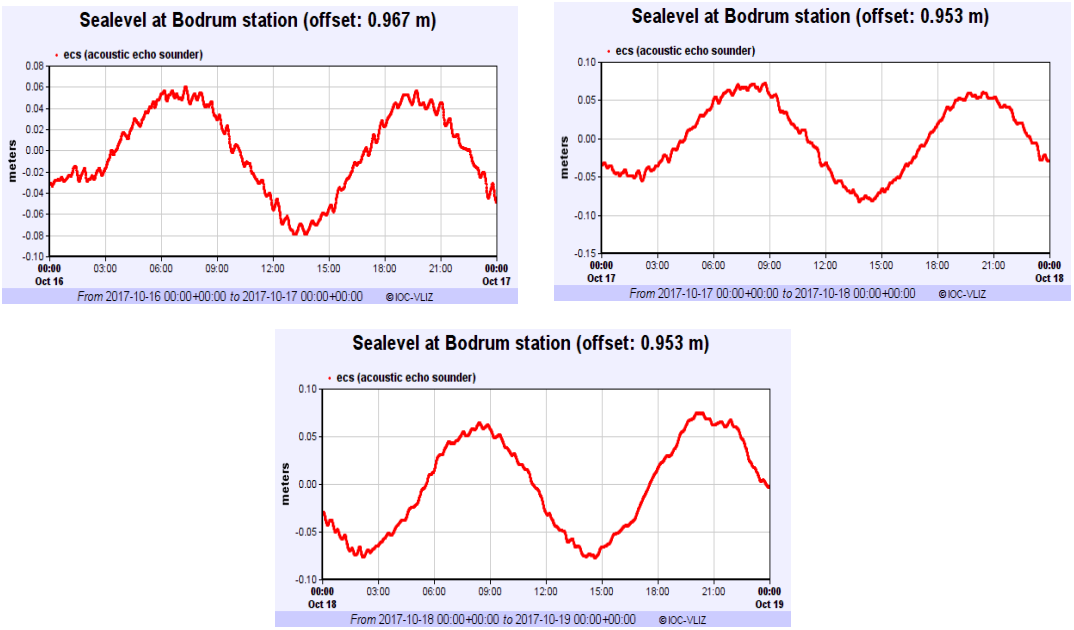

Figure 4.33. Relative Sea Level – October '17

As mentioned in previous sections, an additional case (09 - 20 January – 2016) is modeled to analyze the circulation of the region when extreme conditions are forced. This case is based on the historical data and covers maximum river discharge and maximum wind speed. The open boundary forcing data of this cases are also taken from mareograph station of Fethiye. The sea level observation varies between 0.32 cm and -0.20 cm (Figure 4.34).

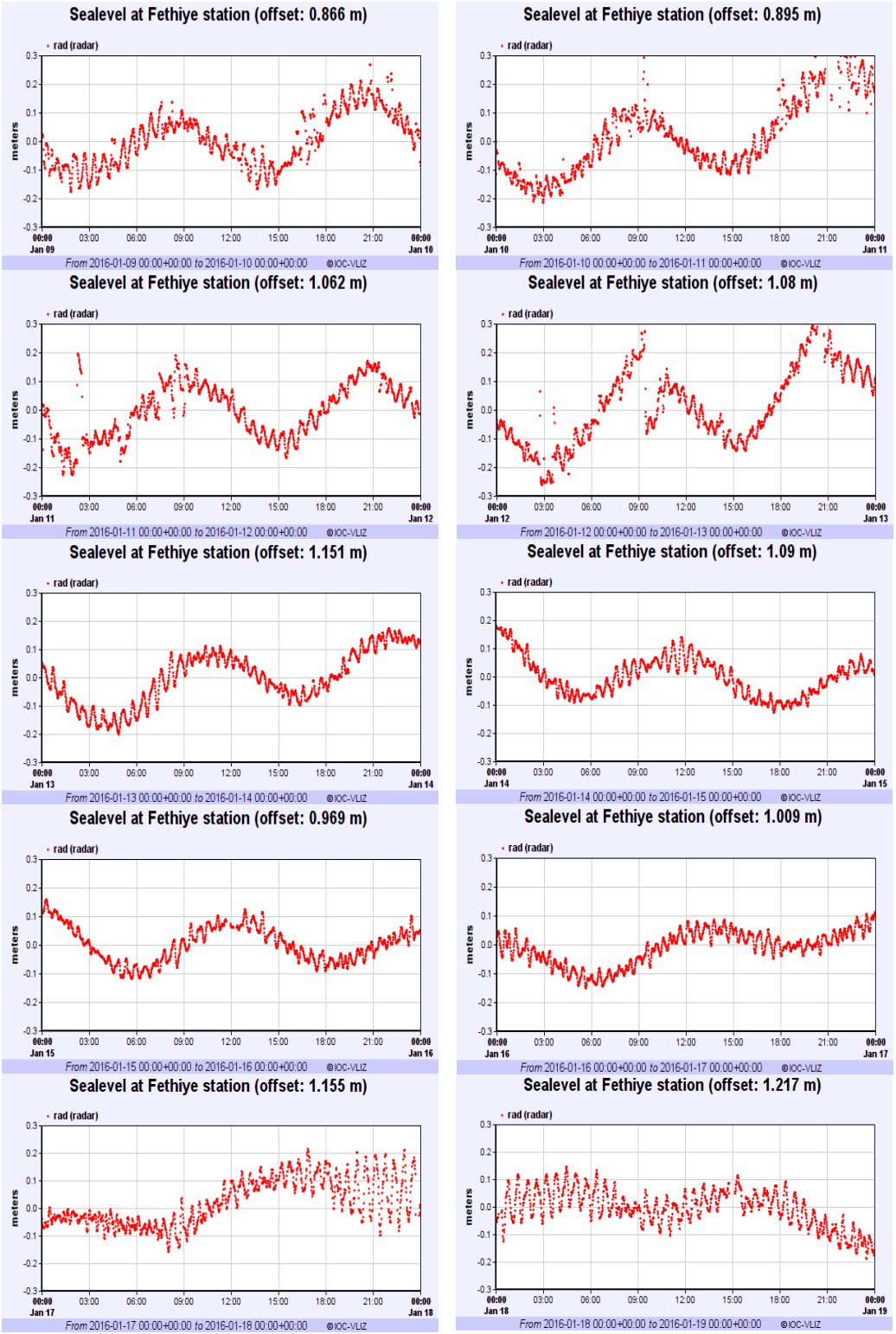

Figure 4.34. Relative Sea Level – 09, 10, 11, 12, 13, 14, 15, 16 January ‘16

CHAPTER 5

THE RESULTS AND THE DISCUSSIONS OF THE MODEL

In this section the model setup and results of six events modeled is presented in detail. Three of these events are the expeditions done by Dr. Dogan Kısacık and his team for the TUBITAK Project – 115Y722. Three additional dates were modeled based on historical data showing the circulation at the river mouth and adjacent coasts under extreme conditions such as maximum and minimum river discharge conditions and wind forcings. These results are discussed considering the assumptions and the data quality.

5.1. FVCOM Model Setup

5.1.1. Computational Domain and The Grid Size

The computational domain is selected to cover the river mouth and adjacent areas such that the study area was bounded by natural physical features (headlands on northern and southern boundaries). On the west, the domain is again naturally limited with island formation. The effect of waves on the circulation is not included in this study since expeditions took place when the sea was calm (very small wave heights, Final Report) and there were no wave measurements for validation of the model. Once the wave component can be neglected, the effect of the island also assumed to be negligible and therefore the computational domain is selected as shown in Figure 5.1.

Figure 5.1. The Computational Domain and the Grid

Figure 5.2 also shows the grid mesh used in the model. The Surface-water Modeling System (SMS) was used to create the unstructured mesh that FVCOM uses. Shoreline data was extracted from EmodNET dataset as explained in the bathymetry section. As also discussed in the bathymetry section, the shoreline map needed to be simplified to be a reasonable approximation of the actual shoreline in order for the grid to be created properly. Advantage of unstructured mesh was utilized by generating higher resolution mesh with 50 m at the shoreline and river mouth while 250m grid size was selected for the open boundary. Special attendance was given to smoothly transition the mesh from coarser to higher resolution. Finally, the mesh has 17170 nodes and 33847 elements.

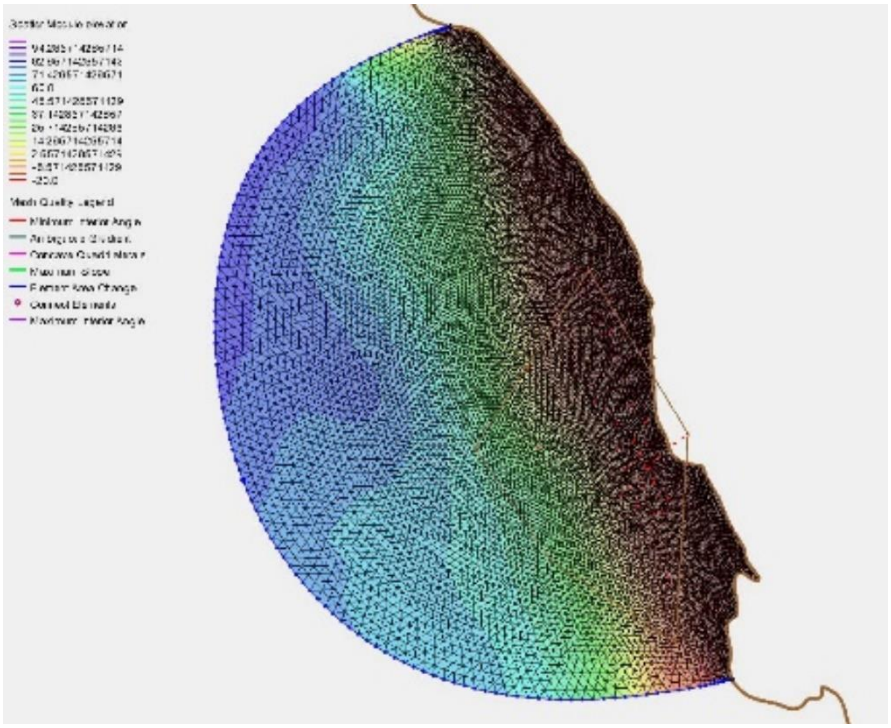

Figure 5.2. The Fine Mesh of the Computational Domain

Although mesh quality check was performed using the quality checker of SMS software and defining the limits recommended by FVCOM, there was problems with stability due to the mesh and computation domain. For initial model runs, it was observed that at some of the boundary nodes and elements, the model started to show instability problems due to very high velocity vector components. Although different mesh sizes and computation time steps were tried, the problem persisted. Finally, the reason for this instability is found to be the handling of FVCOM when a cell is located at the solid boundary. This problem is introduced to the mesh as a result of selecting headlands as natural limits to the study area and the irregular coastline due to delta formation. Although FVCOM tries to handle this problem with ghost cell treatment and it was activated in this study, still, the instability could not be prevented for longer run times. Therefore, sponge nodes were assigned to some of the boundary to artificially reduce the speeds and forces that are calculated on these points. Since the

defined sponge nodes were located at the farthest boundaries and the simulation times were kept fairly limited (mostly 2 days), the effect of reduced values and the progression of the instability along the domain did not reach the study area (river mouth).

5.1.2. The Computational Time Step and Ramp-up Time

For computational efficiency, FVCOM employs a mode-split model with an external 2D mode and an internal 3D mode as discussed in Methodology section. The modes can operate at different time steps with the relationship between the external time step and the internal time step represented by I_{split}. The I_{split} number is chosen as 10 as suggested in literature. As the result; based on the CFL calculation, computational time steps are defined as 1s and 10 s, for the external and internal time steps, sequentially.

The ramp-up time is the duration that is required for a system or a model which start from `zero condition` to the actual initial conditions of the problem. As we are modeling part of a continuous system, it is very important to first have the actual initial conditions of the system to be reflected in the model before any additional forcing is applied. For the ramp-up duration, several studies were inspected in the literature, and it is seen that this initial phase of the analysis varies from 2.5% to 30% of the simulation duration, depending on several factors such as the total simulation time, modules to be included, parameters to be used and etc. For the similar cases used in this study, duration, size and parameters used, there exists a ratio between 15%-30% of the simulation time. To decide the ramp-up duration, four model runs with the inputs of March 2017 case, have been made for a total simulation time of 2 and a half days. The model has been tested for ramp up times of 4, 6, 8, and 12 hours. The results of the model trials can be seen at the figures from 5.3, to 5.6. As it can be seen 6 and 8 hours of ramp-up times fit better that 4 and 12 hours. Considering not only the cell in front of the discharge cell, but all the neighboring cells; 8 hours of ramp-up time is

selected to be the most acceptable time window that the system needs to reach the actual initial conditions of the field.

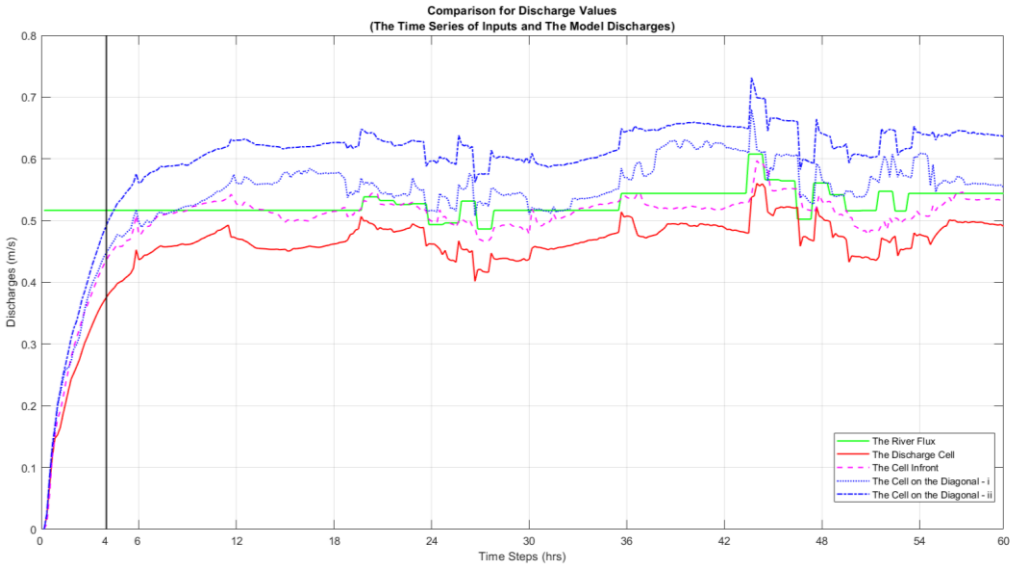

Figure 5.3. Ramp-up Time of 4 Hours

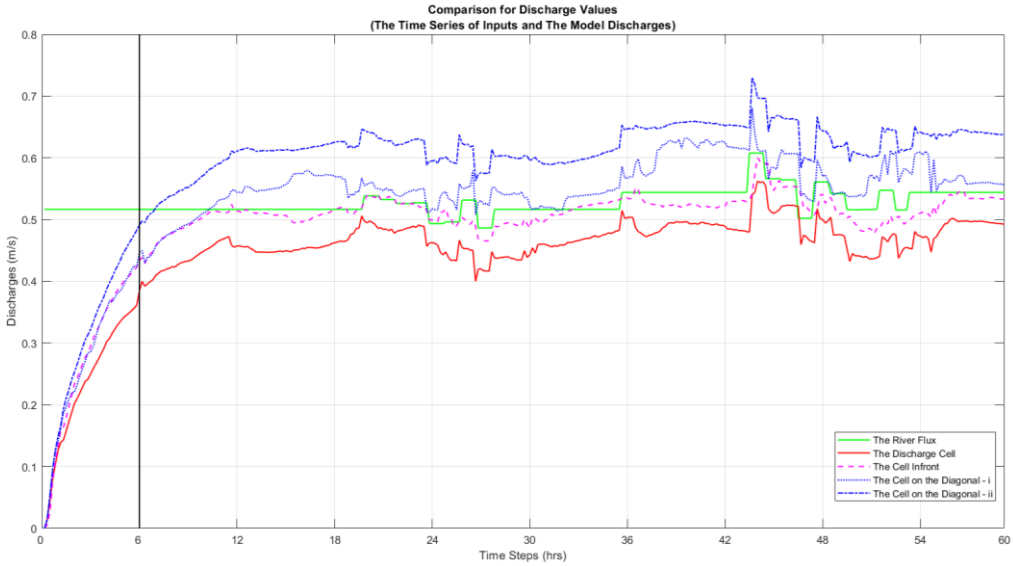

Figure 5.4. Ramp-up Time of 6 Hours

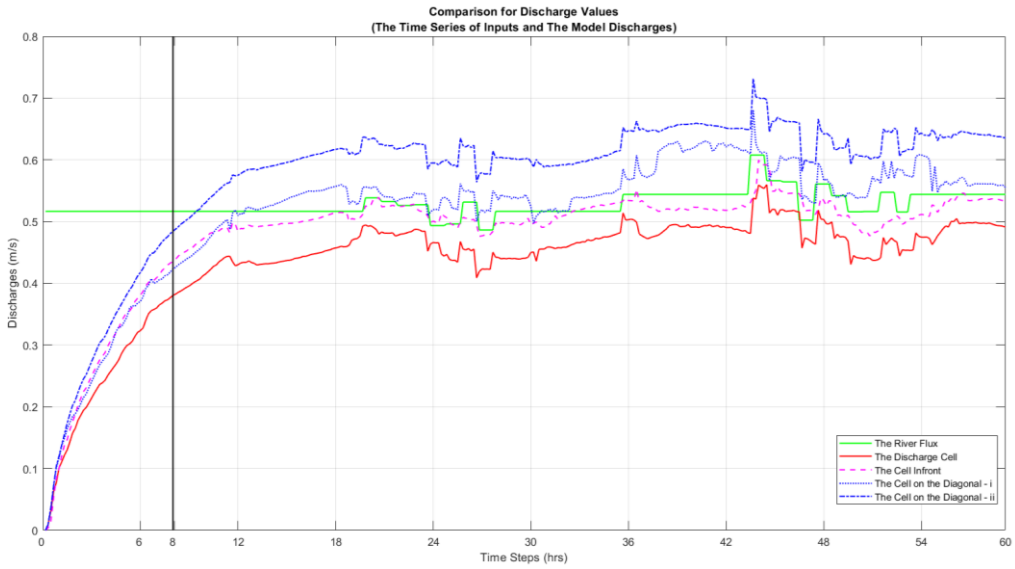

Figure 5.5. Ramp-up Time of 8 Hours

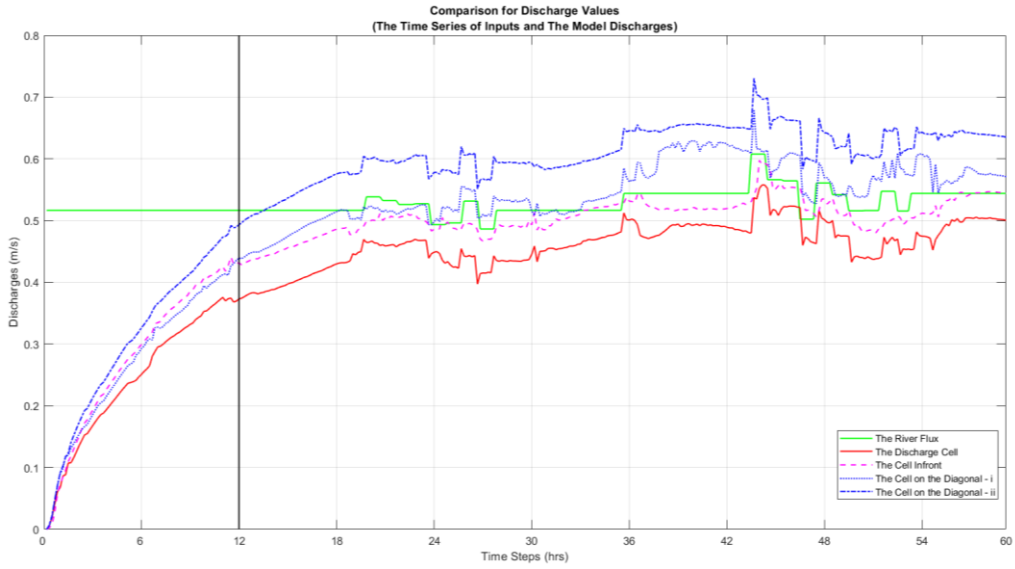

Figure 5.6. Ramp-up Time of 12 Hours

5.1.3. Other Setup Conditions

The following modules of FVCOM was activated to model the circulation of the region:

- WET/DRY to show possible flooding along the coastline under extreme conditions
- TURBULENCE MODEL: MELLOR-YAMADA 2.5 with default values
- RIVER DISTRIBUTION to introduce river forcing
- OPEN BOUNDARY FORCING to introduce tidal forcing
- WIND FORCING to introduce time dependent spatially uniform wind forcing

The analysis conducted on two different computers with processors:

- Intel® Core™ i7-7700HQ (2.8 GHz base frequency, 6 MB cache, 4 cores)
- Intel® Core™ i5-3230M (2.4 GHz base frequency, 3 MB cache , 2 cores)

Depending on the computers and duration of simulation time and forcings, the simulations took 4-40 hours.

5.2. Validation Studies – Expedition Cases of March, May and October 2017

It is important to calibrate numerical models with measurements and observations so that the models can represent the conditions of a region as accurate as possible. Although there are measurement data for the study area, the dataset is not complete and an effective calibration of the model would not be possible. Therefore, the study focused on the capability of FVCOM with its default setting on representing the conditions of the study area based on the available datasets. Several station points are assigned in the model including the stations used in the expeditions to compare current, salinity and temperature results with the observation data.

5.2.1. March ‘17

The first case modeled is based on the expedition done on the 12 - 13 March 2017. The river data is taken from TUBITAK project data. Wind data is from CFSv2 dataset and the open boundary forcing is done by sea level data from Bodrum mareograph station. Constant water temperature and salinity is used throughout the domain as 15.56°C and 37.44 ‰ based on the field measurements. The computational time of 2.5 days took 4-7 hours depending on the processor and forcing types.

The results have been subjected to a smoothing operation via MATLAB for ease of use in statistical calculations of error measures. In order to analyze the contribution of each forcing type on the overall circulation system, several runs were performed such as tide only forcing, wind only forcing, river only forcing. Finally, the actual forcing combination (tide, river and wind together) is modeled. All the runs include the Coriolis effect. The original model output is provided for the case with all forcing types. The rest of the results are presented after the smoothing process.

5.2.1.1. Tide-Only Case

In this case of March ’17, as a forcing parameter, only tide was implemented the model. The change in the sea water elevation used as input is provided in Section 4.3.1.3 and in Figure 4.27. The arbitrary check points and tide input can be seen on the figure 5.7, below. Figure 5.8 shows that the water elevation input forced at the open boundaries is represented accurately across the domain.

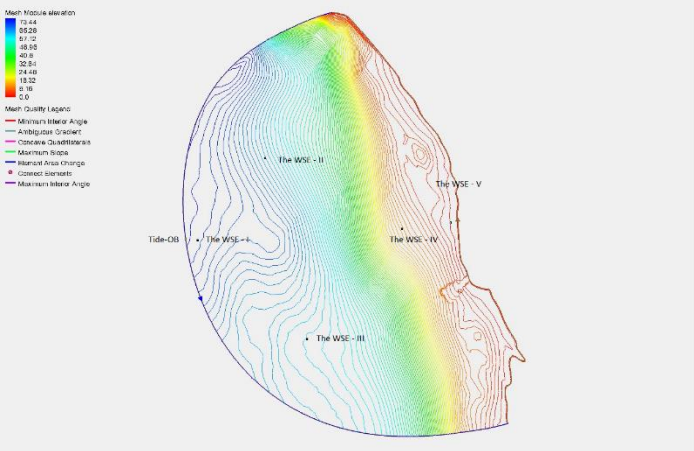

Figure 5.7. The OB and the Tide Check Points

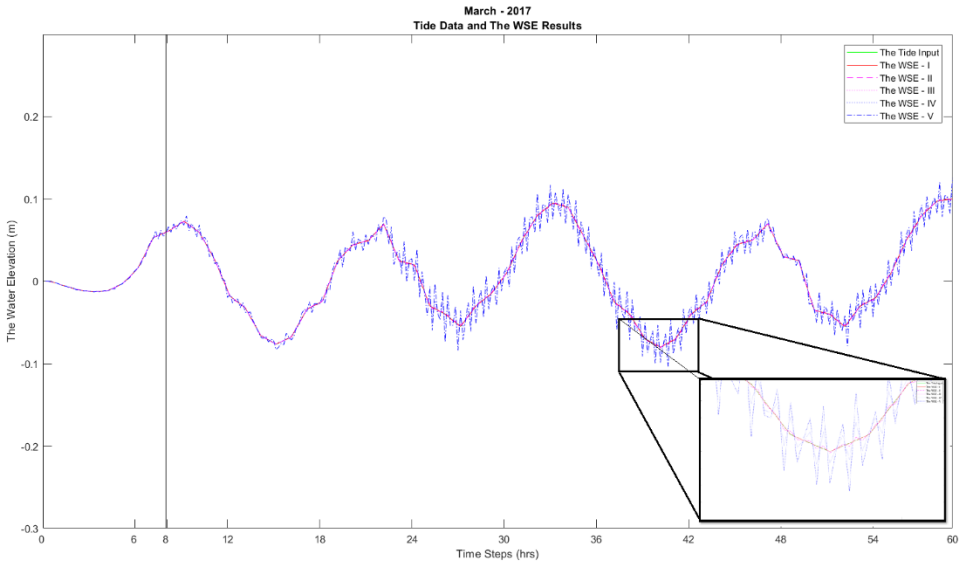

Figure 5.8. The Analysis Result for the OB and the Tide Check Points

Figures 5.9 and 5.10 shows the current speed modeled with respect to the observations at two stations. The tidal forcing produces currents of 0.015 m/s. whereas the observed currents are much higher. Therefore, the contribution of tidal forcing for this case can be assumed as minimum. From the figures 5.9 and 5.10 it is hard to state a clear correlation between the measurements and the analysis.

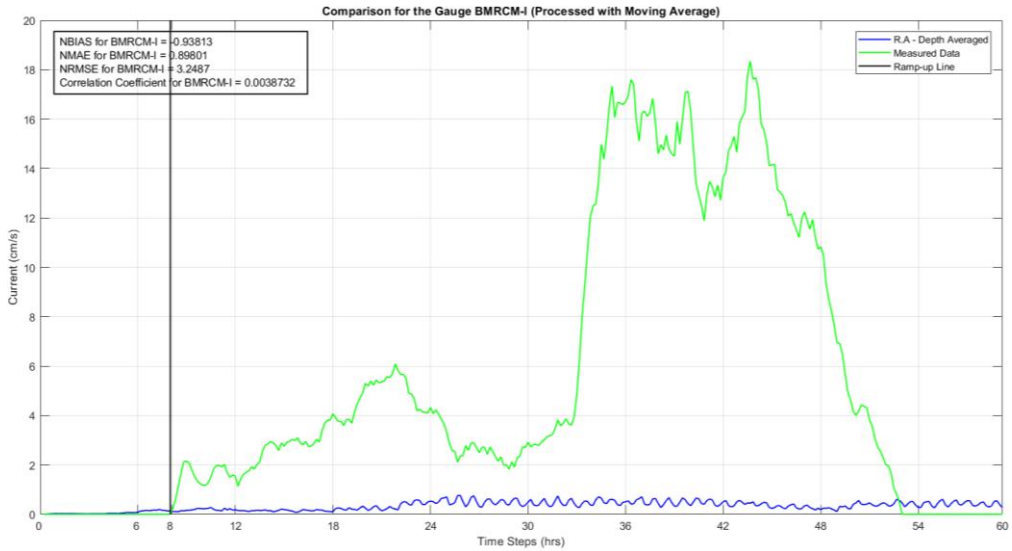

Figure 5.9. The Current Analysis for the Station Point – BMRCM-I (Smoothed)

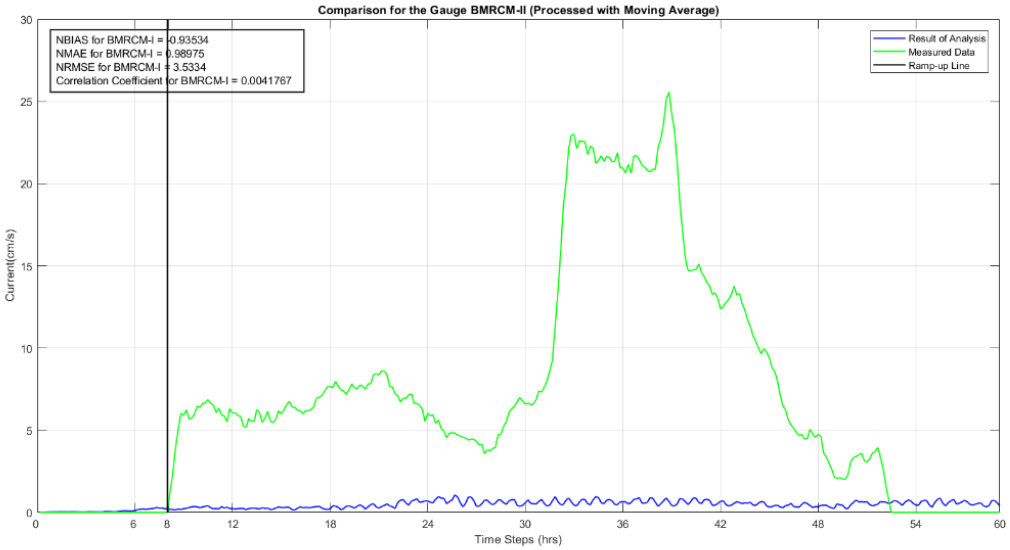

Figure 5.10. The Current Analysis for the Station Point – BMRCM-II (Smoothed)

Consequently, the general circulation pattern, on the hours 32nd, 35th, 38th and 41st, can be seen between the Figures 5.11-5.12. In these figures, it can be understood that; the patterns of 32nd and 38th hours belong to an hour that water elevation gets closer to

mean sea level, on the other hand, the pattern of 35th hour belongs a high tide and 41st, a low tide. As expected, on the hour 35th water moves out of the domain, on the other hand, on the hour 41st, it moves through inside the domain. This result indicates that FVCOM and the model setup can model the tidal forcing and the corresponding currents in the system correctly.

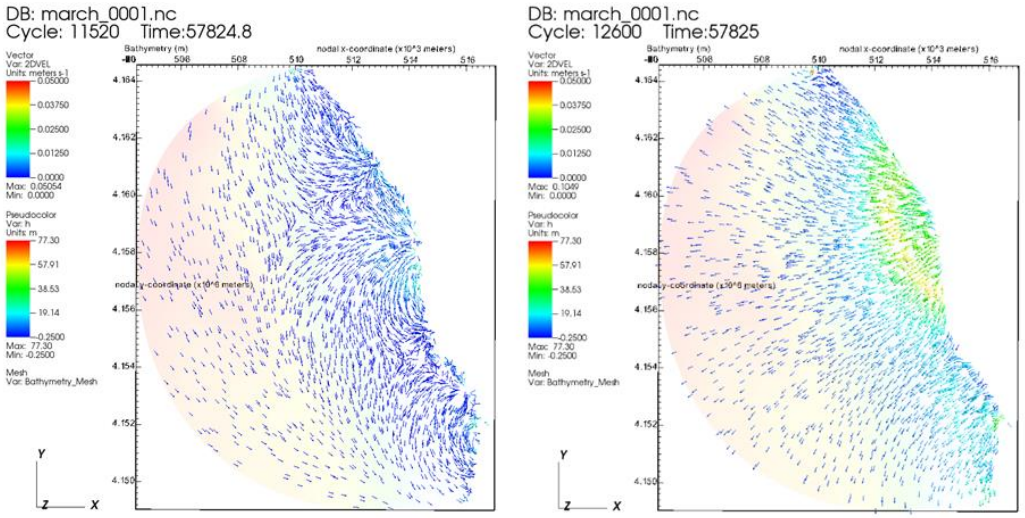

Figure 5.11. Circulation Pattern – March ’17 – Tide Only Case - Hour: 32 and Hour:35

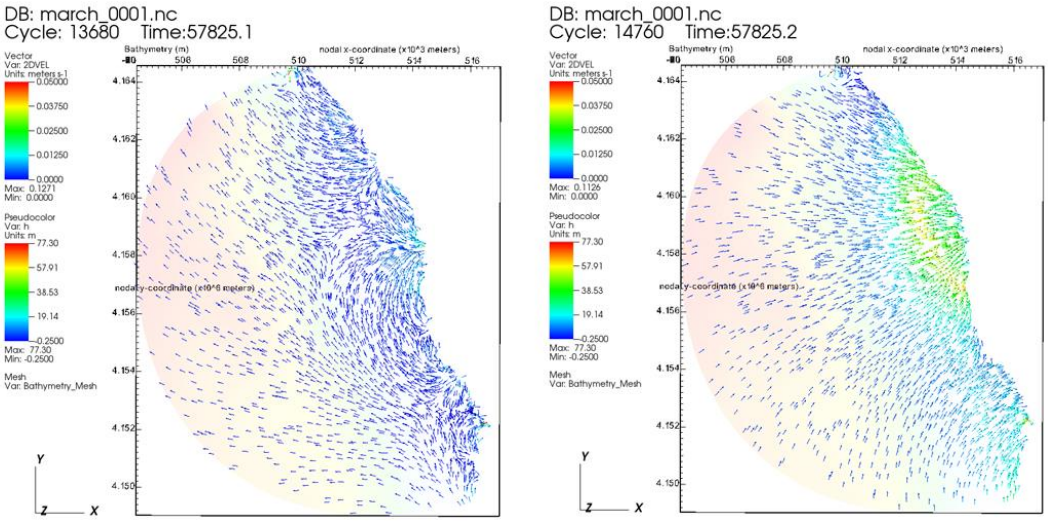

Figure 5.12. Circulation Pattern – March ’17 – Tide Only Case - Hour: 38 and Hour:41

5.2.1.2. River-Only Case

In this case of March ’17, as a forcing parameter, only river was implemented the model. The arbitrary check points and river input can be seen on the figure 5.13 and 5.14, below. Figure 5.14 shows that the river discharge input from the solid boundary where river channel is defined is represented accurately across the domain.

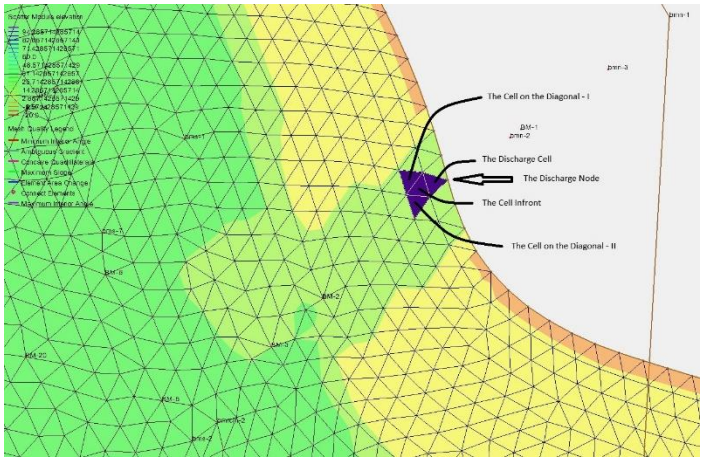

Figure 5.13. The Discharge Node and the Control Cells

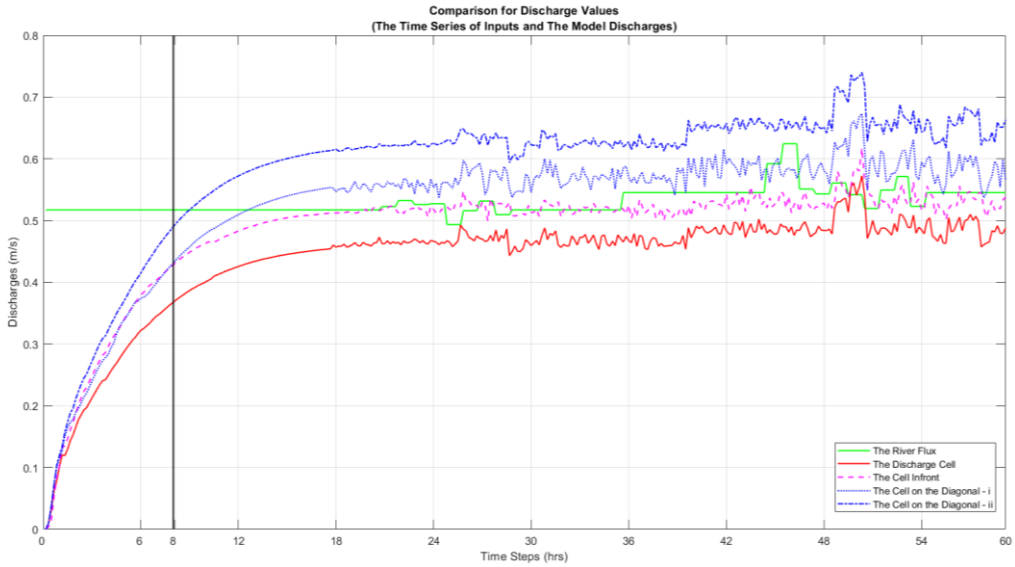

Figure 5.14. The Analysis Result for the Discharge Node and the Control Cells

Figures 5.15 and 5.16 shows the current speed modeled with respect to the observations at two stations at 4 sigma levels from the water surface to the top of final layer. This final layer also corresponds to the depth of the measurement on the field. Therefore, this layer is used for comparison of model results to observation data. The rest of the layers is presented to show the behavior of the model along the vertical domain. Additionally, vertically averaged results are provided to show the performance of the model if used in 2D mode.

For the first station point, the river forcing produces currents of 0.05 m/s on average whereas the observed currents are much higher for the second day. The first day is represented satisfactorily by Layer 4 (the final layer) whereas the rapid increase in the current velocity in 2nd day could not be modeled only with river forcing. The correlation coefficient for this case is calculated as 0.31 which shows that there is some influence of the river as expected but the contribution is limited for this case.

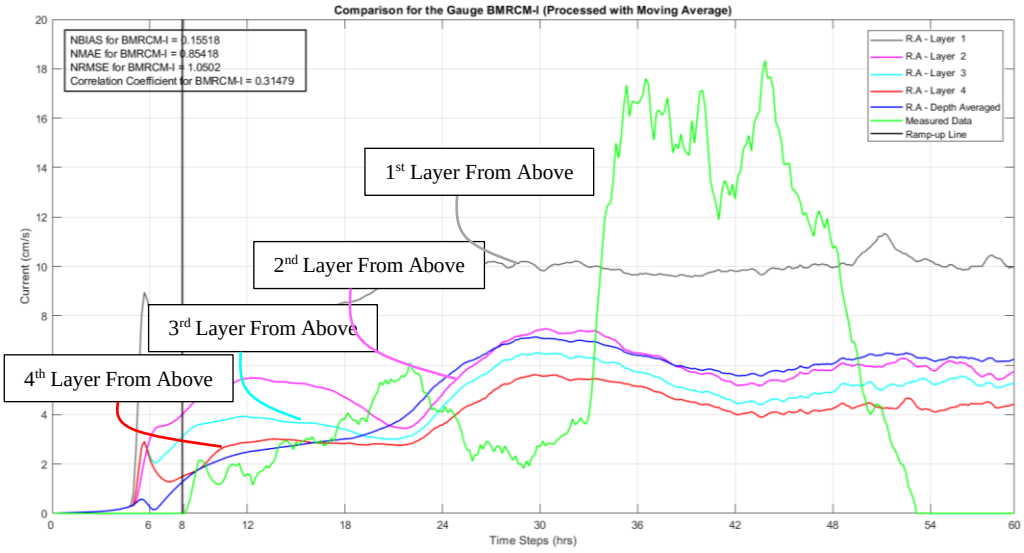

Figure 5.15. The Current Analysis for the Station Point – BMRCM-I (Smoothed)
(1st Layer = 0.89m, 2nd Layer = 2.68m, 3rd Layer = 4.47m, 4th Layer = 6.26m)

For the second station point, currents are higher. The first day is represented fairly well by the depth average approach rather than Layer 4 (the final layer) whereas the

rapid increase in the current velocity in 2nd day could not be modeled only with river forcing. The correlation coefficient for this case is calculated as 0.20702 which shows that there is some influence of the river as expected but the contribution is limited for this case.

Other than that, the meaning of colors are show on the Figure 5.15 in terms of layer numbers. Each layer stands for a different water depth due to the fact that FVCOM uses "terrain following coordinates", in this study, also, this coordinate system has been used, which is named also, Sigma Layers.

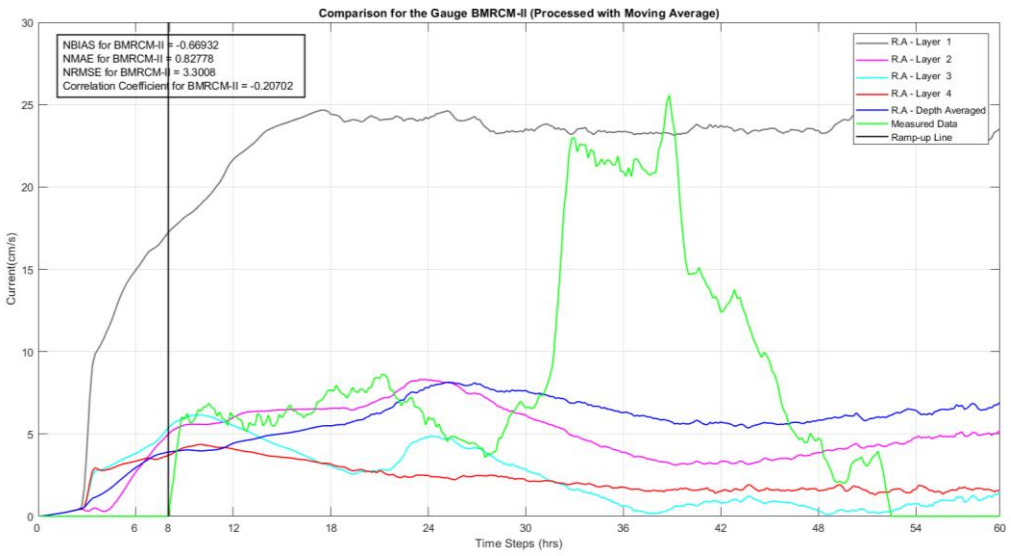

Figure 5.16. The Current Analysis for the Station Point – BMRCM-II (Smoothed)
(1st Layer = 0.37m, 2nd Layer = 1.11m, 3rd Layer = 1.84m, 4th Layer = 2.58m)

Some key features of the circulation system is shown from the Figure 5.17 and Figure 5.18. At the 8th hour, 2 different vortices form up at the offshore of the river mouth. In 8 hours, the one at the lower latitude gets closer to the coastline, and the radius of this one gets bigger. As touching the coast, it advances and moves out of the domain in 14 hours. On the other hand, the other vortex moves towards the offshore and slowly

moves towards the out of domain, from the upper cross section of open boundary and the coastline, leaves the computational domain with a relatively smaller radius, when it is compared to the lower one.

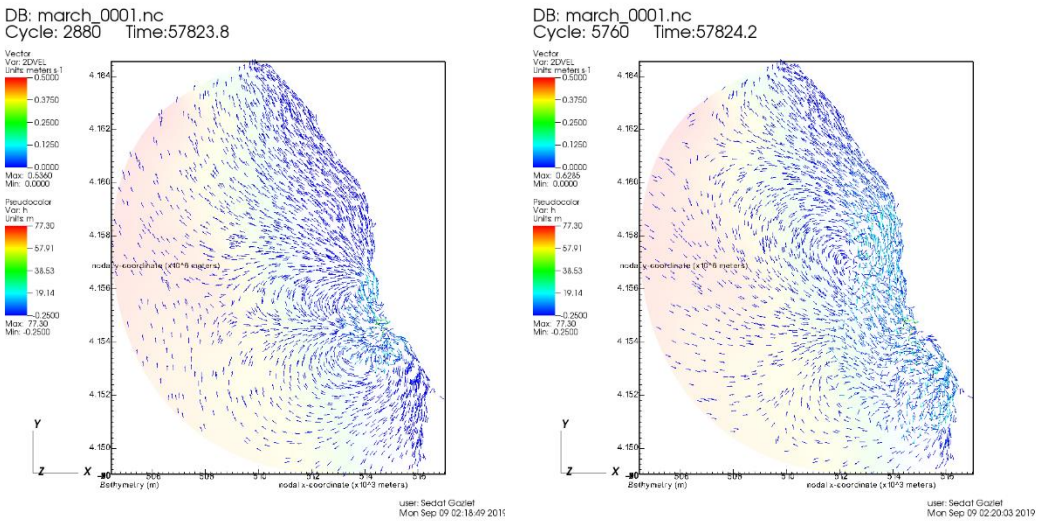

Figure 5.17. Circulation Pattern – March ’17 – River Only Case (Hour: 8)

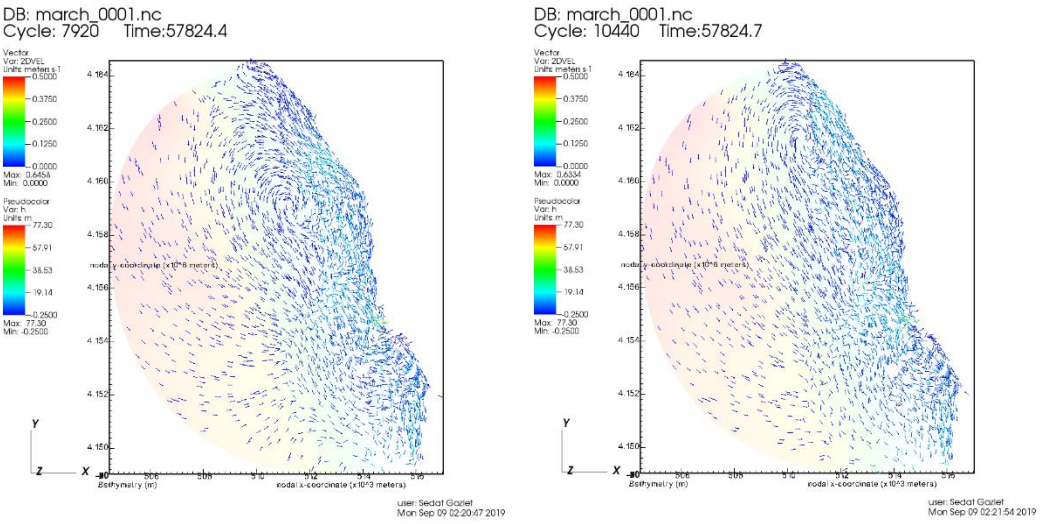

Figure 5.18. Circulation Pattern – March ’17 – River Only Case (Hour: 29)

5.2.1.3. Wind-Only Case

In this case of March ’17, as a forcing parameter, only wind was implemented the model. Figure 5.19 shows that the wind data input over the computation domain is time dependent and spatially uniform as intended. The magnitude and direction of the input data is also represented accurately across the domain. As it can be seen from the Figure 5.19 , the wind speed for the duration of the simulation is on average 4m/s but between the hours 24 and 50, the speed reduced from 6m/s to almost no wind condition. Additionally, the direction changed between +160direction to -160 direction. These changes are expected to be reflected in the circulation pattern in the model results.

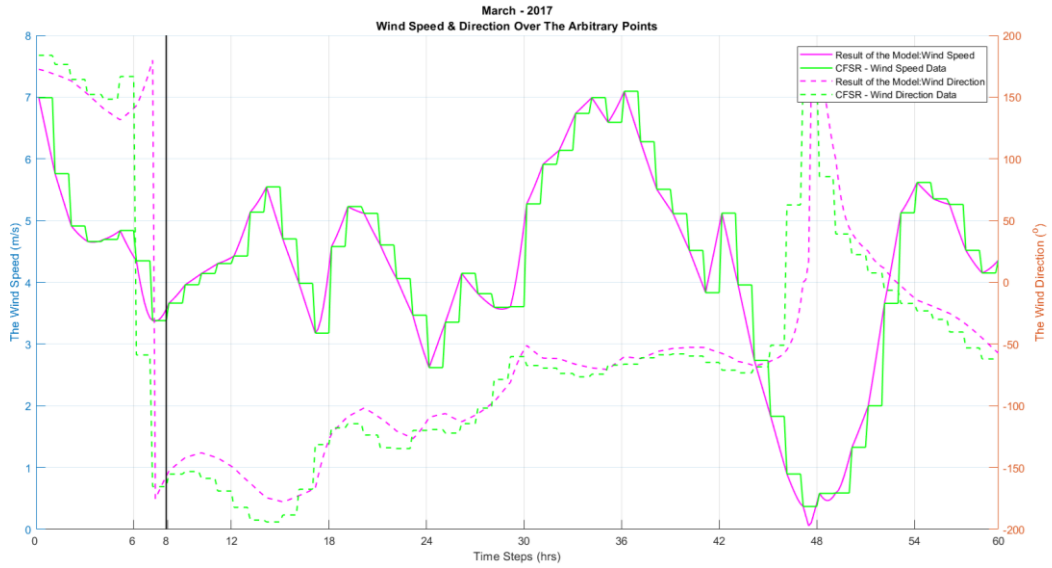

Figure 5.19. The Speed and The Direction of Wind over the Domain (For Direction; 0 Means, Cartesian 0°)

Figures 5.20 and 5.21 shows the current speed modeled with respect to the observations at two stations at 4 sigma levels from the water surface to the top of final layer. This final layer also corresponds to the depth of the measurement on the field. Therefore, this layer is used for comparison of model results to observation data. The rest of the layers is presented to show the behavior of the model along the vertical

domain. Additionally, vertically averaged results are provided to show the performance of the model if used in 2D mode.

For the first station point, the wind forcing produces currents that reflects the trend of the actual measurements at every level for the second day much better. However, the magnitude of the current at final layer which corresponds to the observation is much smaller. The correlation coefficient for this case is calculated as 0.45 which shows that the influence of wind forcing is much more reflected in the current system for this case especially compared to the river forcing at the first station point. Since river forcing represented the first day much better and higher wind speeds were observed in the second day, it can be discussed that for the first day, river was dominant in the current system, while for the second day it was the surface wind component.

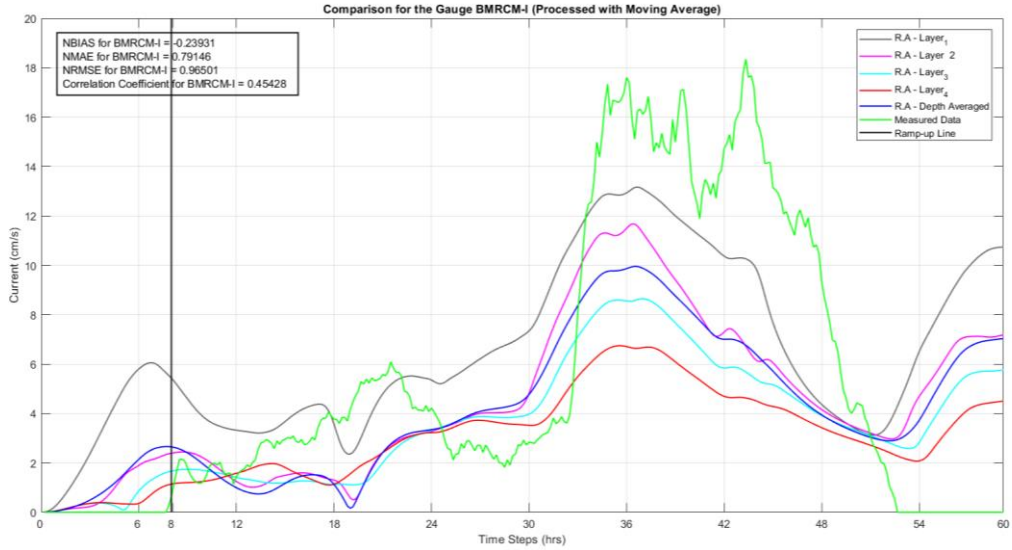

Figure 5.20. The Current Analysis for the Station Point – BMRCM-I (Smoothed)
(1st Layer = 0.89m, 2nd Layer = 2.68m, 3rd Layer = 4.47m, 4th Layer = 6.26m)

For the second station point, currents are higher (Figure 5.21). Similar to first station, the trend of second day was represented better by wind forcing although this is clearly seen in the depth average approach rather than Layer 4 (the final layer). Upper layers

of the water column also reflect the current observation much better both in trend and in magnitude. This output also indicates the impact of wind forcing being more dominant on the second day as the influence of wind would diminish along the water column as it gets deeper. The correlation coefficient for this case is much higher than the previous forcings as well.

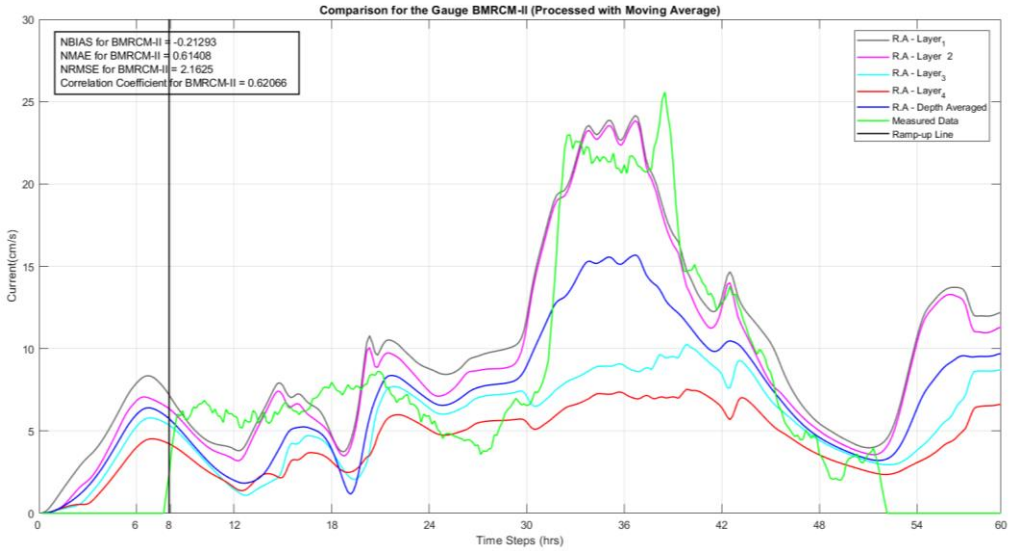

Figure 5.21. The Current Analysis for the Station Point – BMRCM-II (Smoothed)
(1st Layer = 0.37m, 2nd Layer = 1.11m, 3rd Layer = 1.84m, 4th Layer = 2.58m)

Consequently, in the general circulation pattern the first mild increment (20th hour), top of the jump (36th hour), half of the steep slope (42nd hour) and the data belong to lowest wind speed (53rd hour) are shown below, Figure 5.22-5.23. The higher current speeds along the shoreline are seen at 36th hour which is the end of the winds of high speed in the time series given in Figure 5.23. Although the highest wind speed is observed at hour 30, the process of energy transfer from wind to sea surface takes time as is the case with wave generation. Therefore, the full reflection of the wind is expected to be seen after a certain lag. In this case, the lag is around 6 hours, and this

is the 36th hour in the circulation figures with the highest current speeds. These results also show that the model is performing well with wind forcing for the region.

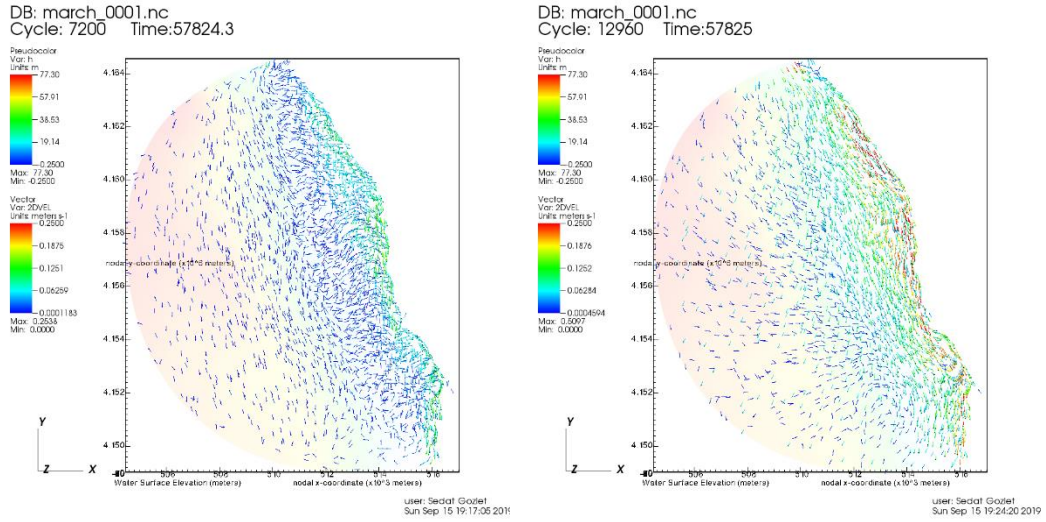

Figure 5.22. Circulation Pattern – March ’17 – Wind Only Case (Hour: 20 & 36)

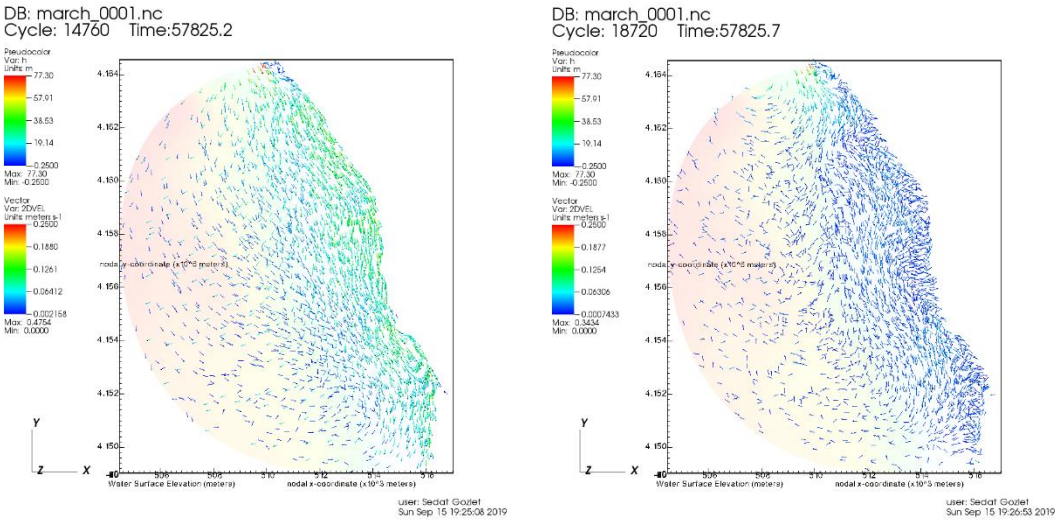

Figure 5.23. Circulation Pattern – March ’17 – Wind Only Case (Hour: 42 & 53)

5.2.1.4. All Parameters Combined Case – Actual Event

In this case tide, river and wind parameters were implemented at the same time as external forcing to represent the actual conditions of the expedition.

Figures 5.24 - 5.27 shows the current speed modeled with respect to the observations at two stations at 4 sigma levels from the water surface to the top of final layer. This final layer also corresponds to the depth of the measurement on the field. Additionally, vertically averaged results are provided to show the performance of the model if used in 2D mode. Both the actual model output as well as the smoothed data is presented for this case.

For the first station point, the combined forcing produces currents that reflects the trend and magnitude of the observations of the first day at the final layer. The depth average results also show a very good representation of the trend of the current observations for the whole duration of observations. For second day, the magnitudes are lower in the model output. However, the final layer cannot model the magnitudes for the second day at all. Still, the trend of the second day is slightly reflected in this layer as well although it can be clearly seen in the upper layers. The correlation coefficient for this case is slightly lower than the wind only case for the same station. The additional current component of the second day could very well be waves generating longshore currents at the shoreline where the stations are located. But this forcing is not included in the model due to lack of data.

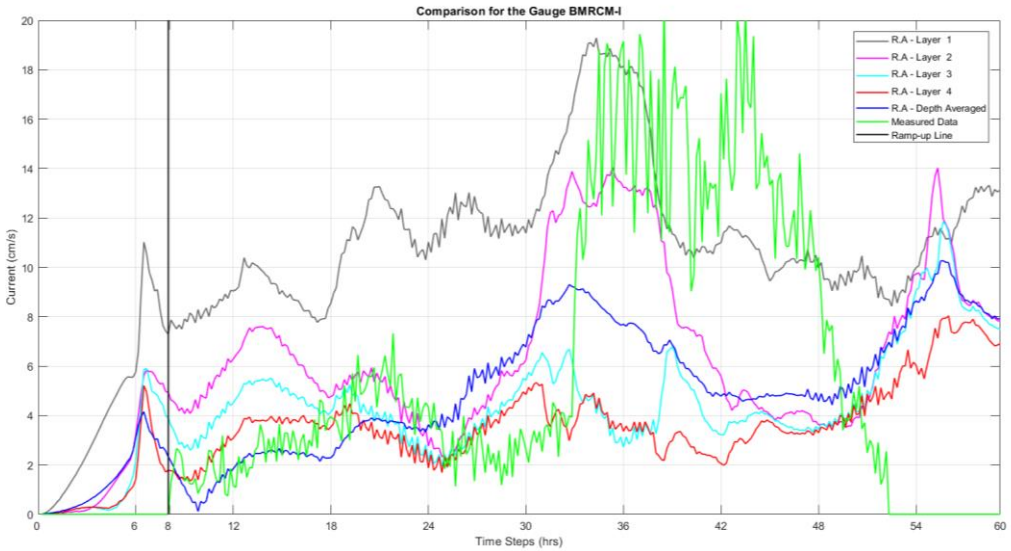

Figure 5.24. The Current Analysis for the Station Point – BMRCM-I
(1st Layer = 0.89m, 2nd Layer = 2.68m, 3rd Layer = 4.47m, 4th Layer = 6.26m)

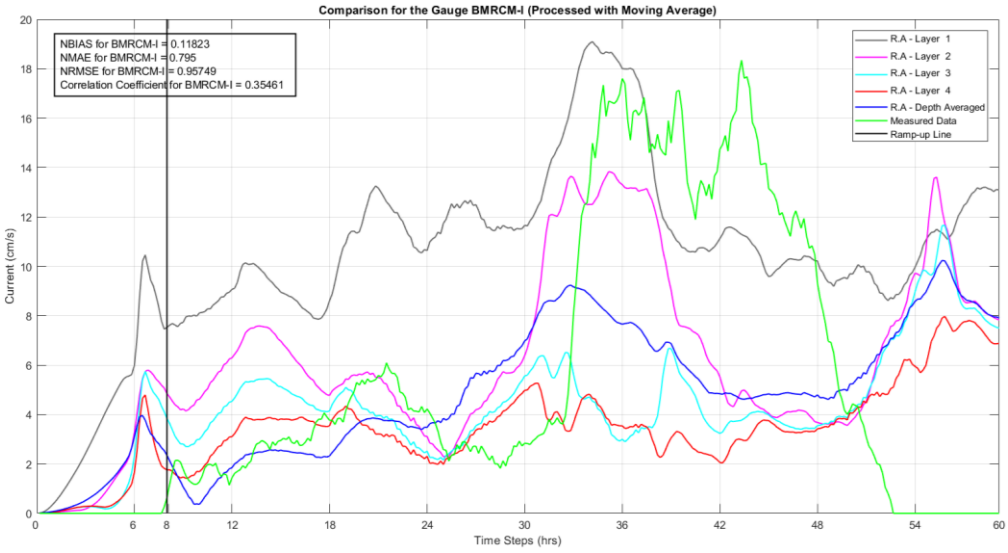

Figure 5.25. The Current Analysis for the Station Point – BMRCM-I (Smoothed)
(1st Layer = 0.89m, 2nd Layer = 2.68m, 3rd Layer = 4.47m, 4th Layer = 6.26m)

For the second station point (Figures 5.26-5.27), the combined forcing produces currents that reflects the trend and magnitude of the observations much better than the first station. Especially, the depth average results show a very good representation of the trend of the current observations for the whole duration of observations. Similar to first station, the magnitudes are lower in the model output for the second day. The correlation coefficient for this station is much higher than first station. But it is slightly lower than the wind only case for the same station.

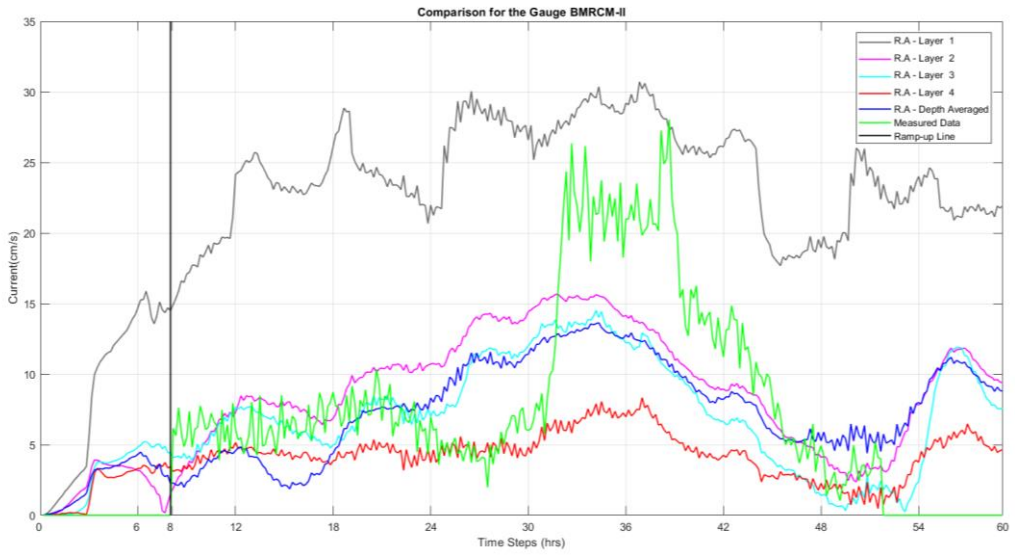

Figure 5.26. The Current Analysis for the Station Point – BMRCM-II
(1st Layer = 0.37m, 2nd Layer = 1.11m, 3rd Layer = 1.84m, 4th Layer = 2.58m)

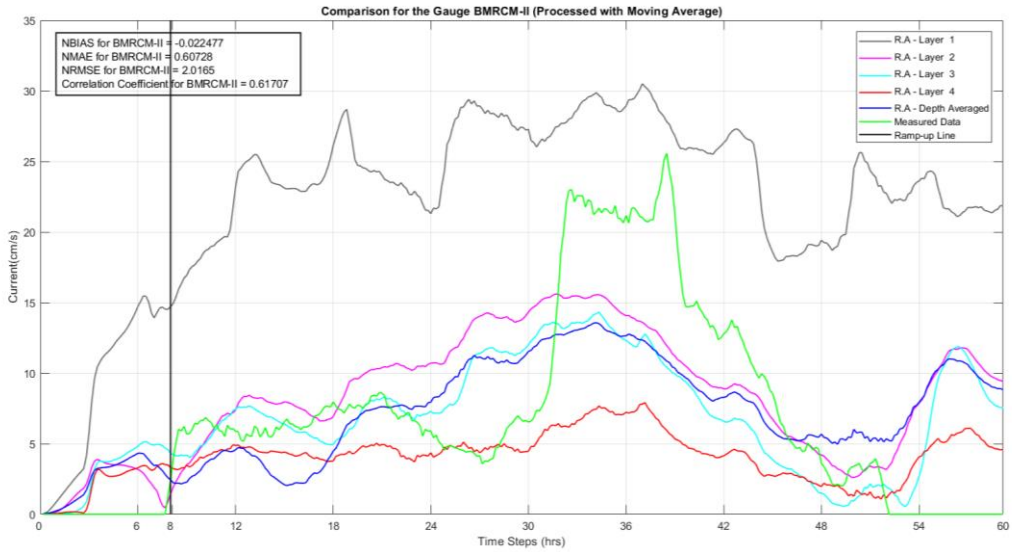

Figure 5.27. The Current Analysis for the Station Point – BMRCM-II (Smoothed)
(1st Layer = 0.37m, 2nd Layer = 1.11m, 3rd Layer = 1.84m, 4th Layer = 2.58m)

Consequently, the general circulation pattern can be seen below, Figure 5.28-5.31. The figures are more common with the wind only case but with higher current speed at the river mouth since there is also the river forcing at this point. The more complex nature of circulation at the river mouth can also be observed from the figures. The model reflects the river flow at the mouth with current vectors directed towards the sea. The maximum and the minimum speeds are achieved at the same hours, from among the previous selected snapshots.

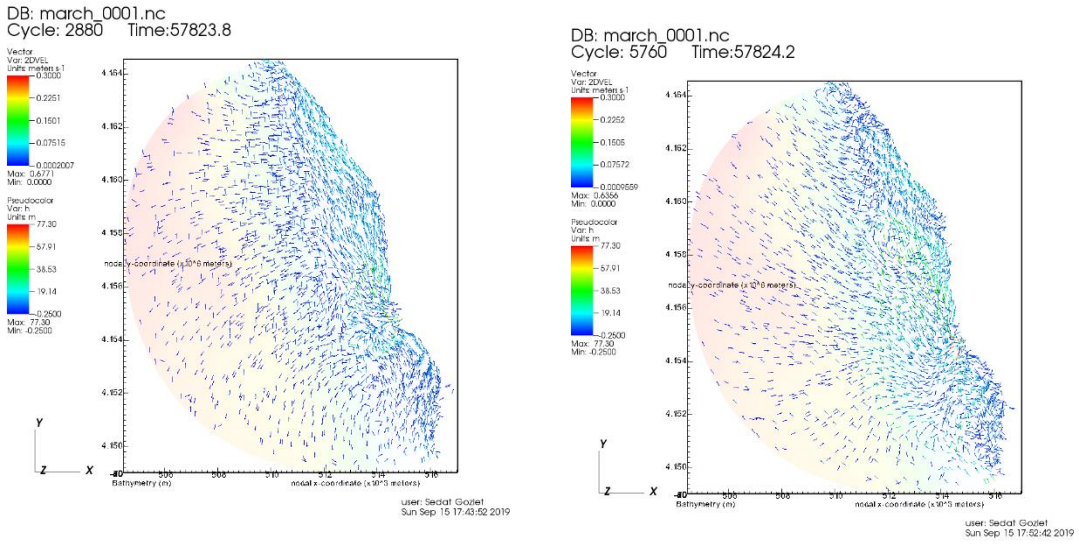

Figure 5.28. Circulation Pattern – March ’17 – All Combined Case (Hour: 8 & 16)

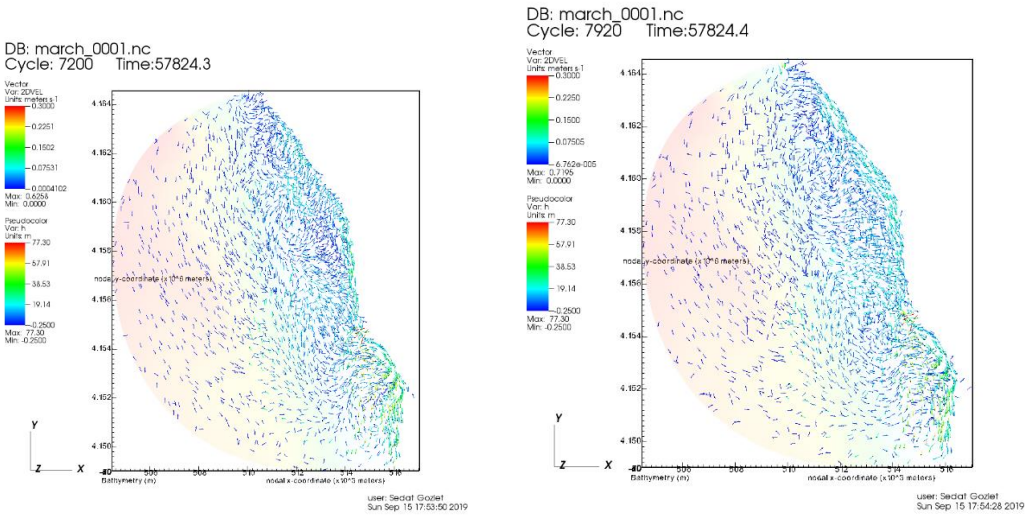

Figure 5.29. Circulation Pattern – March ’17 – All Combined Case (Hour: 20 & 22)

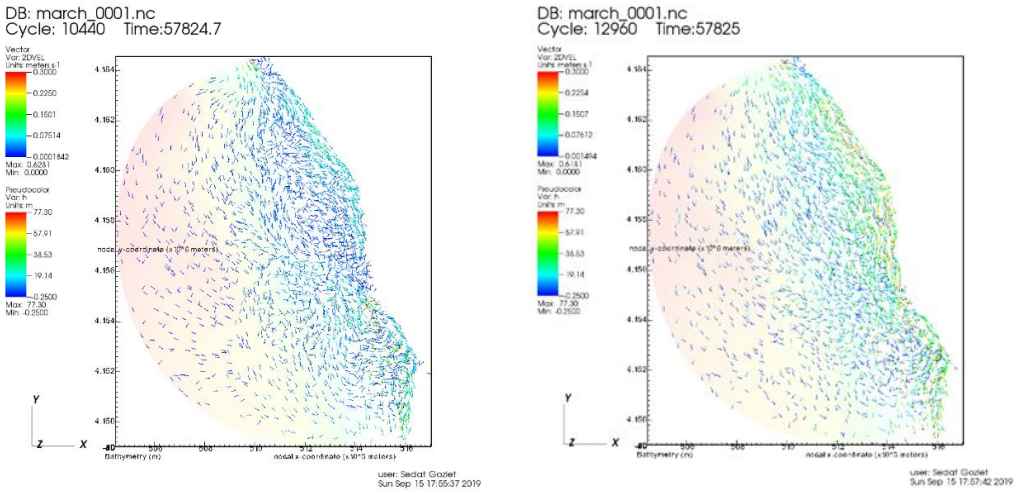

Figure 5.30. Circulation Pattern – March ’17 – All Combined Case (Hour: 29 & 36)

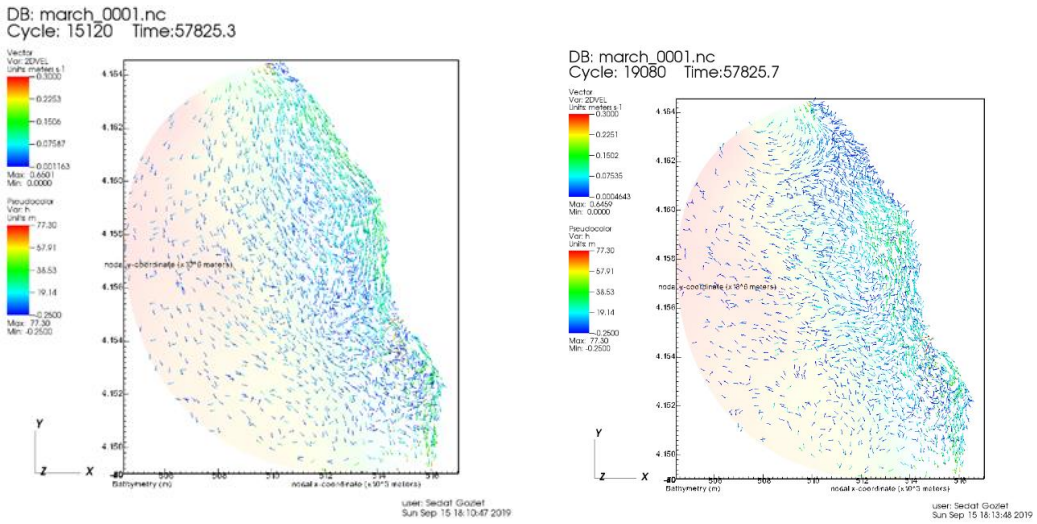

Figure 5.31. Circulation Pattern – March ’17 – All Combined Case (Hour: 42 & 53)

Furthermore, the salinity and the temperature data collected during the expedition at several stations are compared to the model output. The stations were presented in chapter 4. The results are presented in Figures 5.32, and 5.33. The salinity outputs of the model are usually in good agreement with the measurements at most stations and along the water column (Figure 5.32). The stations closer to river mouth shows the mixing of salt-water and fresh water and this transition is reflected in the model results as well. Some stations are in very shallow depths and for those stations the model did not perform very well for the surface layer. On the other hand, the temperature results do not show the same level of accuracy as the salinity. The trend along the water column is modeled well in most of the stations but the magnitudes were not compatible with the observations.

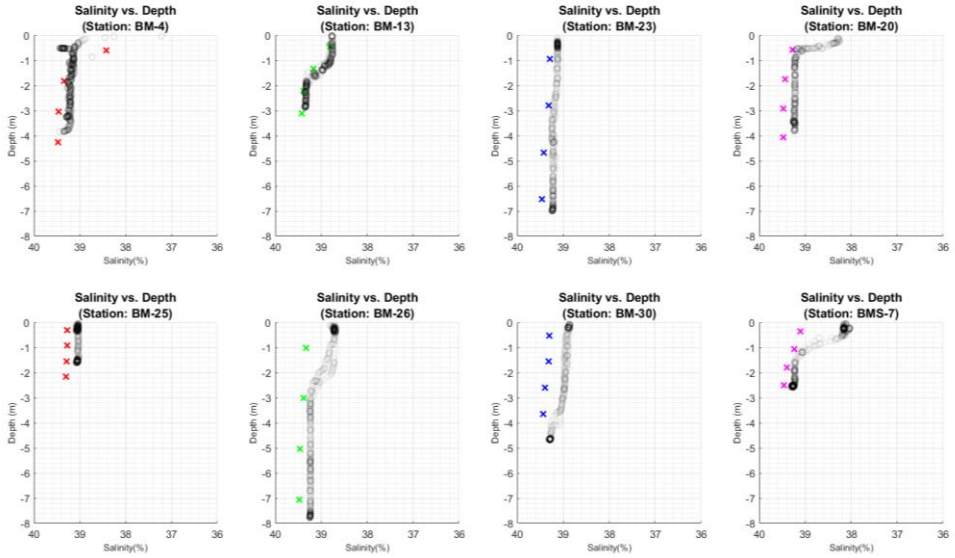

Figure 5.32. Salinity - March '17

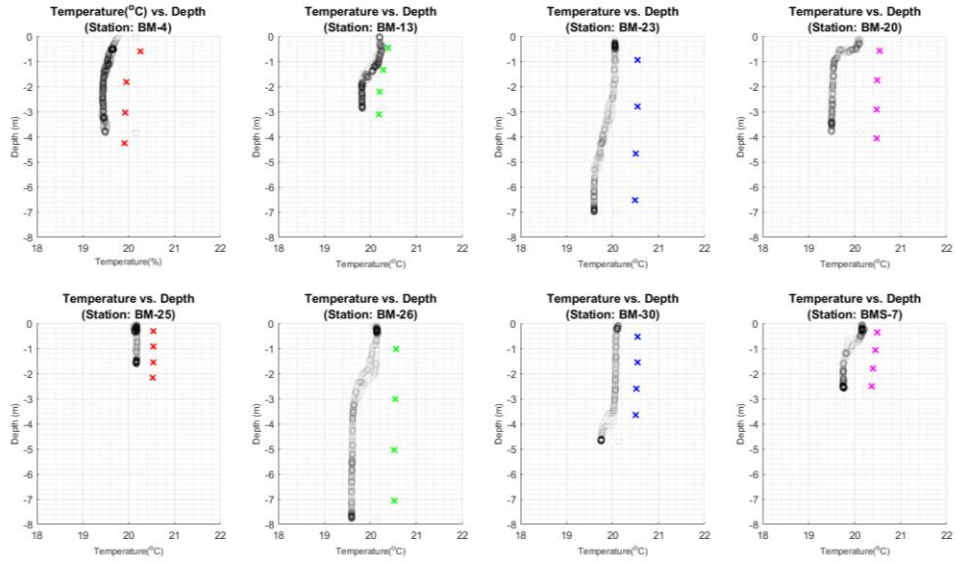

Figure 5.33. Temperature - March '17

One possible reason is could be the selection of the initial temperature condition for sea and river. Salinity and temperature are two variables that change in time and spatially. For salinity, the difference between the sea and the river causes a mixing

process which create a chaotic environment where a local circulation occurs. Furthermore, for the temperature change, this phenomenon happens faster than salinity change, and its results are not close to the in-situ data when they have compared to salinity. On the account of both parameters, one other reason for their analysis results differs from the real data, each of these parameters vary not only in horizontal plane, but also in depth as well, see the Figures 5.34 and 5.35. But in this study, these parameters were considered spatially uniform.

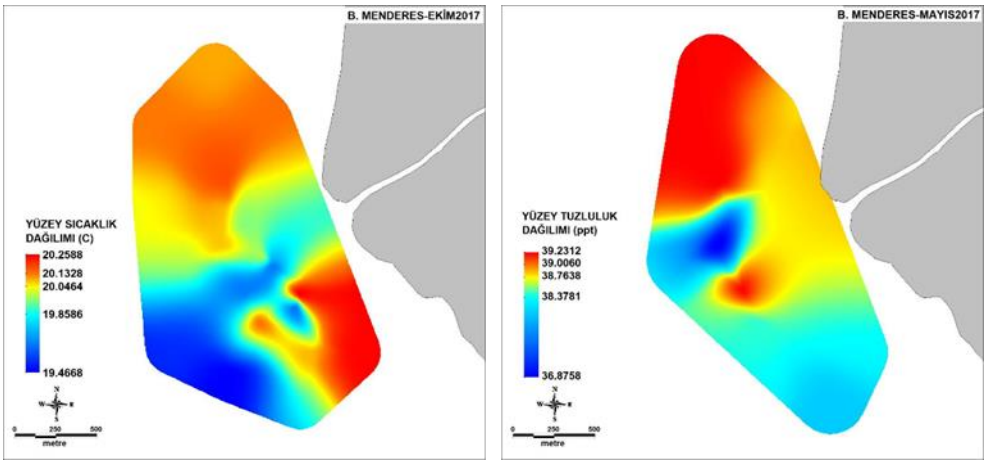

Figure 5.34. Salinity and Temperature Distribution on the Surface (Retrieved from the TUBITAK Report, Kısacık et al., 2017)

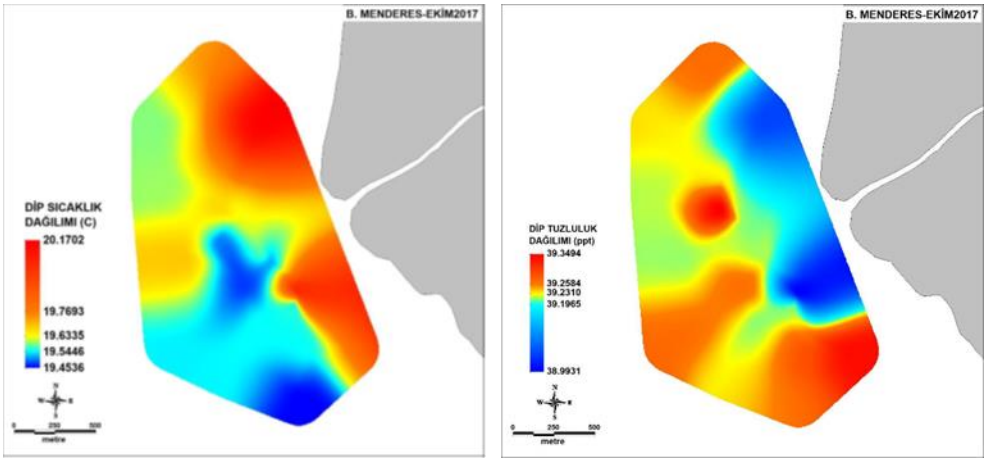

Figure 5.35. Salinity and Temperature Distribution at the Bottom (Retrieved from the TUBITAK Report, Kısacık et al., 2017)

5.2.2. May ‘17

The second case modeled is based on the expedition done on the 23 & 24 May 2017. The river data is taken from TUBITAK project data. Wind data is from CFSv2 dataset and the open boundary forcing is done by sea level data from Bodrum mareograph station. Constant water temperature and salinity is used throughout the domain as 22.68°C & 39.41 ‰ based on the field measurements. The computational time of 2.5 days took 4-7 hours depending on the processor and forcing types.

The results have been subjected to a smoothing operation via MATLAB for ease of use in statistical calculations of error measures. In order to analyze the contribution of each forcing type on the overall circulation system, several runs were performed such as tide only forcing, wind only forcing, river only forcing. Finally, the actual forcing combination (tide, river and wind together) is modeled. All the runs include the Coriolis effect. The original model output is provided for the case with all forcing types. The rest of the results are presented after the smoothing process.

5.2.2.1. Tide-Only Case

In this case of May ’17, as a changing parameter, only tide was implemented the model. Figure 5.36 shows that the water elevation input forced at the open boundaries is represented accurately across the domain.

The result of the analysis on the station points BM-4, BM-14 and BM-24 by means of current speeds are in order of magnitude 0.025 cm/s. From the figures 5.37, 5.38 and 5.39 it is hard to state a clear correlation between the measurements and the analysis.

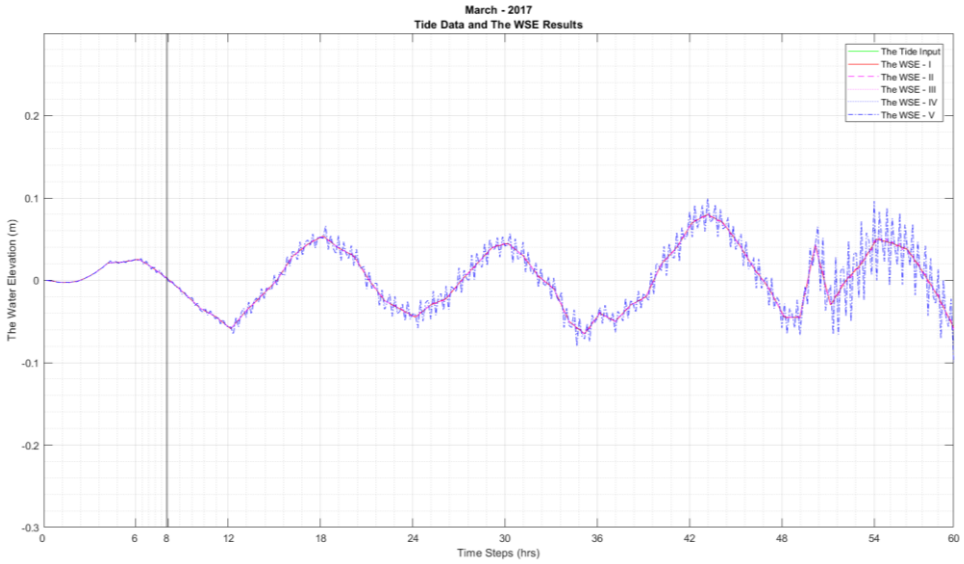

Figure 5.36. The Analysis Result for the OB and the Tide Check Points

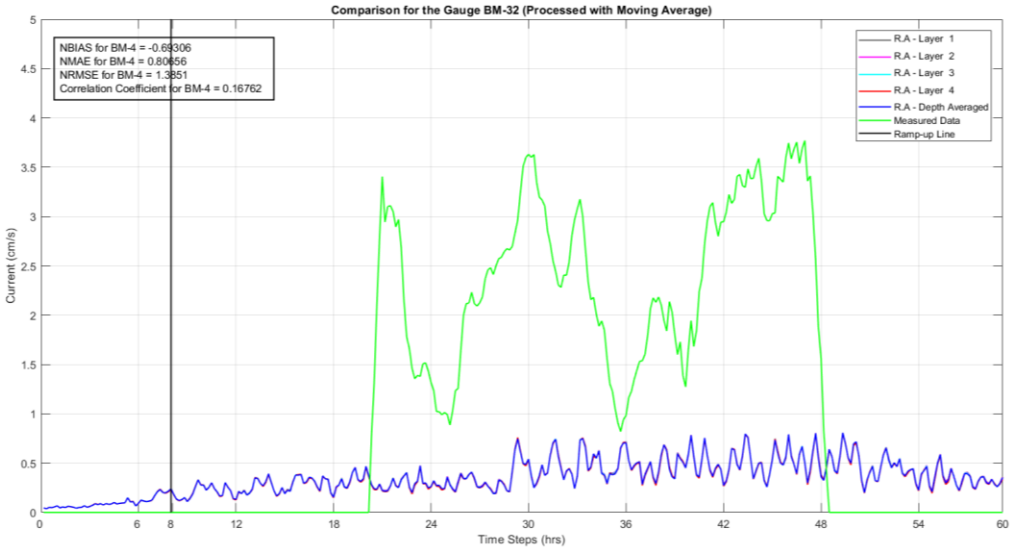

Figure 5.37. The Current Analysis for the Station Point – BM-32 (Smoothed)

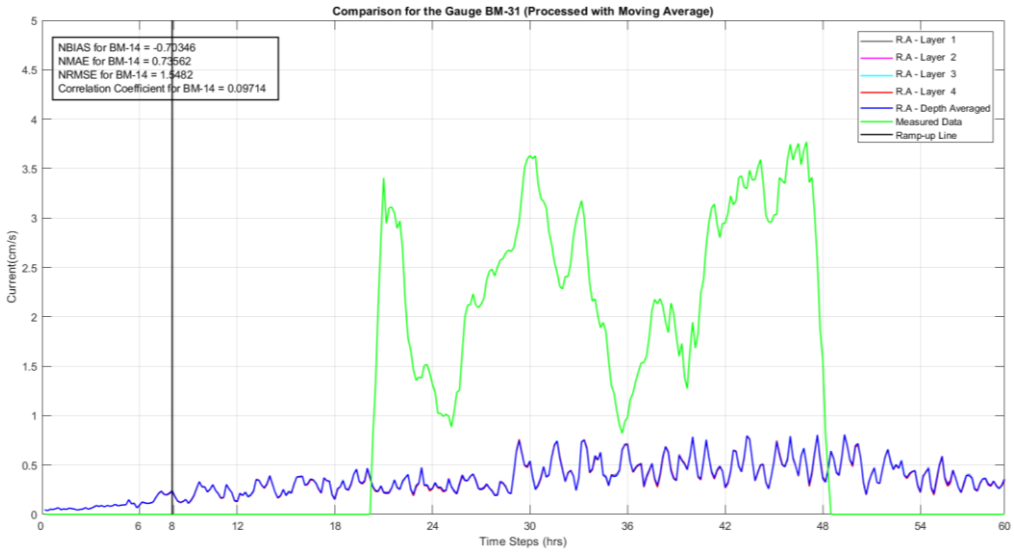

Figure 5.38. The Current Analysis for the Station Point – BM-31 (Smoothed)

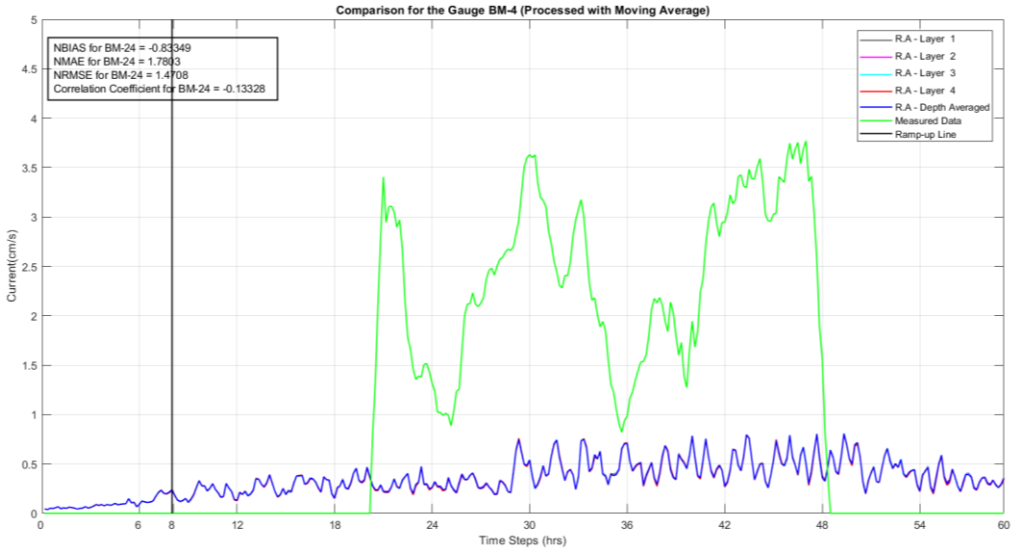

Figure 5.39. The Current Analysis for the Station Point – BM-4 (Smoothed)

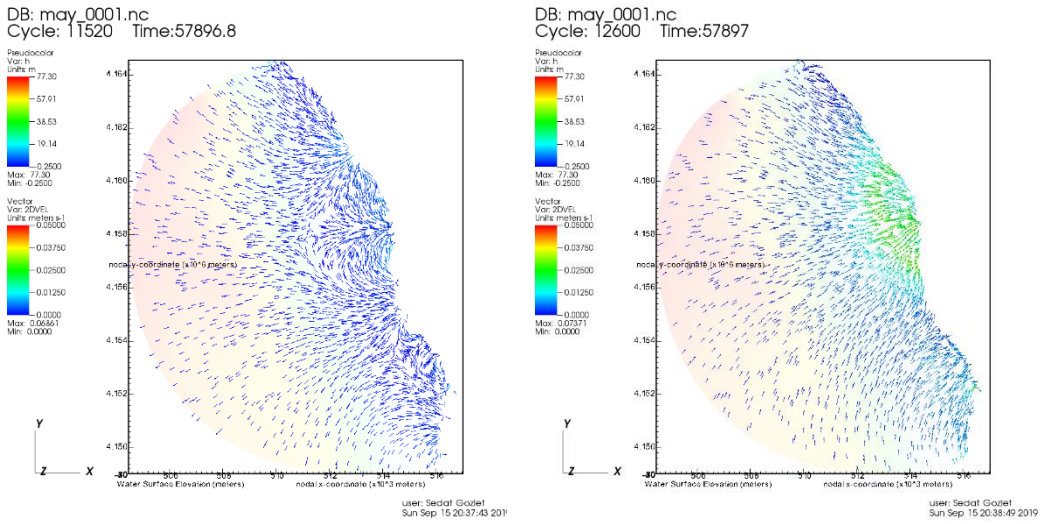

Figure 5.40. Circulation Pattern – May ’17 – Tide Only Case (Hour: 36 & 39)

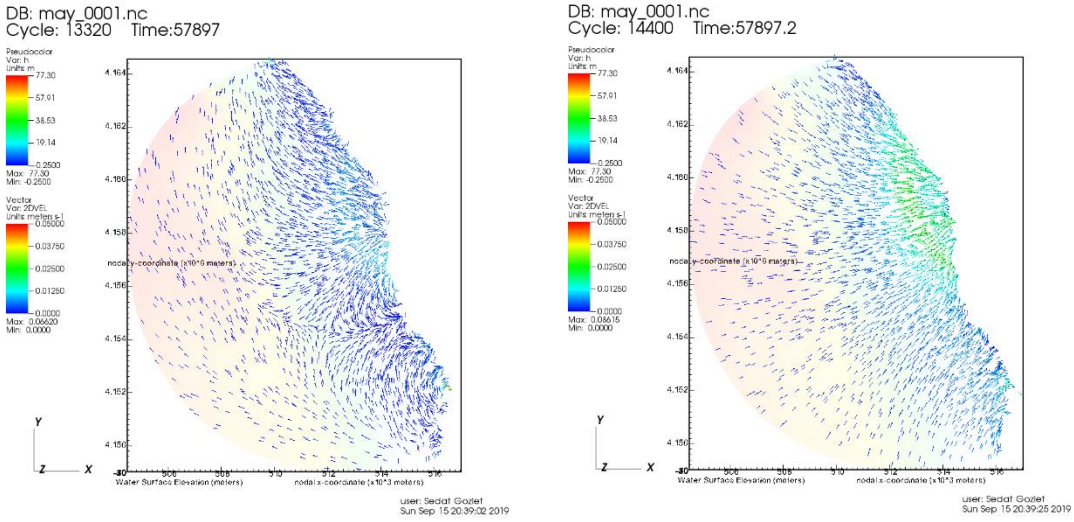

Figure 5.41. Circulation Pattern – May ’17 – Tide Only Case (Hour: 42 & 44)

Therefore, the circulation pattern generally, on the hours 36nd, 39th, 42th and 44st, can be seen between the Figures 5.40-5.41. In these figures, it can be understood that; the patterns of 36nd and 39th hours belong to an hour that water elevation gets closer to

mean sea level, on the other hand, the pattern of 42th hour belongs a high tide and 44st, a low tide. As expected, on the hour 39th water moves out of the domain, on the other hand, on the hour 44nd, it moves through inside the domain.

5.2.2.2. River-Only Case

In this case of May ’17, as a changing parameter, only river was implemented the model. The arbitrary check points and tide input can be seen on the Figure 5.42. As the data source DSI was used, which has a time resolution of 12 hours. Salinity and temperature changes observed due to the river transport of those parameters.

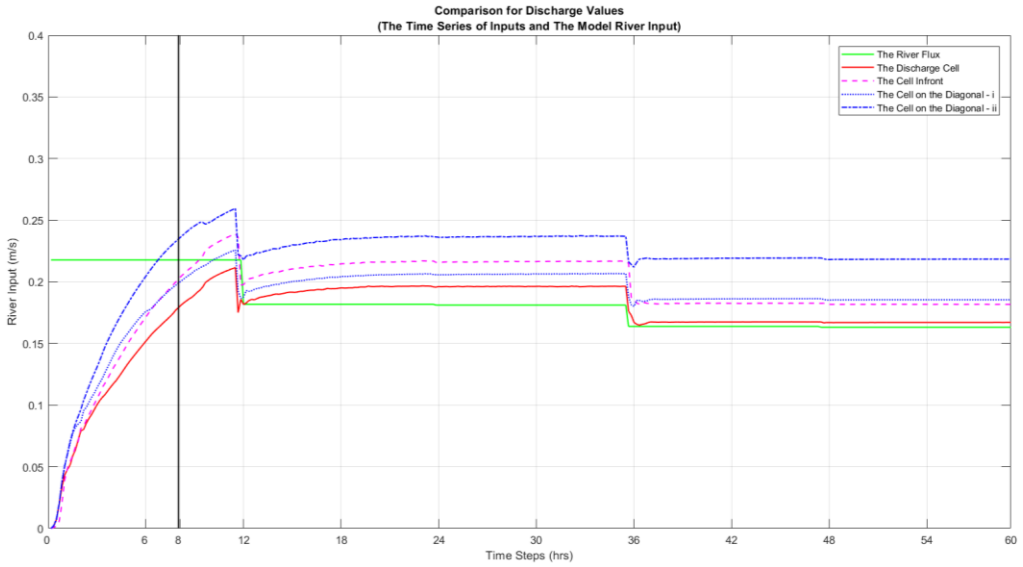

Figure 5.42. The Analysis Result for the Discharge Node and the Control Cells

The result of the analysis on the station points BM-4, BM-14 and BM-24 by means of current speeds are in order of magnitude 0.05 m/s. The data has a stable shape parallel with the changes in the direction of decrease as accordance with the daily data.

The discharge node and the control cells around can be seen on the Figure 5.13.

The Figures from 5.43 to 5.45, are belong to the stations BM-4, BM-14 and BM-24, respectively. For all the figures of the measurements, the magnitude of order of current speed was barely predicted by the model; the first half of the observations are approximated within the uppermost layer of the BM-4 and BM-14 stations. On the other hand, in Figure 5.45, 2nd and the 3rd layer caught the magnitude of observation better than the 1st and the 4th layers for the station BM-24. Nevertheless, the last jump in the observations, which starts approximately around 40th hour of the analysis, could not be represented any of the layers at any of the stations.

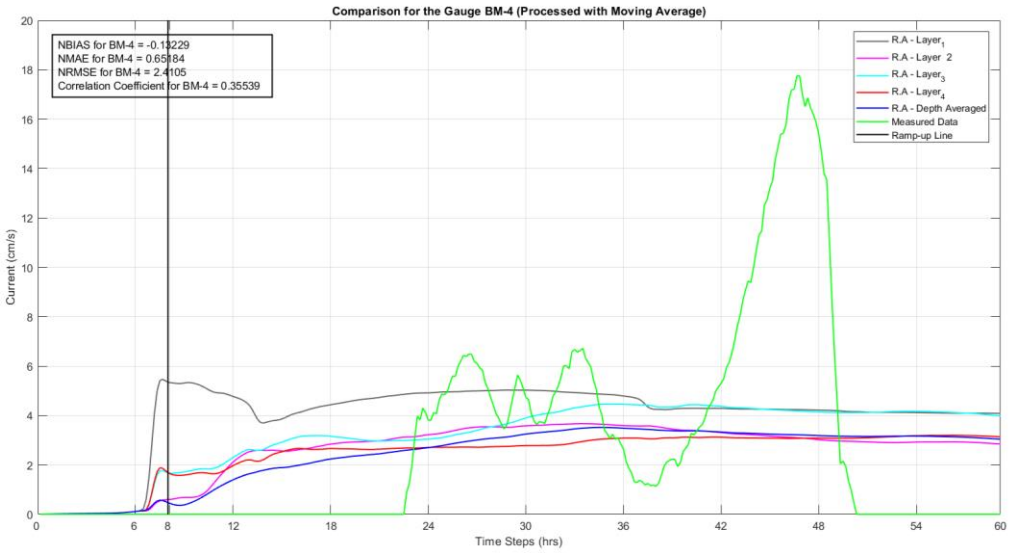

Figure 5.43. The Current Analysis for the Station Point – BM-4 (Smoothed)
(1st Layer = 0.61m, 2nd Layer = 1.82m, 3rd Layer = 3.03m, 4th Layer = 4.24m)

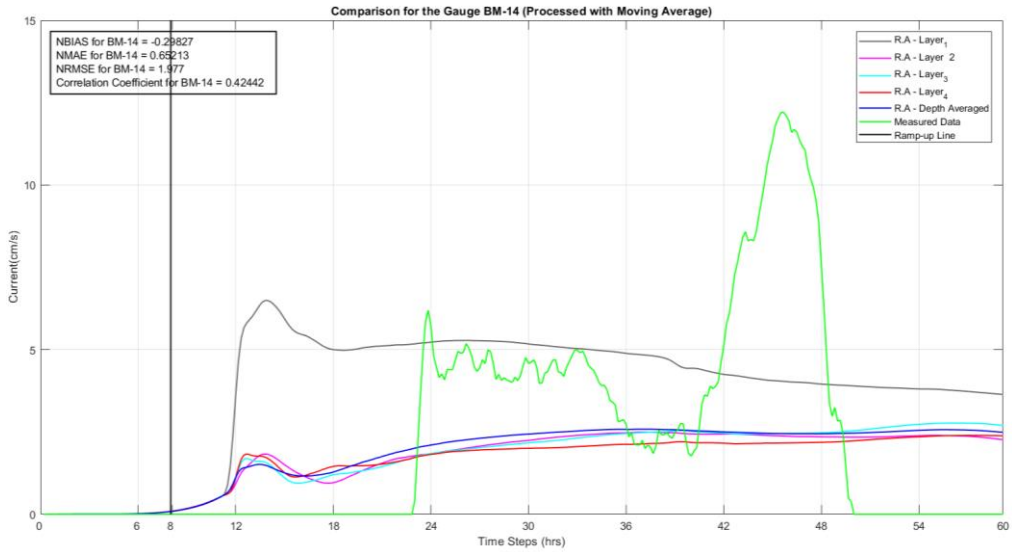

Figure 5.44. The Current Analysis for the Station Point – BM-14 (Smoothed)
(1st Layer = 0.86m, 2nd Layer = 2.58m, 3rd Layer = 4.30m, 4th Layer = 6.02m)

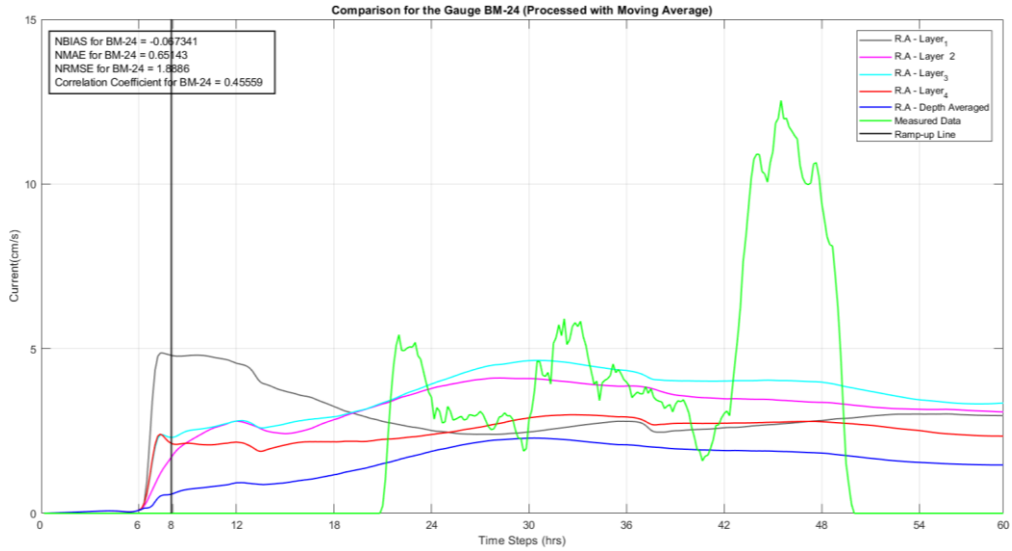

Figure 5.45. The Current Analysis for the Station Point – BM-24 (Smoothed)
(1st Layer = 0.50m, 2nd Layer = 1.49m, 3rd Layer = 2.48m, 4th Layer = 3.47m)

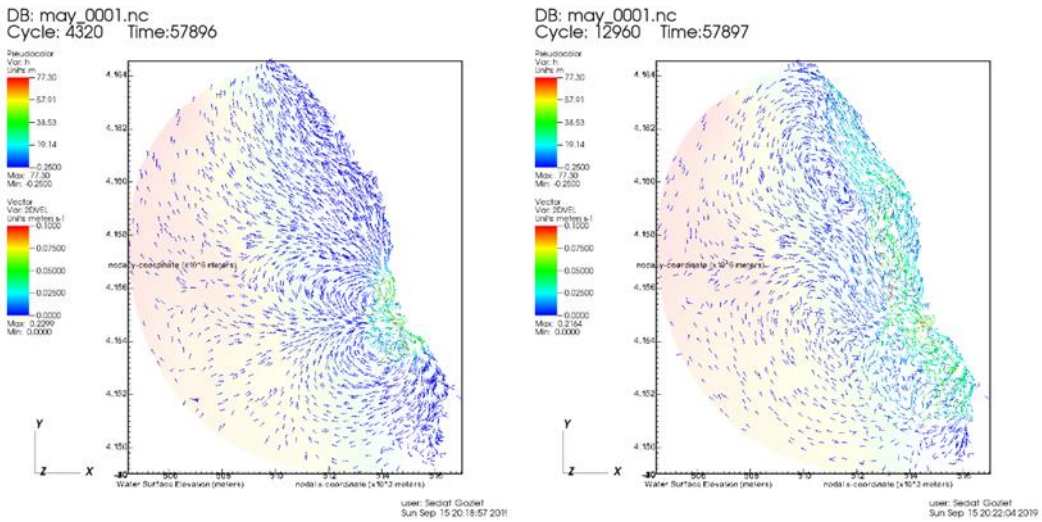

Figure 5.46. Circulation Pattern – May ’17 – River Only Case (Hour: 12 & 36)

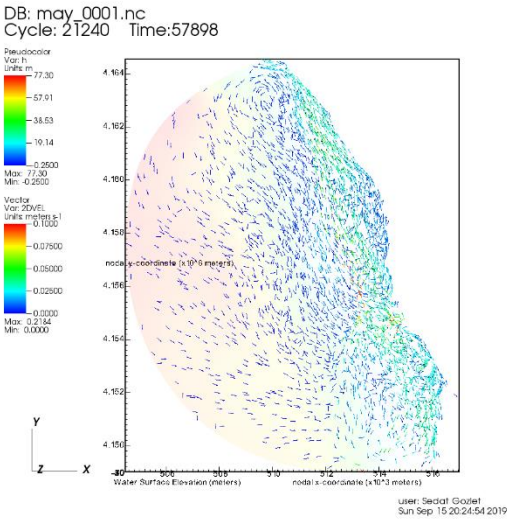

Figure 5.47. Circulation Pattern – May ’17 – River Only Case (Hour: 59)

The general circulation pattern, as expected, shaped by the vortices caused by the river that can be seen at the above, from the Figure 5.45 and 5.47 since there is no critical change after the system has been stabilized, three snapshots of the system enough for it to summarize the behavior.

5.2.2.3. Wind-Only Case

In this case of May ’17, as the only parameter, wind was implemented the model. The change in the wind speed and direction can be seen from the Figure 5.48, clearly. It can be seen from the plot, the wind speed for the duration of the simulation is on average 5m/s but it fluctuates between the values of 10m/s and 1m/s. Companying the slow degradation, three peaks can be seen from the figure, distinctly. Furthermore, the direction change is relatively steady, it oscillates between the directions 0° and -100°.

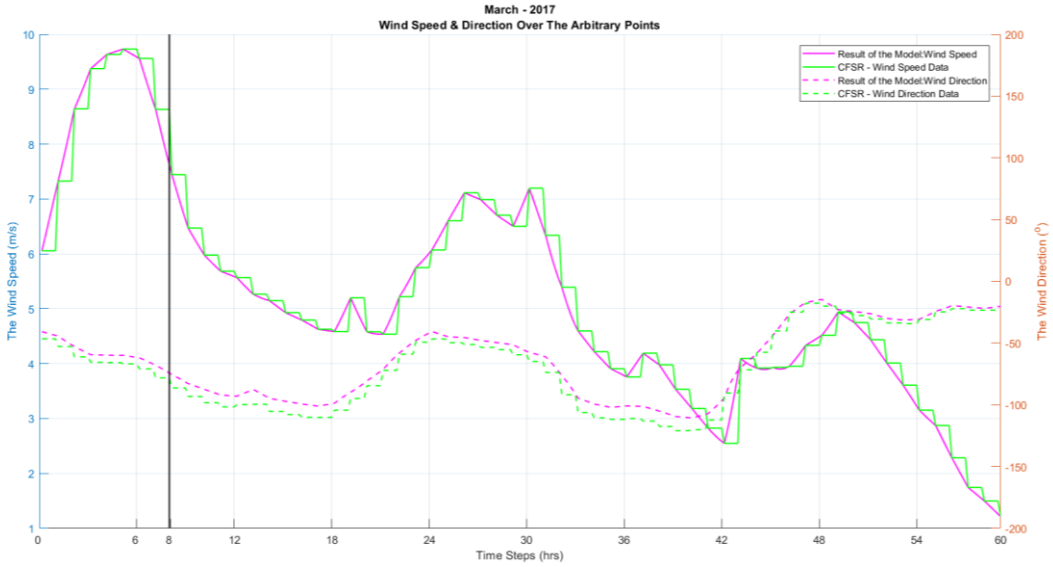

Figure 5.48. The Speed and The Direction of Wind over the Domain

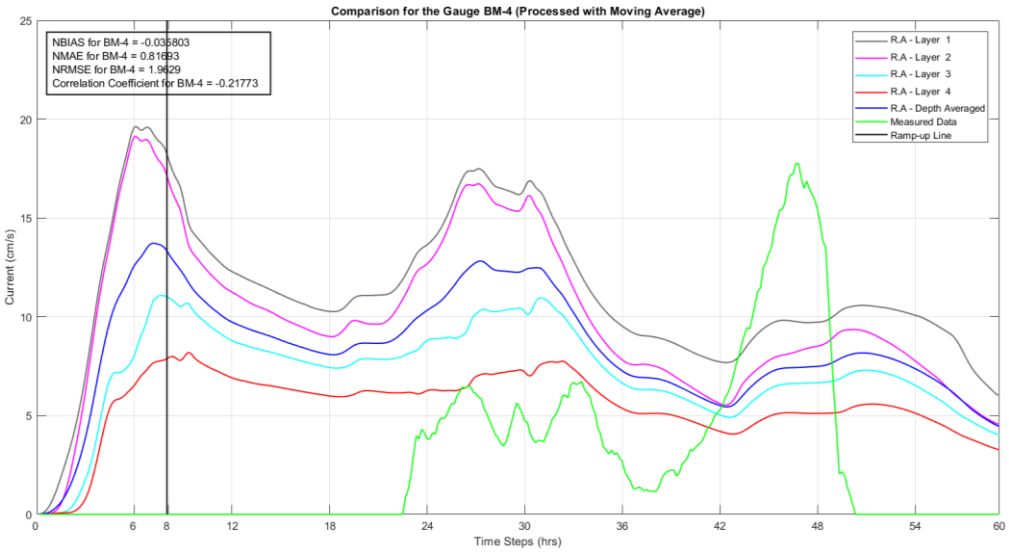

Figure 5.49. The Current Analysis for the Station Point – BM-4 (Smoothed)
(1st Layer = 0.61m, 2nd Layer = 1.82m, 3rd Layer = 3.03m, 4th Layer = 4.24m)

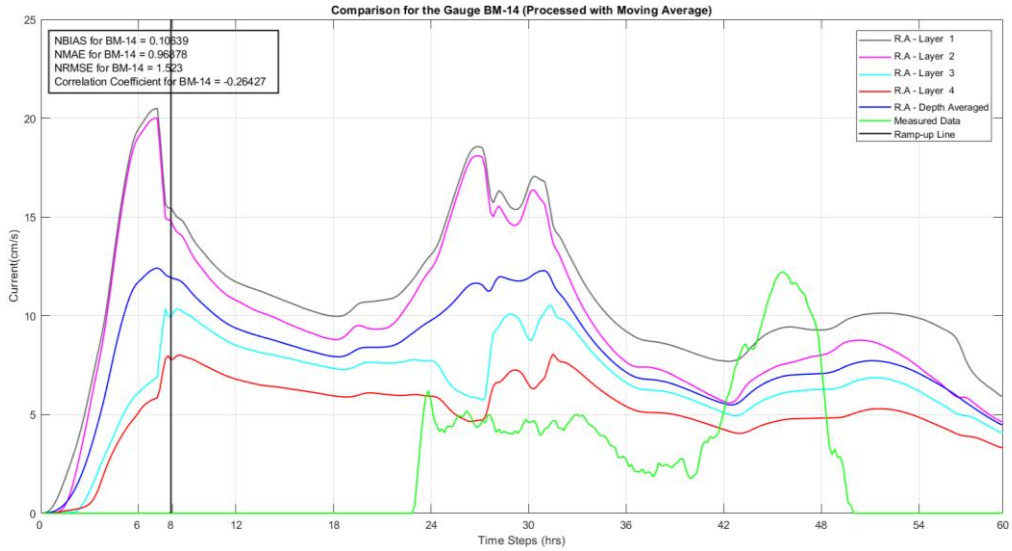

Figure 5.50. The Current Analysis for the Station Point – BM-14 (Smoothed)
(1st Layer = 0.86m, 2nd Layer = 2.58m, 3rd Layer = 4.30m, 4th Layer = 6.02m)

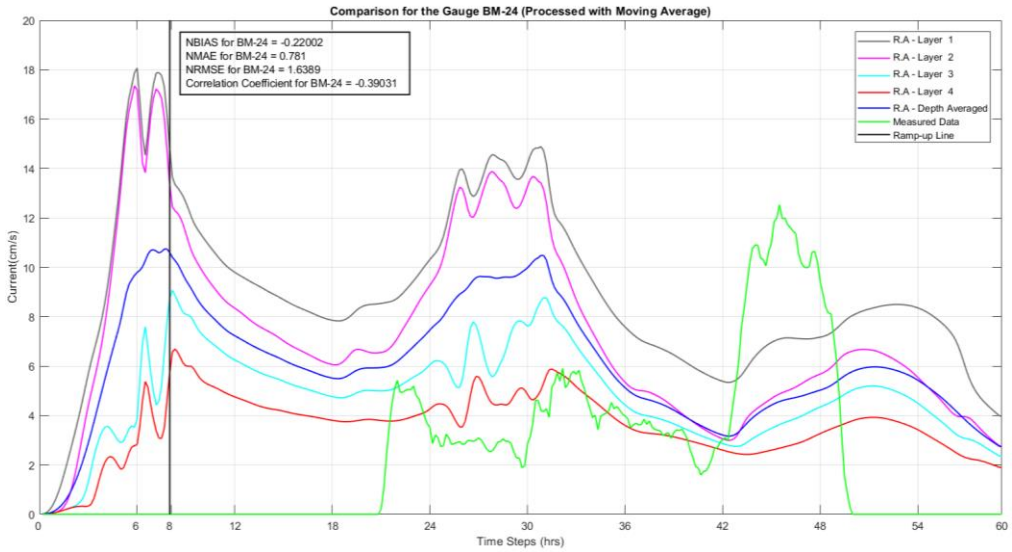

Figure 5.51. The Current Analysis for the Station Point – BM-24 (Smoothed)
(1st Layer = 0.50m, 2nd Layer = 1.49m, 3rd Layer = 2.48m, 4th Layer = 3.47m)

The result of the analysis reflected both of the input data characteristics and the measurement behavior, up to a point. To generally speaking, on the station points BM-4, BM-14 and BM-24 by means of current speeds are in order of magnitude 0.20 cm/s. The trend of the data behaves similarly for all sampling window, especially on the stations BM-14 and BM-24 up to the 42nd hour (Figure 5.60-5.61) in layer-4, which is the bottom layer, behaved very close to the measurements as it was expected to be. Nonetheless, the model again missed the last jump between the hours of 42nd and 47th which is present in in-situ data as well. Yet, apart from the March ’17 analysis, in this analysis the model caught the trend in a clearer way, but the 4th layer missed the magnitude as having a value of one third of the real data.

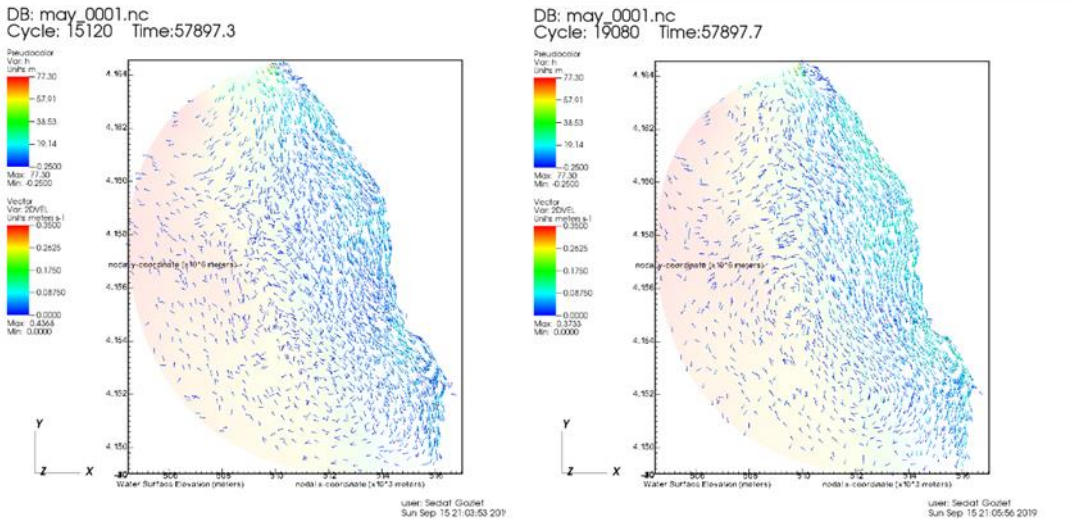

Figure 5.52. Circulation Pattern – May ’17 – Wind Only Case (Hour: 18 & 29)

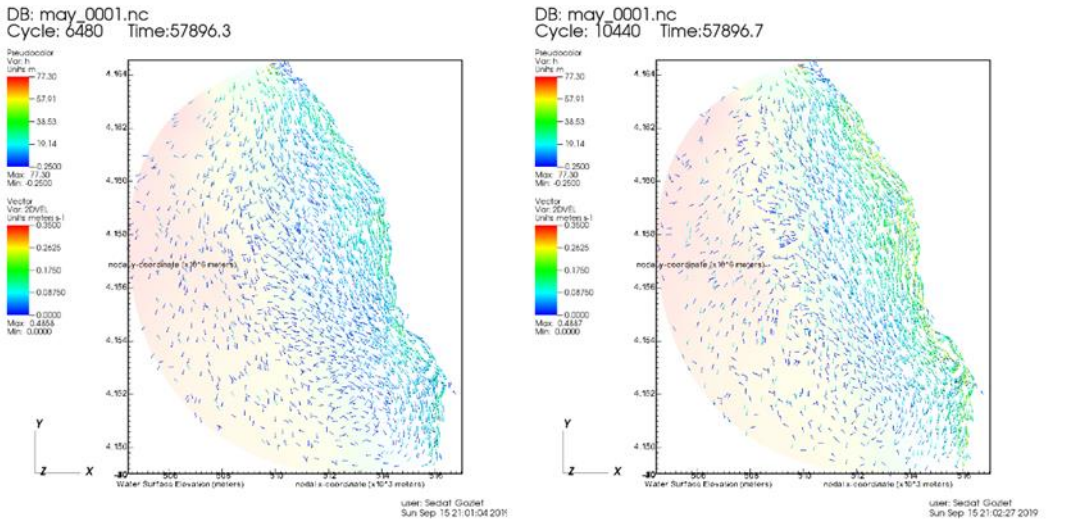

Figure 5.53. Circulation Pattern – May ’17 – Wind Only Case (Hour: 42 & 53)

For the general circulation pattern, firstly, concave up regime (18th hour), then, top of the jump (29th hour), then second concave up (42nd hour) and finally the data belong to concave down shapes (53rd hour) are shown below, Figure 5.52-5.53.

5.2.2.4. All Parameters Combined Case – Actual Event

In this case tide, river and wind parameters were implemented the software as time series. The Coriolis forcing was open.

Salinity and temperature changes observed due to the river transport of those parameters.

For circulation pattern and the observation stations, the previous changes will be tried to be observed in this combined case. These forces either will superpose or damp each other.

Starting from the 23rd hour, the combined forcing produces currents that reflects the trend and magnitude of the observations until the 42nd hour in a good way, even in the BM-14 the 1st layer, which is the closest to the water surface, behaves very close to the third jump both in the mean of magnitude of order and the trend, yet it over predicts the earlier events in dataset. Beside that the depth average results also show a very good representation of the trend of the current observations for the whole duration of observations. For the rest of the stations and the layers, the magnitudes are lower in the model output. Still, the trend of the second day is slightly reflected in this layer as well although it can be clearly seen in the upper layers. The correlation coefficient for this case is slightly lower than the wind only case for the same station. The additional current component of the second day could very well be waves generating longshore currents at the shoreline where the stations are located. But this forcing is not included in the model due to lack of data.

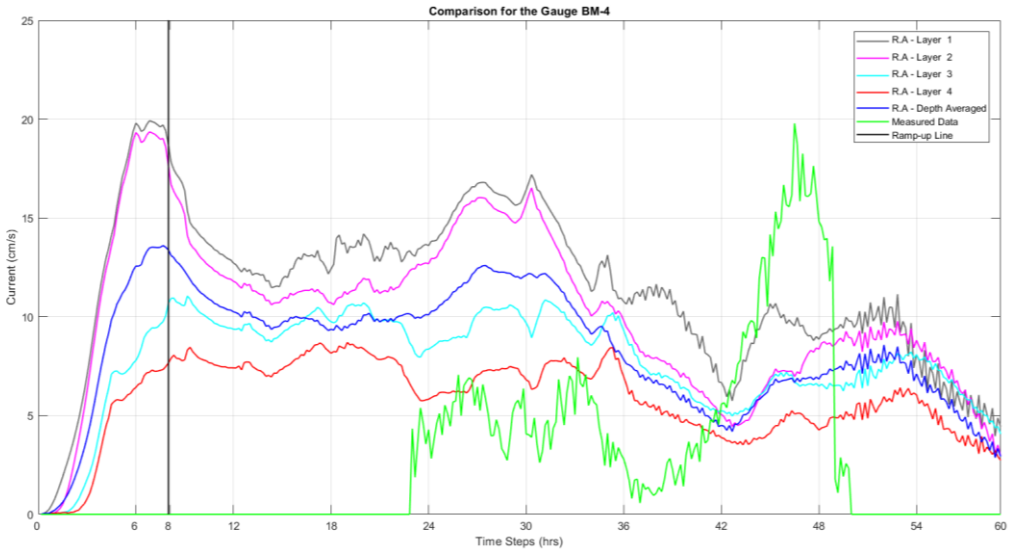

Figure 5.54. The Current Analysis for the Station Point – BM-4

(1st Layer = 0.61m, 2nd Layer = 1.82m, 3rd Layer = 3.03m, 4th Layer = 4.24m)

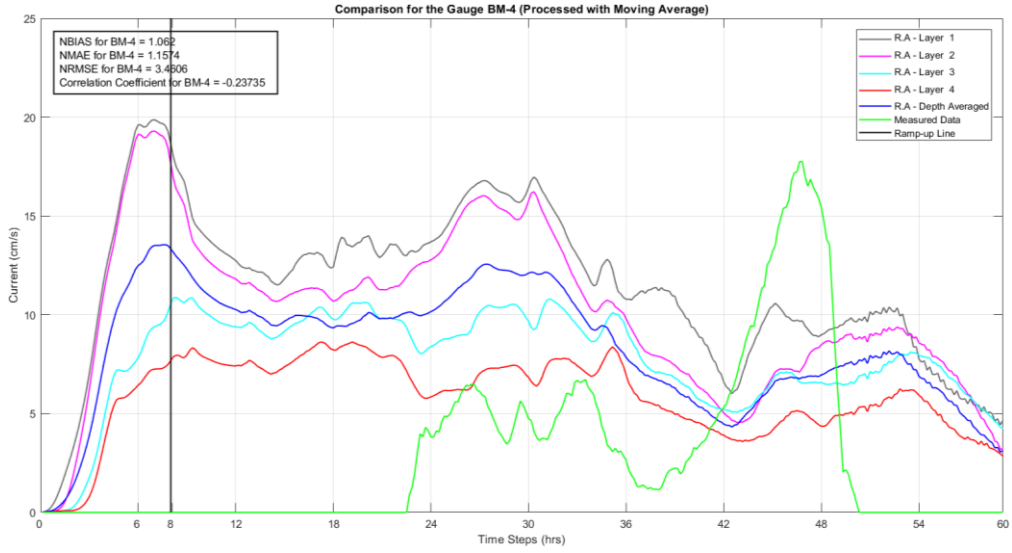

Figure 5.55. The Current Analysis for the Station Point – BM-4 (Smoothed)

(1st Layer = 0.61m, 2nd Layer = 1.82m, 3rd Layer = 3.03m, 4th Layer = 4.24m)

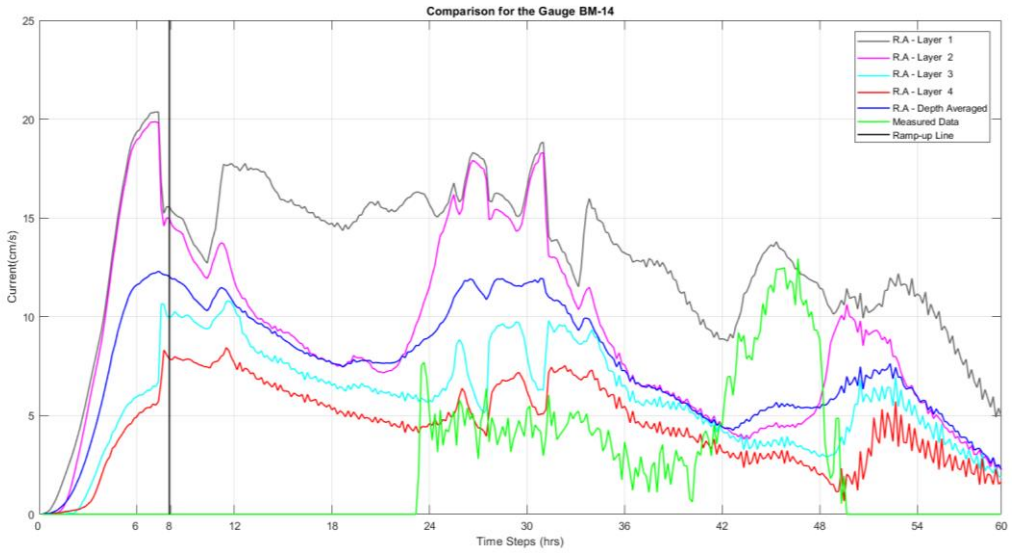

Figure 5.56. The Current Analysis for the Station Point – BM-14

(1st Layer = 0.86m, 2nd Layer = 2.58m, 3rd Layer = 4.30m, 4th Layer = 6.02m)

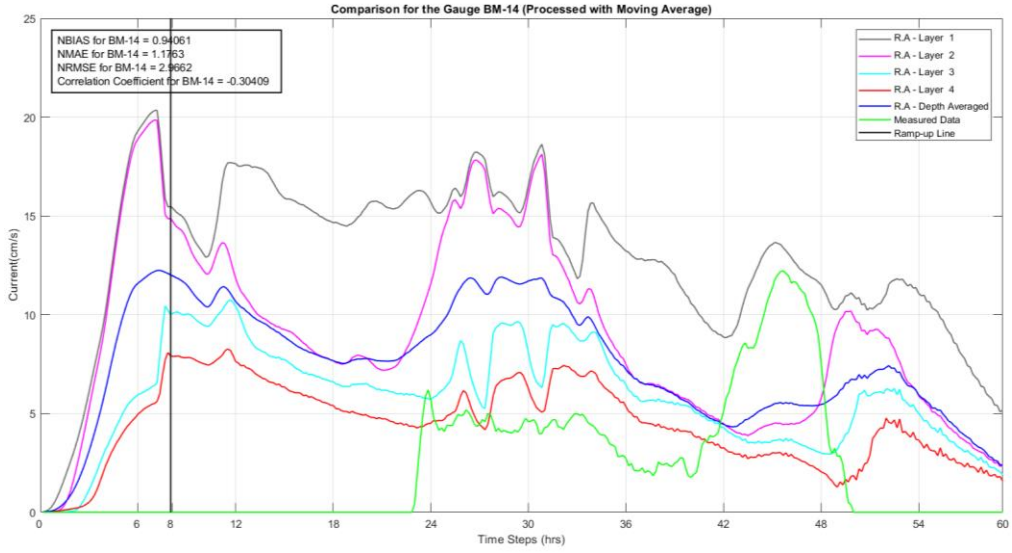

Figure 5.57. The Current Analysis for the Station Point – BM-14 (Smoothed)

(1st Layer = 0.86m, 2nd Layer = 2.58m, 3rd Layer = 4.30m, 4th Layer = 6.02m)

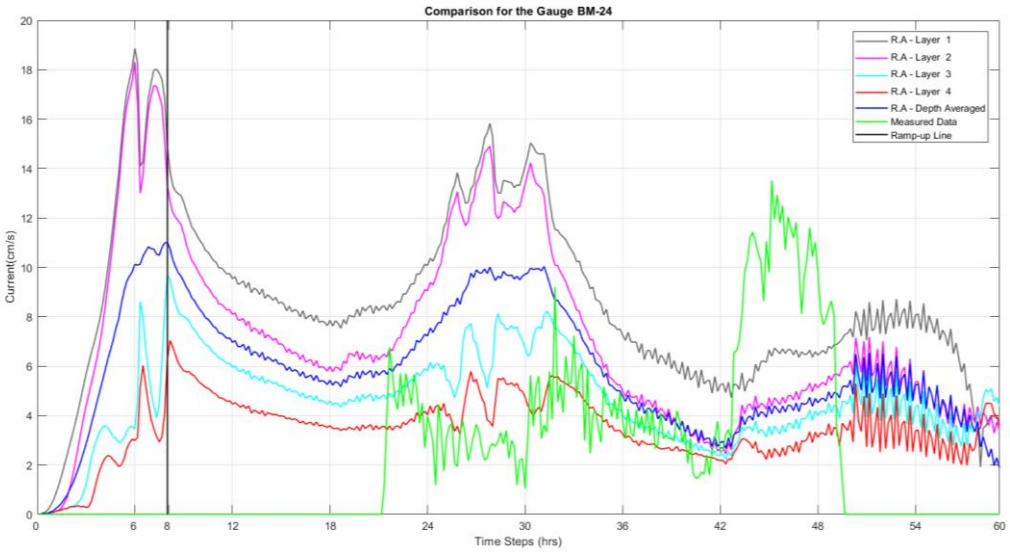

Figure 5.58. The Current Analysis for the Station Point – BM-24

(1st Layer = 0.50m, 2nd Layer = 1.49m, 3rd Layer = 2.48m, 4th Layer = 3.47m)

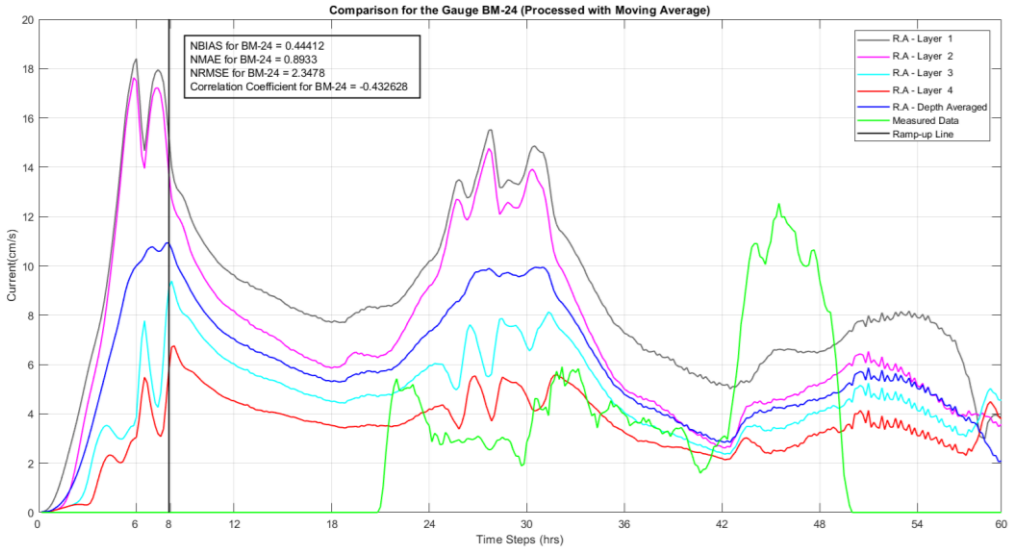

Figure 5.59. The Current Analysis for the Station Point – BM-24 (Smoothed)

(1st Layer = 0.50m, 2nd Layer = 1.49m, 3rd Layer = 2.48m, 4th Layer = 3.47m)

The result of the analysis on the station points BM-4, BM-14 and BM-24 shows that in the combined case, the model catches the trend and the magnitude of order in a better fashion. Yet, at some points like; the jump at the 45th hour, the model missed it on every station point (Figures 5.54-5.59).

Consequently, the general circulation pattern can be seen below, Figure 5.60-63, with the patterns are compatible with the previous solo cases. The maximum and the minimum speeds are achieved at the same hours, from among the previous selected punctual aspects.

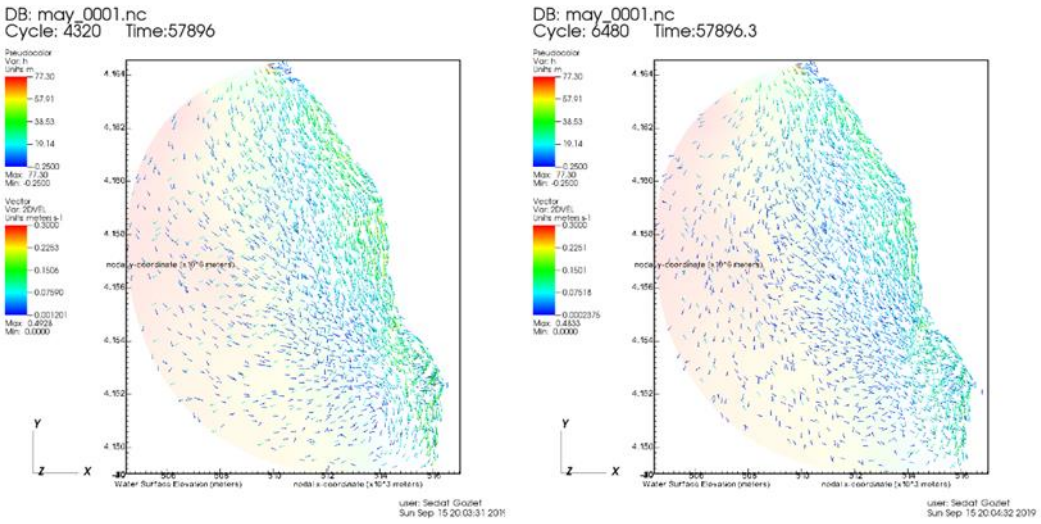

Figure 5.60. Circulation Pattern – May ’17 – All Combined Case (Hour: 12 & 18)

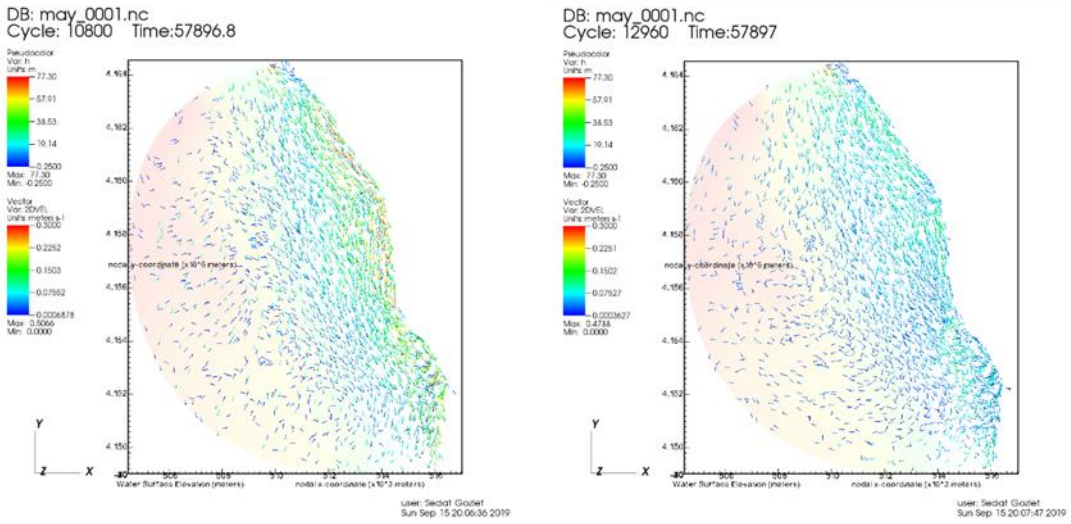

Figure 5.61. Circulation Pattern – May ’17 – All Combined Case (Hour: 30 & 36)

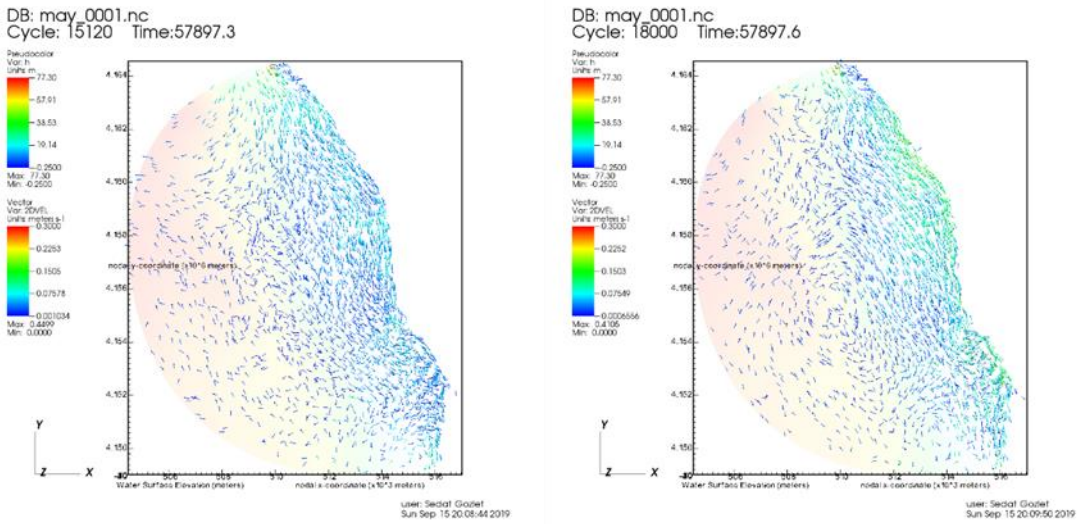

Figure 5.62. Circulation Pattern – May ’17 – All Combined Case (Hour: 42 & 50)

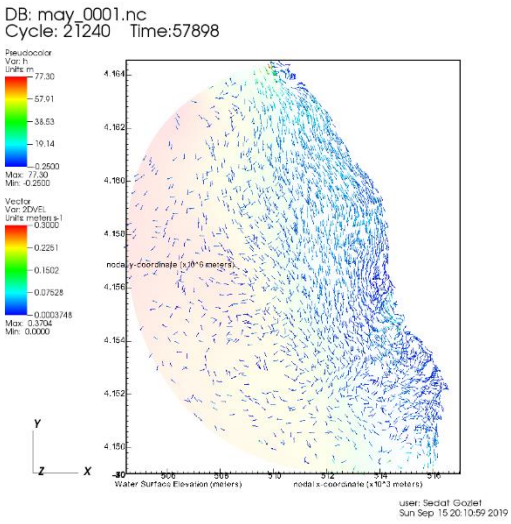

Figure 5.63. Circulation Pattern – May ’17 – All Combined Case (Hour: 59)

Furthermore, the salinity and the temperature analyze results can be seen on the figures; 5.64 and 5.65. Even the salinity results have a good proximity, the temperature results do not have a considerable disagreement.

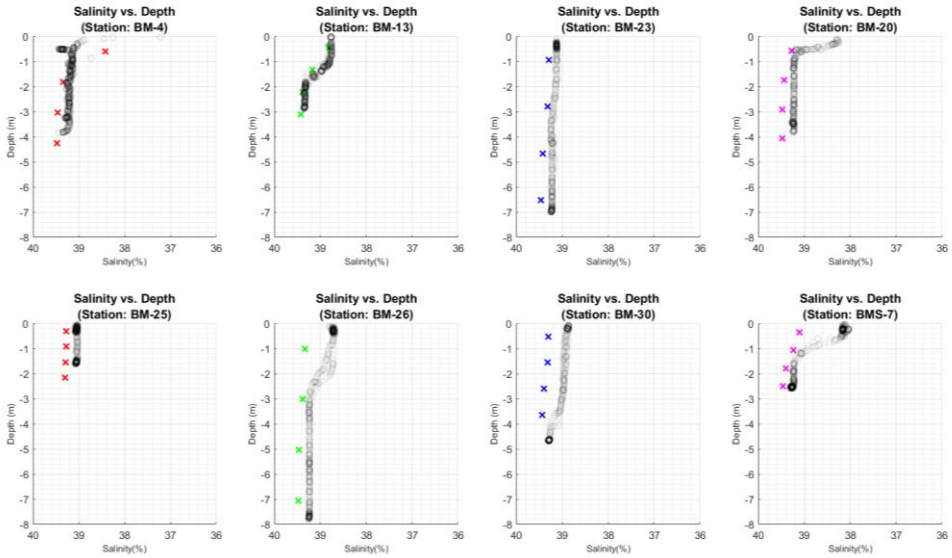

Figure 5.64. Salinity - May ’17

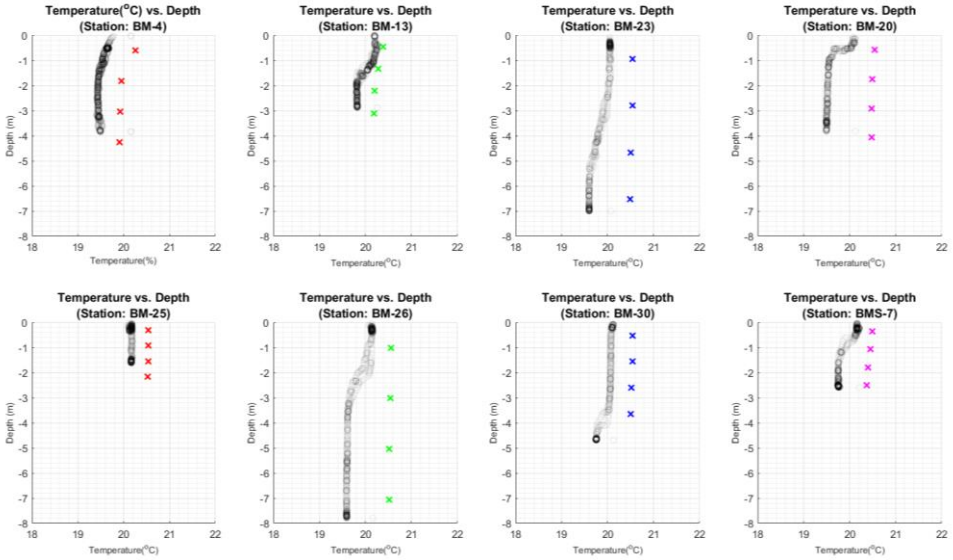

Figure 5.65. Temperature - May ’17

As for the salinity and the temperature data collected during the expedition at several stations are compared to the model output. The stations were chosen as closer as for the similarity for all cases. The results are presented in Figures 5.64, and 5.65. The salinity outputs of the model are usually in good agreement with the measurements at most stations and along the water column (Figure 5.64). The stations closer to river mouth shows the mixing of salt-water and fresh water and this transition is reflected in the model results as well. Some stations are in very shallow depths and for those stations the model did not perform very well for the surface layer.

5.2.3. October ‘17

The third case modeled is based on the expedition done on the 18 & 19 March 2017. The river data is taken from TUBITAK project data. Wind data is from CFSv2 dataset and the open boundary forcing is done by sea level data from Bodrum mareograph station. Constant water temperature and salinity is used throughout the domain as 20.61°C & 39.48 ‰ based on the field measurements. The computational time of 2.5 days took 4-7 hours depending on the processor and forcing types.

The results have been subjected to a smoothing operation via MATLAB for ease of use in statistical calculations of error measures. In order to analyze the contribution of each forcing type on the overall circulation system, several runs were performed such as tide only forcing, wind only forcing, river only forcing. Finally, the actual forcing combination (tide, river and wind together) is modeled. All the runs include the Coriolis effect. The original model output is provided for the case with all forcing types. The rest of the results are presented after the smoothing process.

5.2.3.1. Tide-Only Case

In this case of May – ’17, as a changing parameter, only tide was implemented the model. The arbitrary check points and tide input can be seen on the figure 5.66.

As of no river input exists, there was no salinity and temperature alterations.

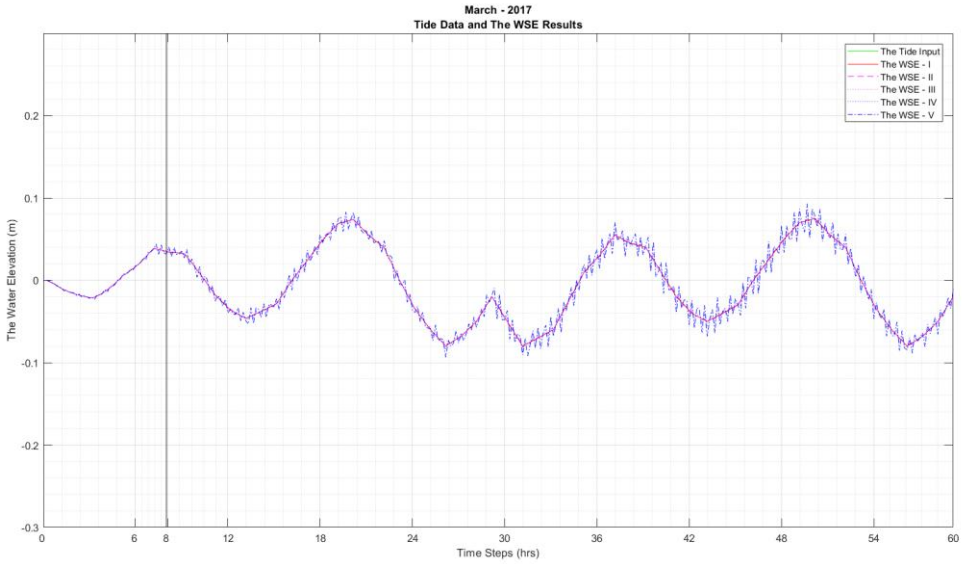

Figure 5.66. The Analysis Result for the OB and the Tide Check Points

The result of the analysis on the station points BM-32, BM-31 and BM-4 by means of current speeds are in order of magnitude 0.015 cm/s. From the figures 5.67 - 5.69. It is hard to state a clear correlation between the measurements and the analysis.

Consequently, the general circulation pattern, on the hours 43nd, 47th, 50th and 53st, can be seen between the Figures 5.70-5.71. In these figures, it can be understood that; the patterns of 47th and 53th hours belong to an hour that water elevation gets closer to mean sea level, on the other hand, the pattern of 50th hour belongs a high tide and 43rd, a low tide. As expected, on the hour 53rd water moves out of the domain, on the other hand, on the hour 47th, it moves through inside the domain.

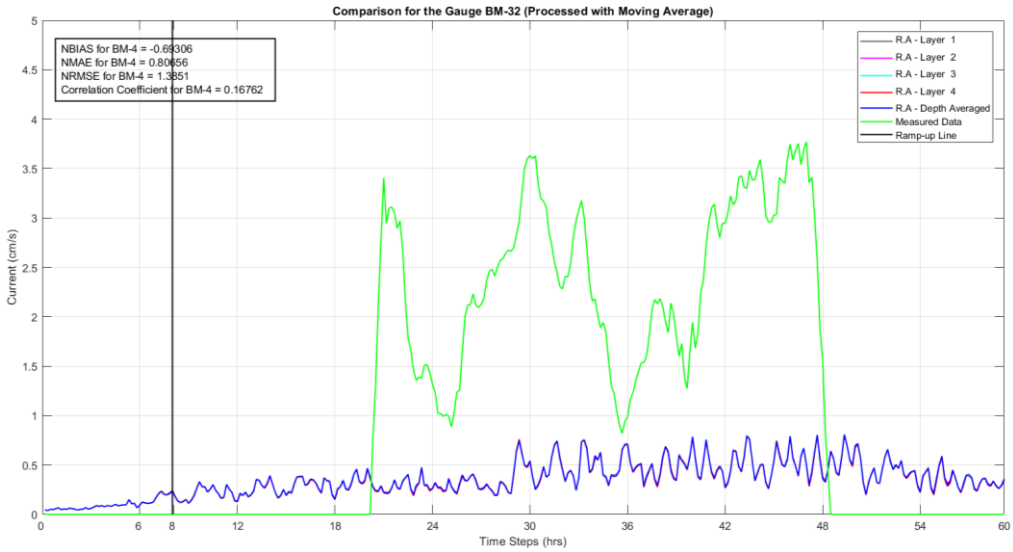

Figure 5.67. The Current Analysis for the Station Point – BM-32 (Smoothed)

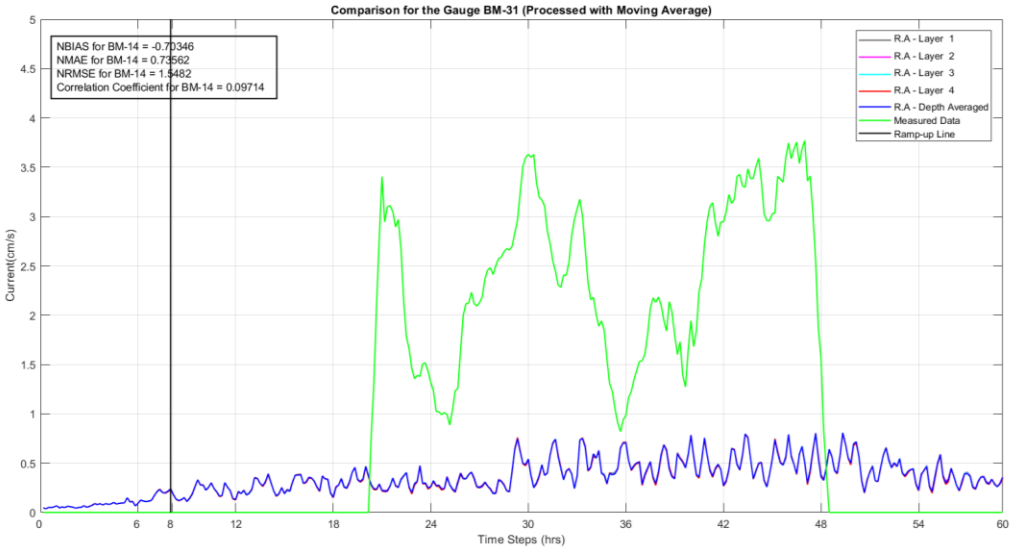

Figure 5.68. The Current Analysis for the Station Point – BM-31 (Smoothed)

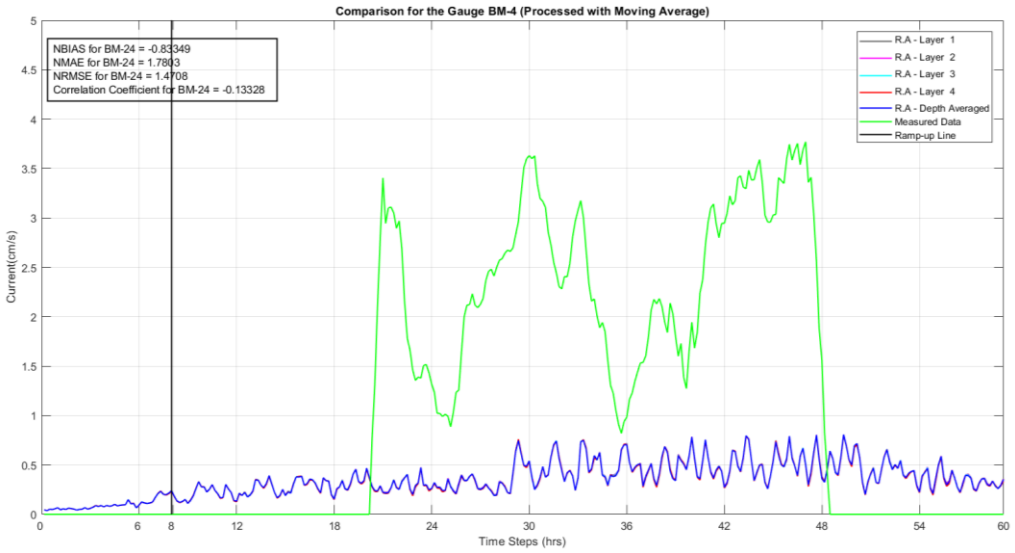

Figure 5.69. The Current Analysis for the Station Point – BM-4 (Smoothed)

Except for the May ’17 case, Tide-Only case for October ‘17 is shown again due to its importance for the all combined case. From the Figures 5.67 to 5.69 it is clear that tidal forcing has an effect on the current stations approximately 10 to 15 per cent.

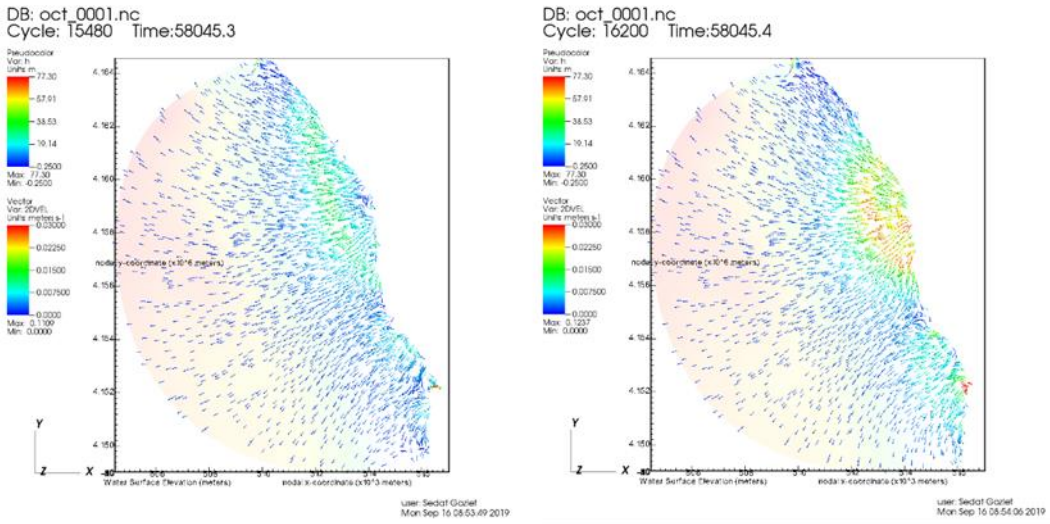

Figure 5.70. Circulation Pattern – May ’17 – Tide Only Case (Hour: 42 & 46)

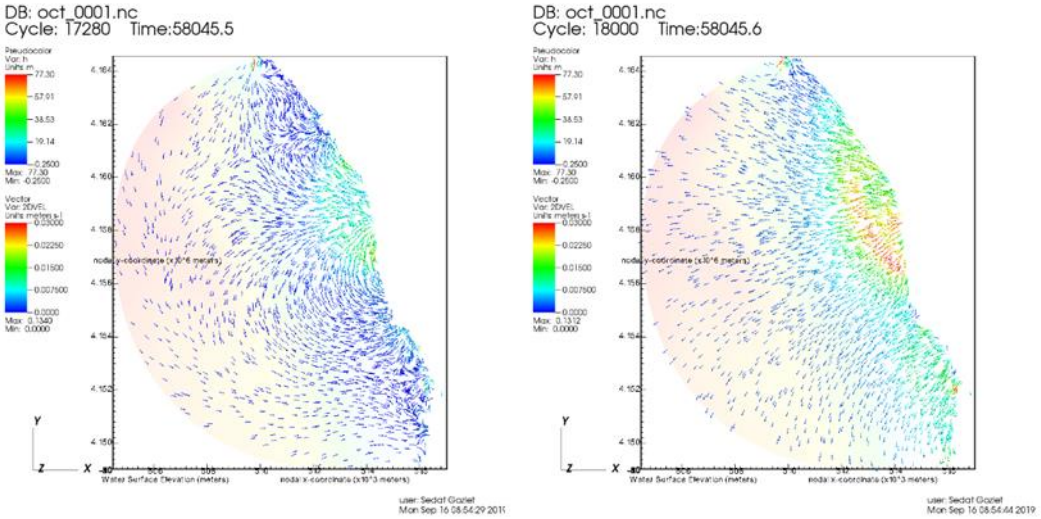

Figure 5.71. Circulation Pattern – May ’17 – Tide Only Case (Hour: 50 & 53)

Finally, the pattern for circulation, on the hours 42nd, 46th, 50th and 53st, can be seen between the Figures 5.70-5.71. In these figures, it can be understood that; the patterns of 42nd and 46th hours belong to an hour that water elevation gets closer to mean sea level, on the other hand, the pattern of 46th hour belongs a high tide and 50th, a low tide. As expected, on the hour 50th water moves out of the domain, on the other hand, on the hour 53rd, it moves through inside the domain.

5.2.3.2. River-Only Case

In this case of May – ’17, as a changing parameter, only river was implemented the model. The arbitrary check points and river input can be seen on the Figure 5.72. As the data source DSI was used, which has a time resolution of 12 hours. Salinity and temperature changes observed due to the river transport of those parameters.

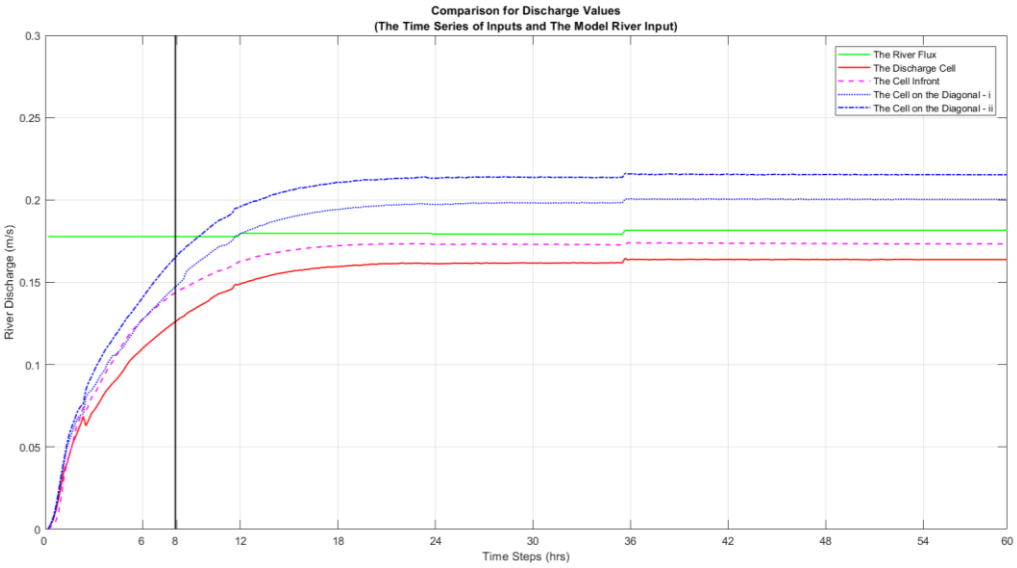

Figure 5.72. The Analysis Result for the Discharge Node and the Control Cells

The result of the analysis on the station points BM-32, BM-31 and BM-4 by means of current speeds are in order of magnitude 0.05 m/s. The data has a stable shape parallel with the changes in the direction of decrease as accordance with the daily data

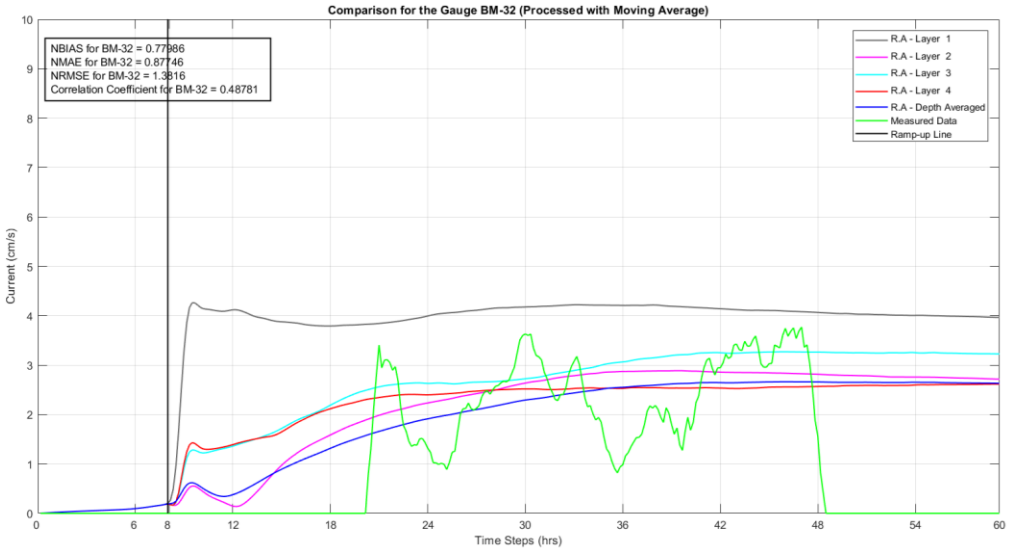

Figure 5.73. The Current Analysis for the Station Point – BM-32 (Smoothed)
(1^{st} Layer = 0.61m, 2^{nd} Layer = 1.82m, 3^{rd} Layer = 3.03m, 4^{th} Layer = 4.24m)

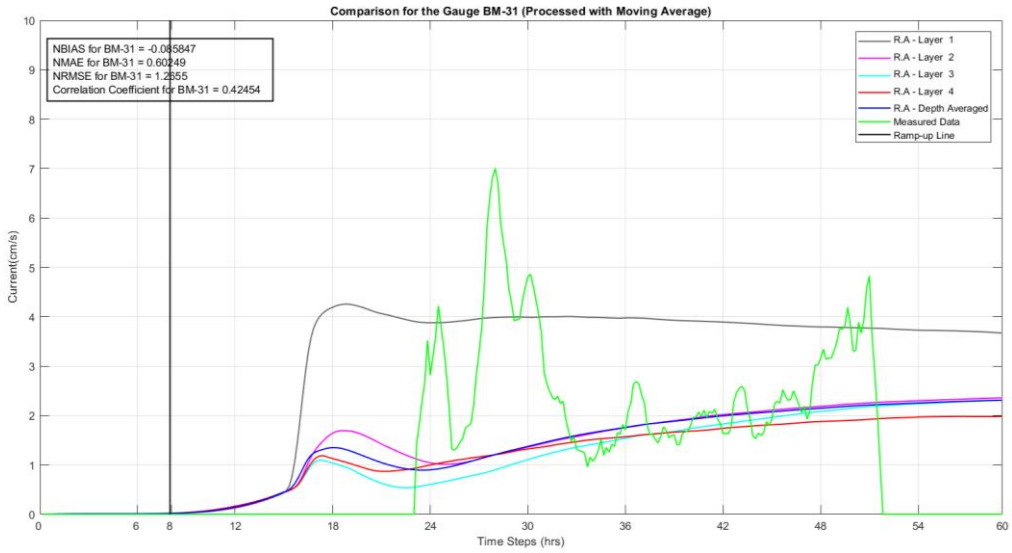

Figure 5.74. The Current Analysis for the Station Point – BM-31 (Smoothed)
(1st Layer = 0.49m, 2nd Layer = 1.48m, 3rd Layer = 2.47m, 4th Layer = 3.46m)

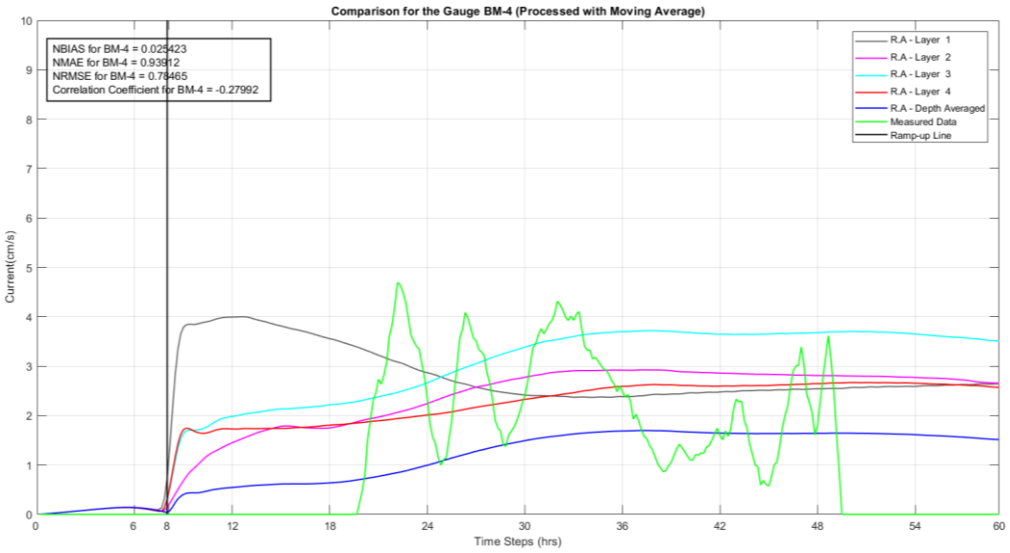

Figure 5.75. The Current Analysis for the Station Point – BM-4 (Smoothed)
(1st Layer = 0.61m, 2nd Layer = 1.82m, 3rd Layer = 3.03m, 4th Layer = 4.24m)

Consequently, the general circulation pattern can be seen at the below, from the Figure 5.76, and 5.77 since there is no critical change after the system has been stabilized, three snapshots of the system enough for it to summarize the behavior. Since the river runs a speed that very close constant 0.2 m/s, there exist no drastic direction or magnitude change. Only at the offshore part of the domain, vortices occur, and they don't dissipate.

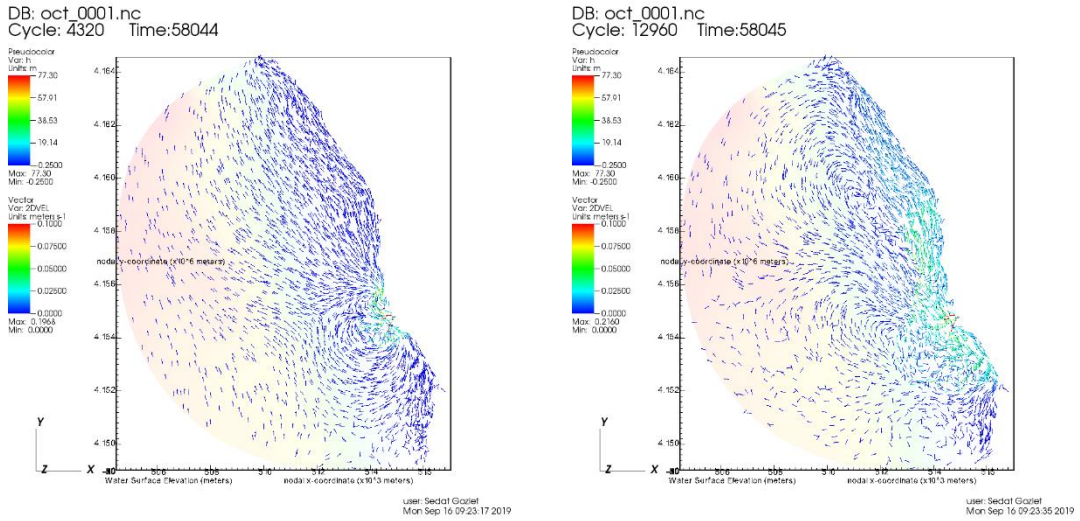

Figure 5.76. Circulation Pattern – May '17 – River Only Case (Hour: 12 & 36)

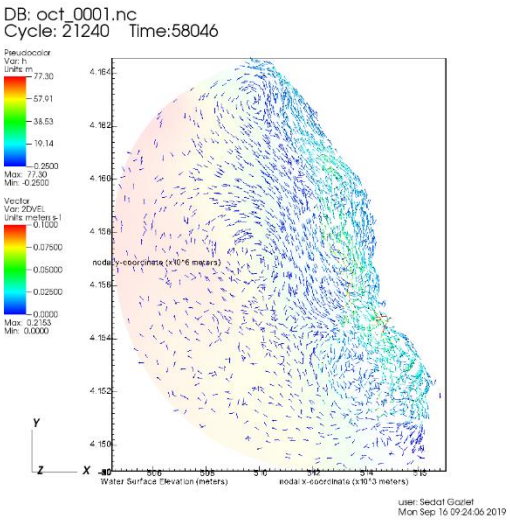

Figure 5.77. Circulation Pattern – May '17 – River Only Case (Hour: 59)

5.2.3.3. Wind-Only Case

In this case of May – ’17, as a changing parameter, only wind was implemented the model. The change in the wind speed can be seen from the Figure 5.78.

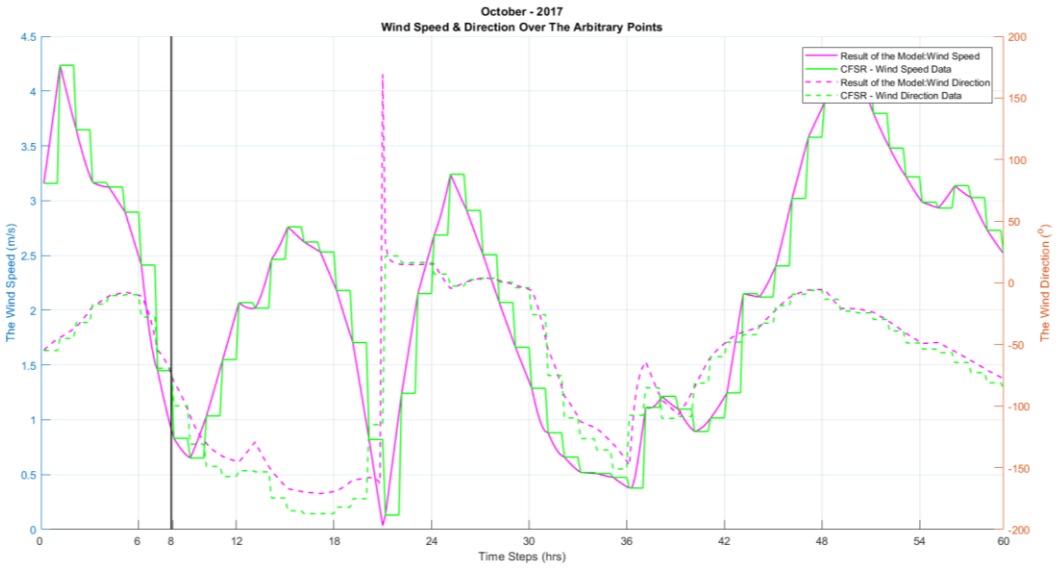

Figure 5.78. The Speed and The Direction of Wind over the Domain

As it can be seen from the Figure 5.78 above, on the hours 15, 25 and 50, the wind makes local maximums and on the hours 21 and 36 the wind make local minimums, where changes in the circulation pattern will be observed, either by means of magnitude or direction, depending on the change in the wind direction and magnitude.

The result of the analysis on the station points BM-32, BM-31 and BM-4 by means of current speeds are in order of magnitude 0.05 cm/s. The trend of the data behaves similarly for all sampling period, especially on the stations BM-32, BM-31 and partially BM-4 (Figure 5.79-5.81).

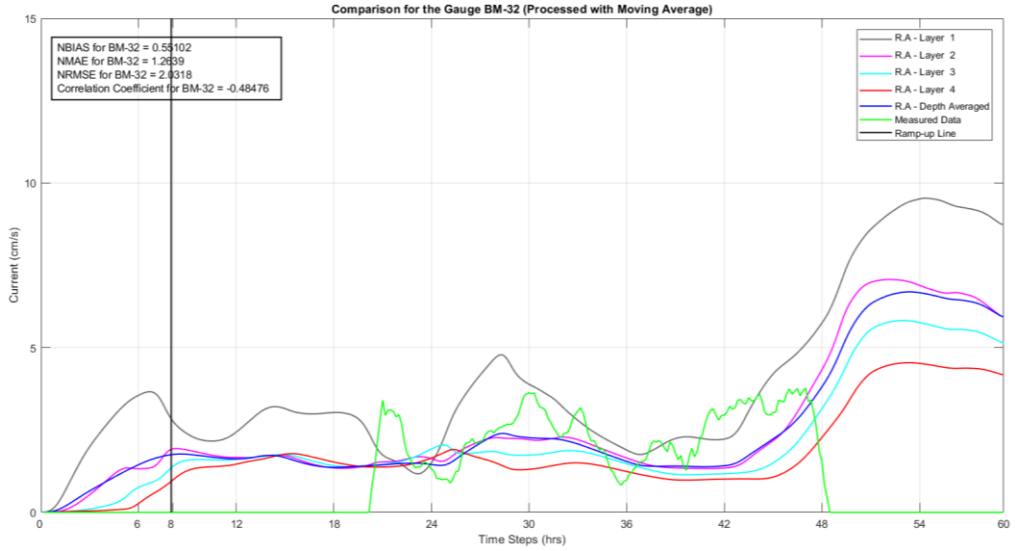

Figure 5.79. The Current Analysis for the Station Point – BM-32 (Smoothed)
(1st Layer = 0.49m, 2nd Layer = 1.48m, 3rd Layer = 2.47m, 4th Layer = 3.46m)

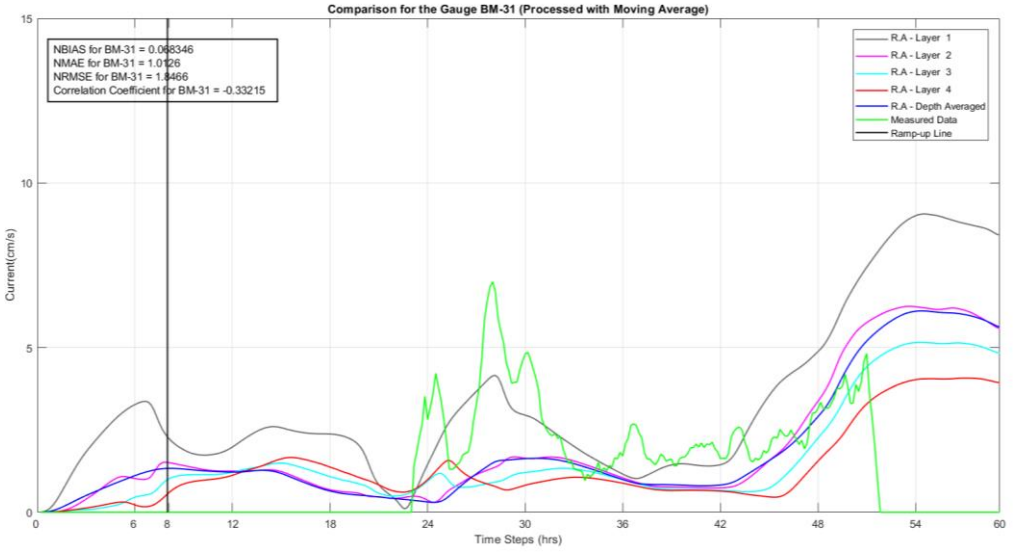

Figure 5.80. The Current Analysis for the Station Point – BM-31 (Smoothed)
(1st Layer = 0.59m, 2nd Layer = 1.78m, 3rd Layer = 2.96m, 4th Layer = 4.15m)

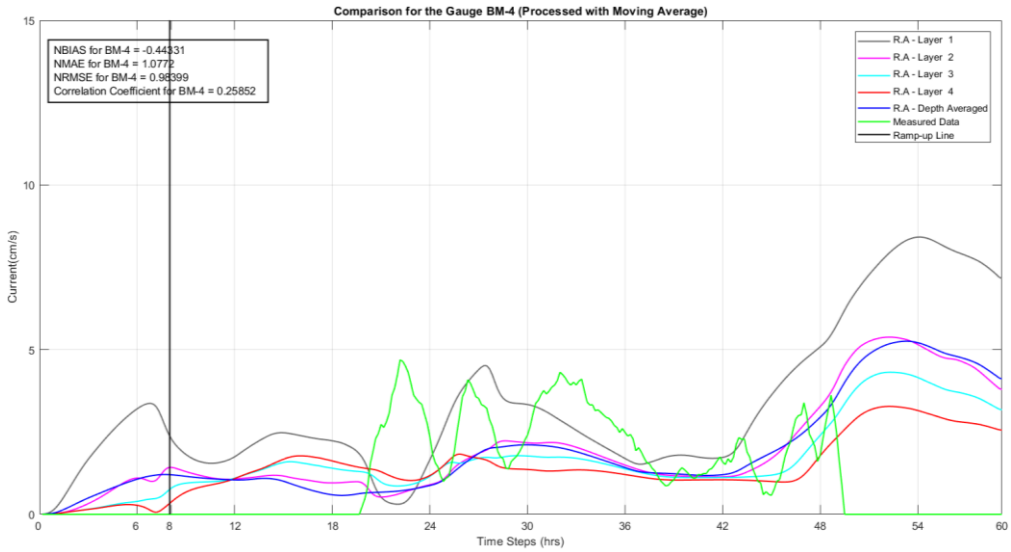

Figure 5.81. The Current Analysis for the Station Point – BM-4 (Smoothed)
(1^{st} Layer = 0.61m, 2^{nd} Layer = 1.82m, 3^{rd} Layer = 3.03m, 4^{th} Layer = 4.24m)

The result of the analysis reflected both of the input data characteristics and the measurement behavior, up to a point. The general circulation pattern firstly, mild slope regime (15^{th} hour), then, local maximums (28^{th} and 54^{th} hour), then local minima (42^{nd} hour) are shown below, Figure 5.82-5.83.

The effect of the fourth peak (see the Figure 5.78) can be seen clearly at the shallow depths of the region, ignoring the values penetrating from the northern part, which were reduced with the sponge nodes, the highest current speeds were achieved within this local maxima up to a value of 0.12 m/s, nearly.

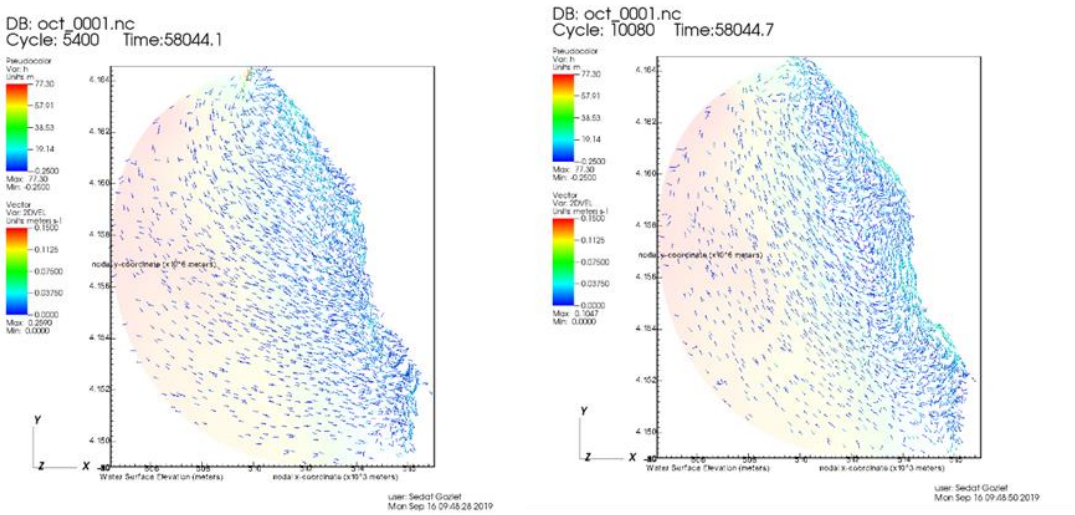

Figure 5.82. Circulation Pattern – October ’17 – Wind Only Case (Hour: 15 & 28)

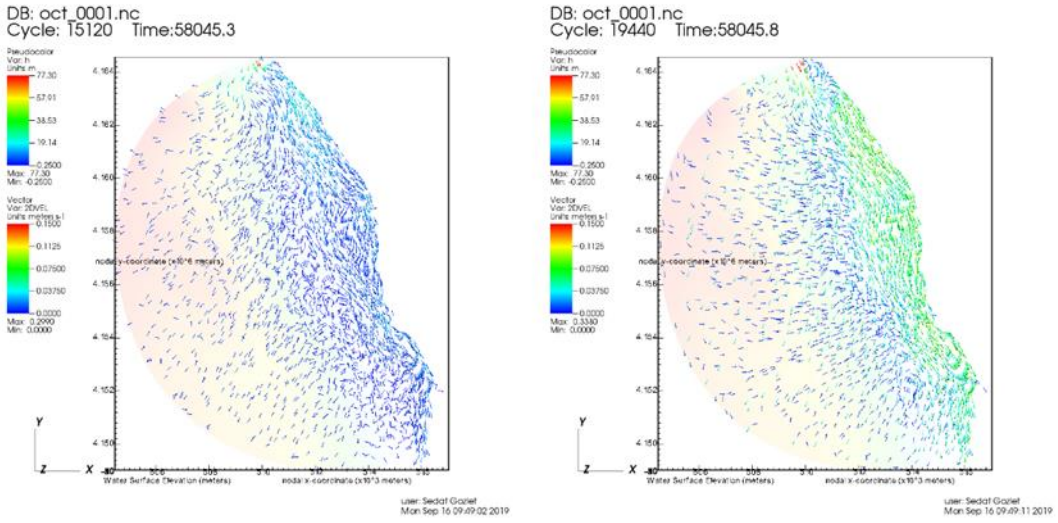

Figure 5.83. Circulation Pattern – October ’17 – Wind Only Case (Hour: 42 & 54)

5.2.3.4. All Parameters Combined Case - Actual Event

In this case tide, river and wind parameters were implemented the software as time series. The Coriolis forcing was open.

Salinity and temperature changes observed due to the river transport of those parameters.

For circulation pattern and the observation stations, the previous changes will be tried to be observed in this combined case. These forces either will superpose or damp each other.

The result of the analysis on the station points BM-32, BM-31 and BM-4 shows that in this calibrated case, the model catches the trend and the magnitude of order in a better fashion. Yet, there are some points that the model missed the trend of observation data (Figures 5.84-5.89).

Not only the depth average results, but also the data collected for each layer show a very good representation of the trend of the current observations for the stations 31 and 32, in terms of magnitude and trend. For the station named BM-4 the trends cannot be reflected with the station data, on the other hand the magnitude of order was achieved.

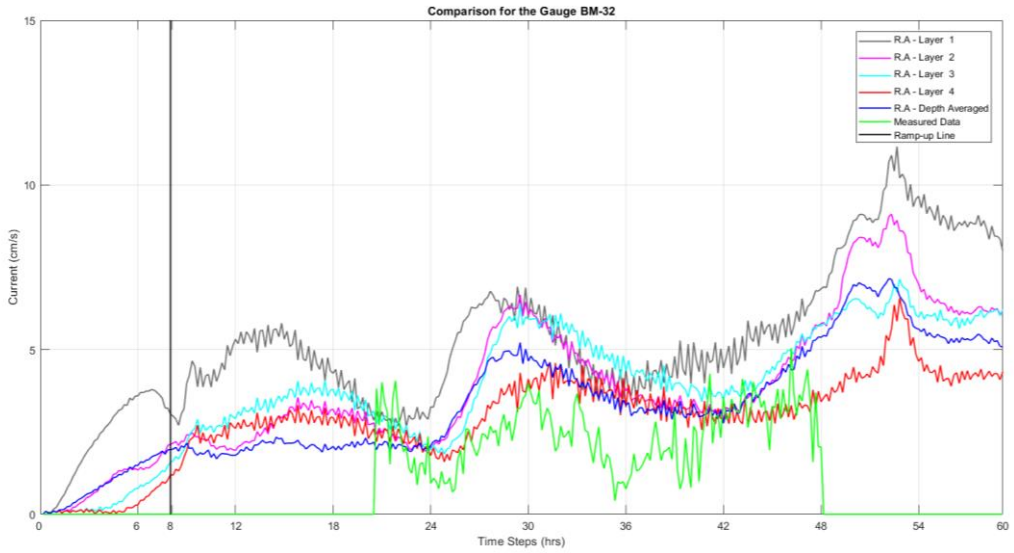

Figure 5.84. The Current Analysis for the Station Point – BM-32

(1st Layer = 0.49m, 2nd Layer = 1.48m, 3rd Layer = 2.47m, 4th Layer = 3.46m)

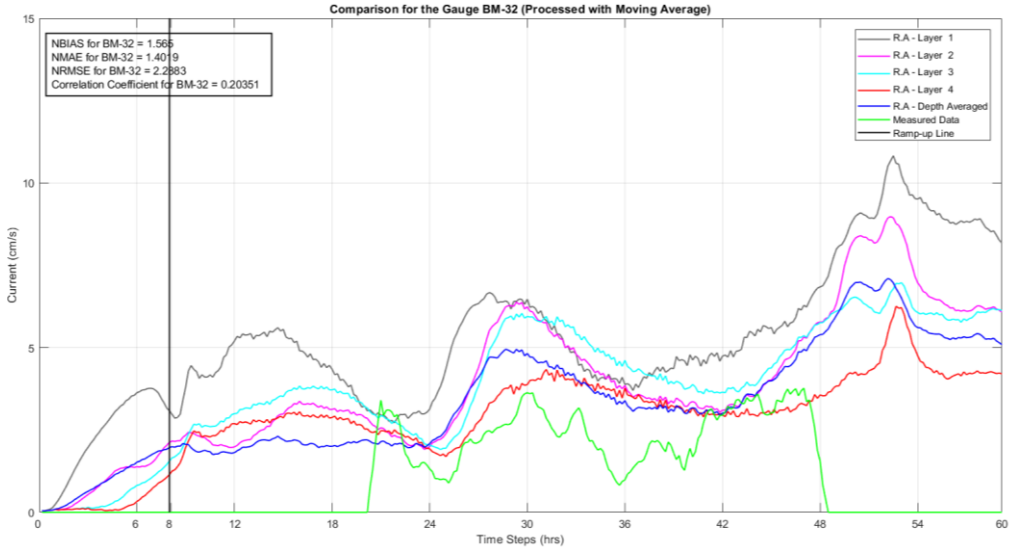

Figure 5.85. The Current Analysis for the Station Point – BM-32 (Smoothed)

(1st Layer = 0.49m, 2nd Layer = 1.48m, 3rd Layer = 2.47m, 4th Layer = 3.46m)

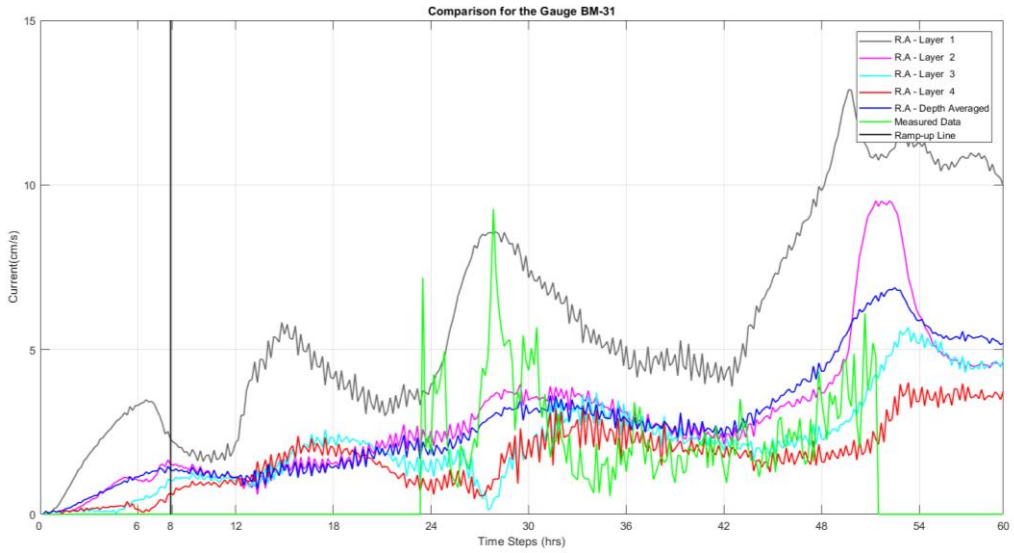

Figure 5.86. The Current Analysis for the Station Point – BM-31

(1st Layer = 0.59m, 2nd Layer = 1.78m, 3rd Layer = 2.96m, 4th Layer = 4.15m)

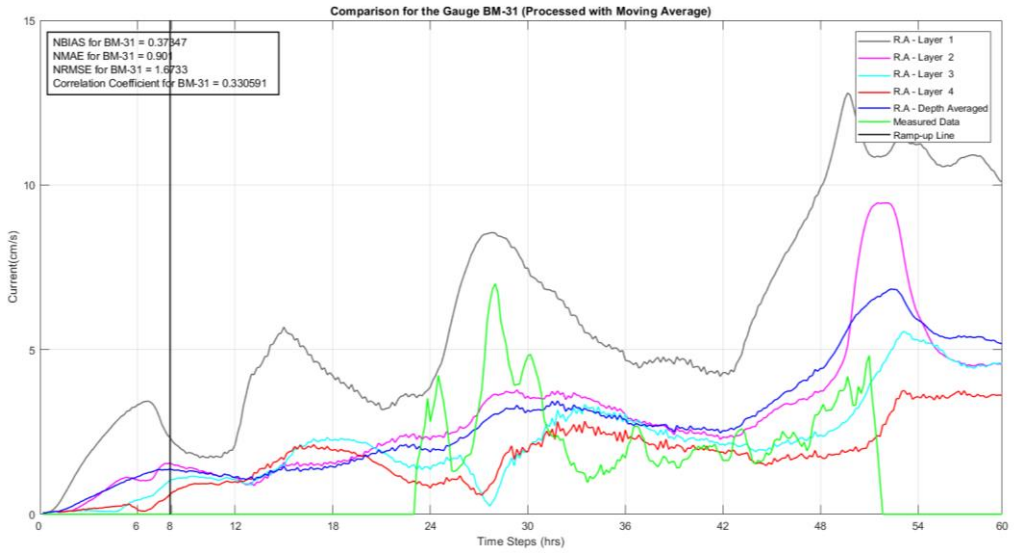

Figure 5.87. The Current Analysis for the Station Point – BM-31(Smoothed)

(1st Layer = 0.59m, 2nd Layer = 1.78m, 3rd Layer = 2.96m, 4th Layer = 4.15m)

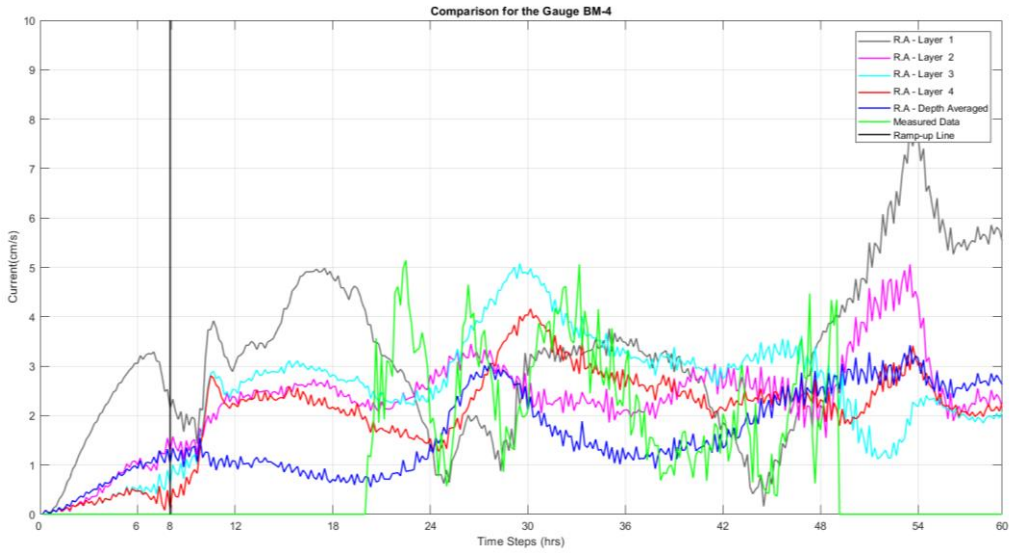

Figure 5.88. The Current Analysis for the Station Point – BM-4

(1st Layer = 0.61m, 2nd Layer = 1.82m, 3rd Layer = 3.03m, 4th Layer = 4.24m)

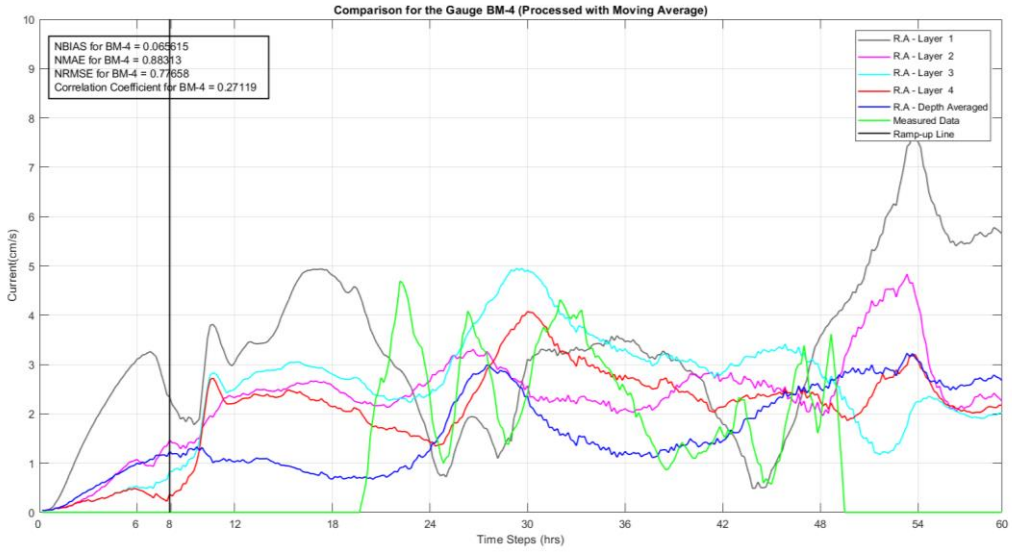

Figure 5.89. The Current Analysis for the Station Point – BM-4 (Smoothed)

(1st Layer = 0.61m, 2nd Layer = 1.82m, 3rd Layer = 3.03m, 4th Layer = 4.24m)

The circulation pattern can be seen below, Figure 5.90-93, with the patterns are compatible with the previous solo cases. The maximum and the minimum speeds are achieved at the same hours, from among the previous selected punctual aspects. In this case the wind component is the main driving factor for the region, the direction and the magnitude of current are in align with this component. Yet, from the previous cases (March and May), the tide component is stronger, and the river component has a slightly less influence on the current regime inside the bay.

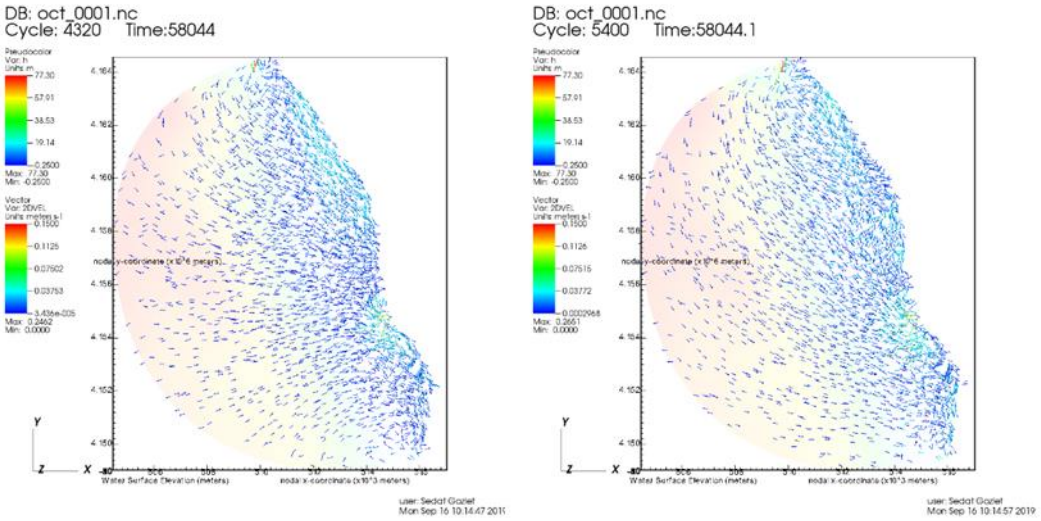

Figure 5.90. Circulation Pattern – October ’17 – All Combined Case (Hour: 12 & 15)

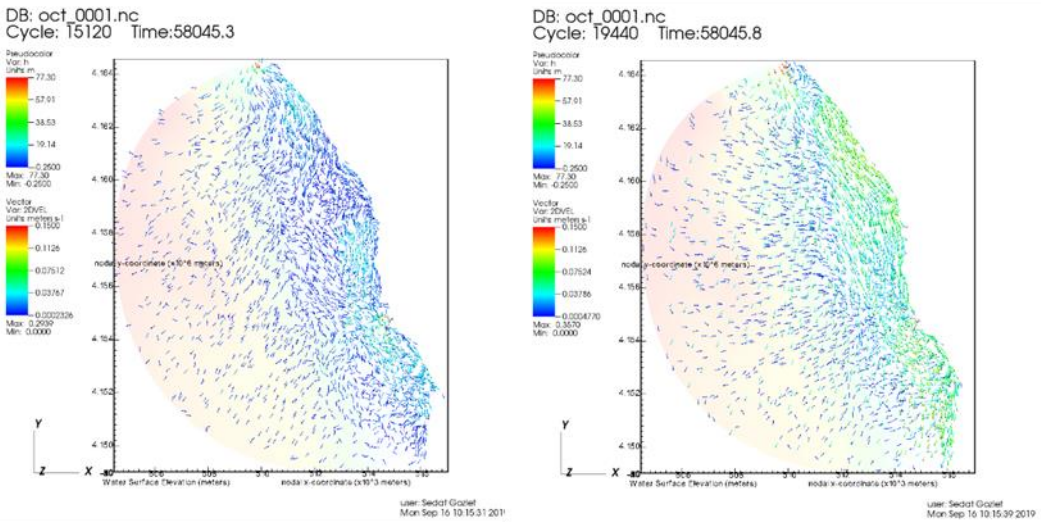

Figure 5.91. Circulation Pattern – October ’17 – All Combined Case (Hour: 28 & 36)

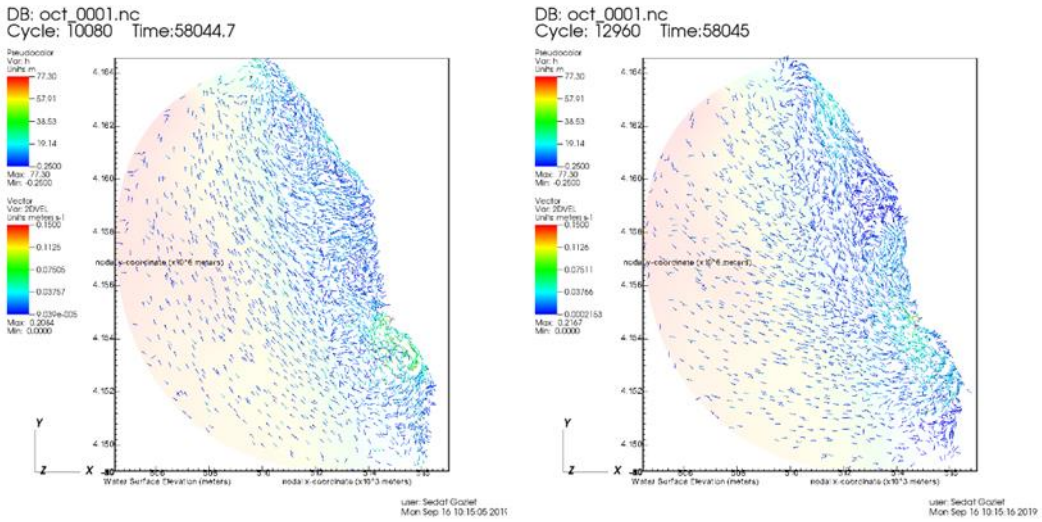

Figure 5.92. Circulation Pattern – October ’17 – All Combined Case (Hour: 42 & 54)

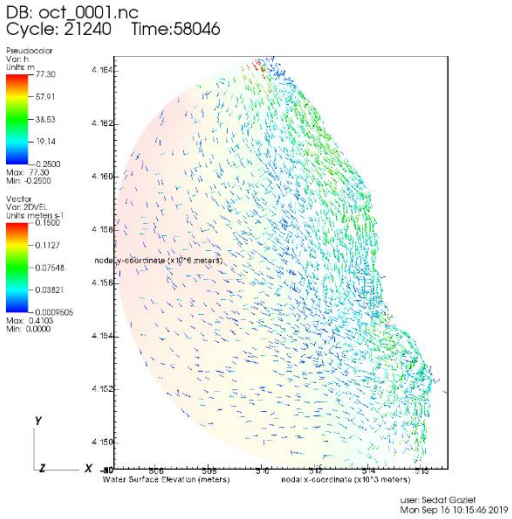

Figure 5.93. Circulation Pattern – October ’17 – All Combined Case (Hour: 59)

Furthermore, the salinity and the temperature analyze results can be seen on the Figures 5.94 and 5.95. Even the salinity results have a good proximity, the temperature results do not have a considerable disagreement. The stations nearer to river discharge point demonstrates the blending of salt-water and fresh water and this progress is

reflected in the model outcomes too. A few stations are in shallow profundities and for those stations the model didn't perform very well for the surface layer. Then again, the temperature results do not demonstrate a similar degree of precision as the saltiness. The pattern along the water segment is displayed well in the majority of the stations however the extents were not good with the perceptions.

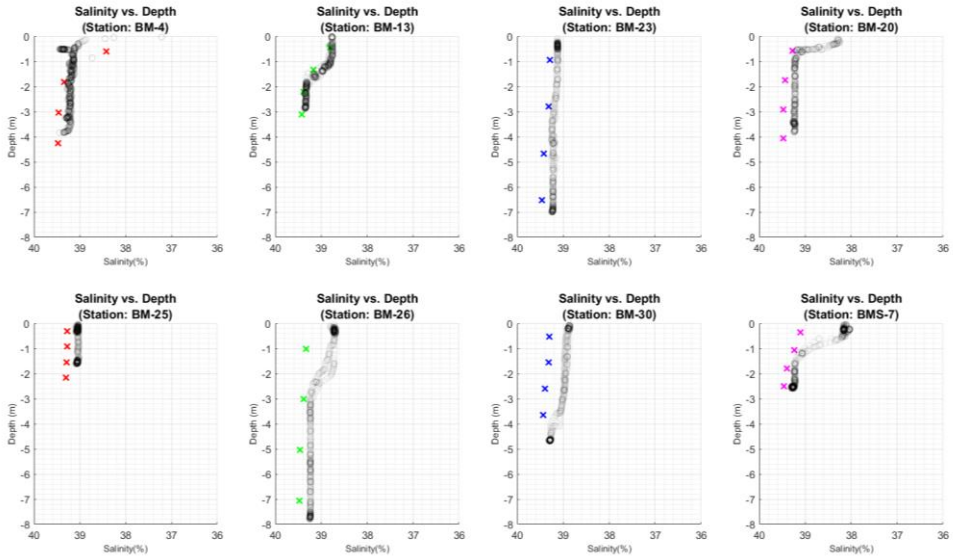

Figure 5.94. Salinity - October ’17

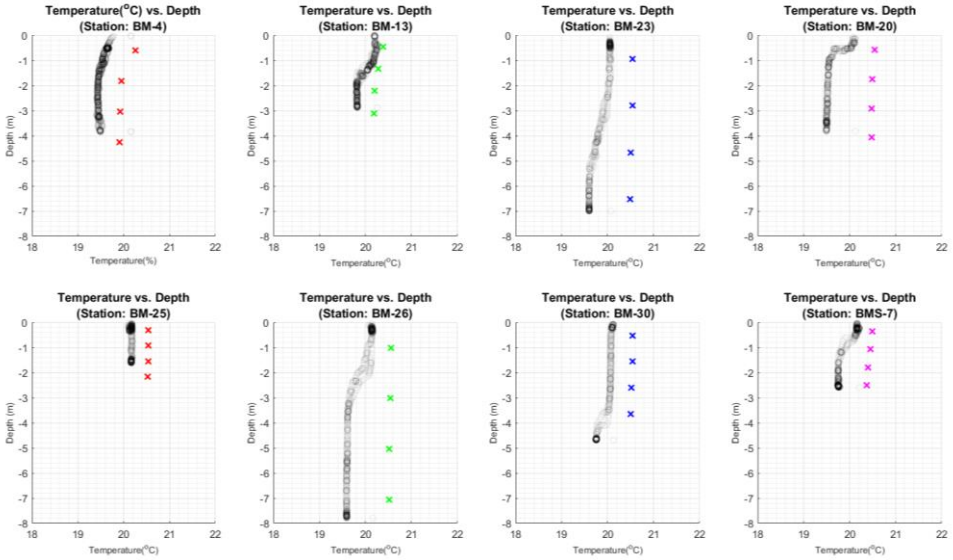

Figure 5.95. Temperature - October ’17

5.3. The Extreme Case – Actual Event

The model results of validation cases reflect the trend of the currents at the observation stations, the magnitudes are not very well matched. A calibration study could improve the performance of the model however the lack of data in terms of wind and waves makes it not practical. However, trends being matched with observations indicates that the model setup can represent the circulation patterns with a certain confidence. Therefore, a time period corresponding to extreme wind and river forcing is modeled to present the possible circulation pattern of the region.

This period is selected to represent two extreme forcing conditions back to back. January 9-19, 2016 represent the case with minimum river discharge while the last three days were the storm condition with the maximum wind speed. The river discharge and wind data are presented in Figure 5.96 and 5.97. The ramp-up time of the model was selected as 15 hours of simulation time. Temperature and salinity of the sea was used as 15.56°C and 37.44 ‰. The computational time of the simulation was approximately 34 hours. The circulation patterns as outputs of the model are presented in Figures 5.98 - 5.102.

This analysis is a combination of two different cases, in which the first case is between the dates 09-15 January that was included because it is a minimum case where the river runs its minimum values throughout the available data set. Furthermore, 15-19 January has been included in the analysis, due to having the maximum wind speed of allover the 40 years' data. The extreme wind analysis was conducted to detect this 'peak' value.

Moreover, the alignment of those two different cases, gave the chance of seeing the transition behavior from minimum to maximum.

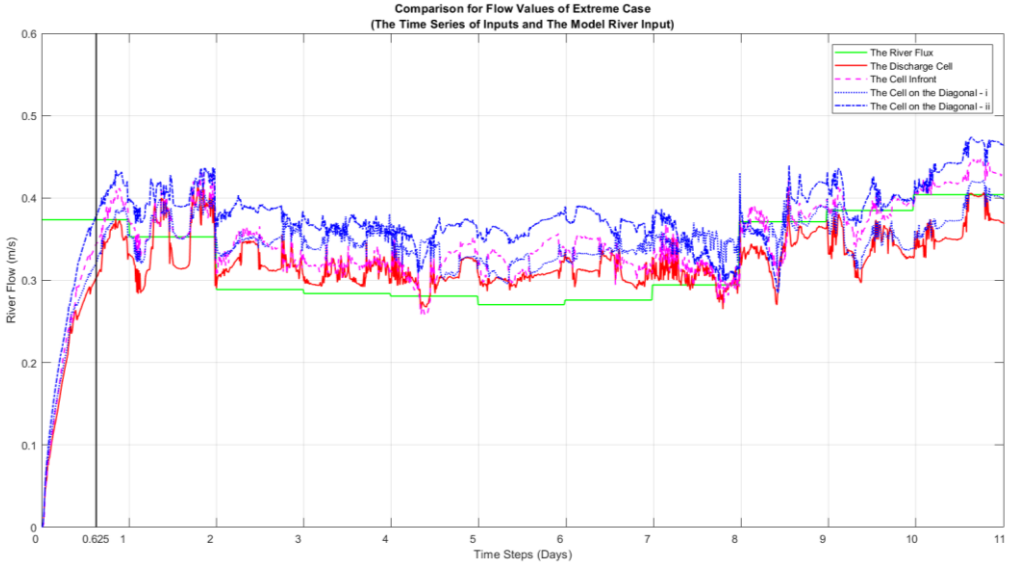

Figure 5.96. The Analysis Result for the Discharge Node and the Control Cells

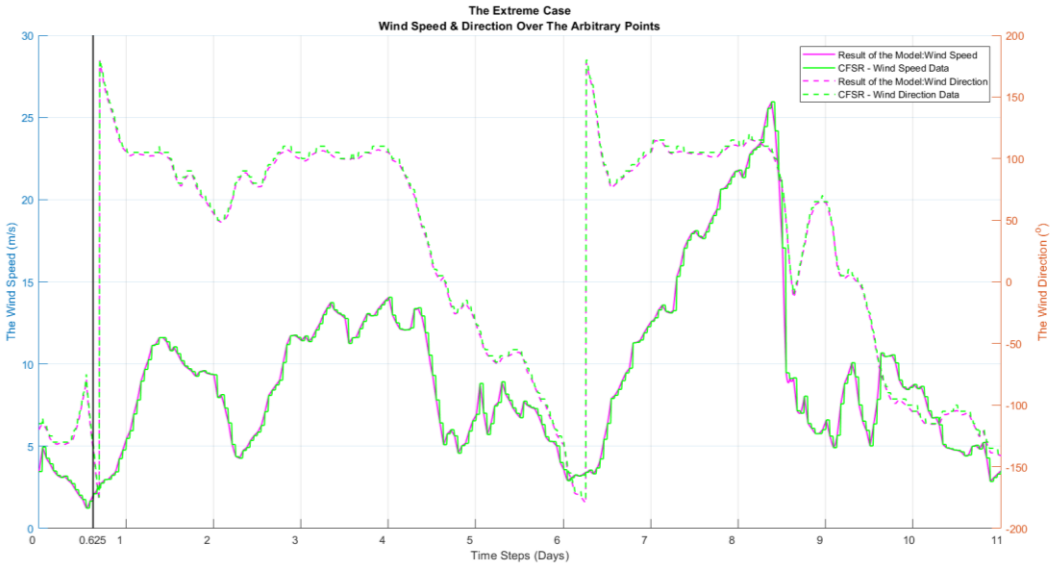

Figure 5.97. The Speed and The Direction of Wind over the Domain

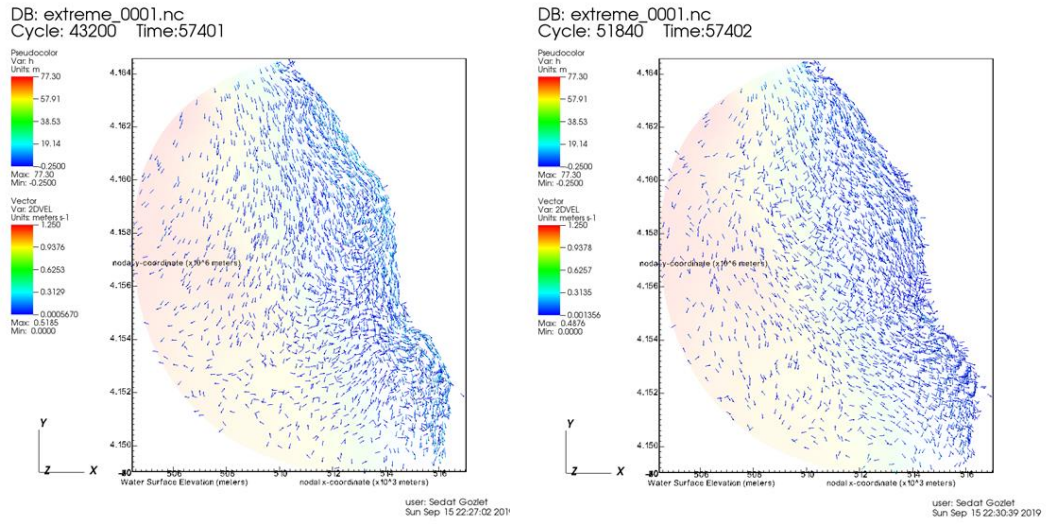

Figure 5.98. Circulation Pattern – The Extreme Case (Hour: 24 & 48)

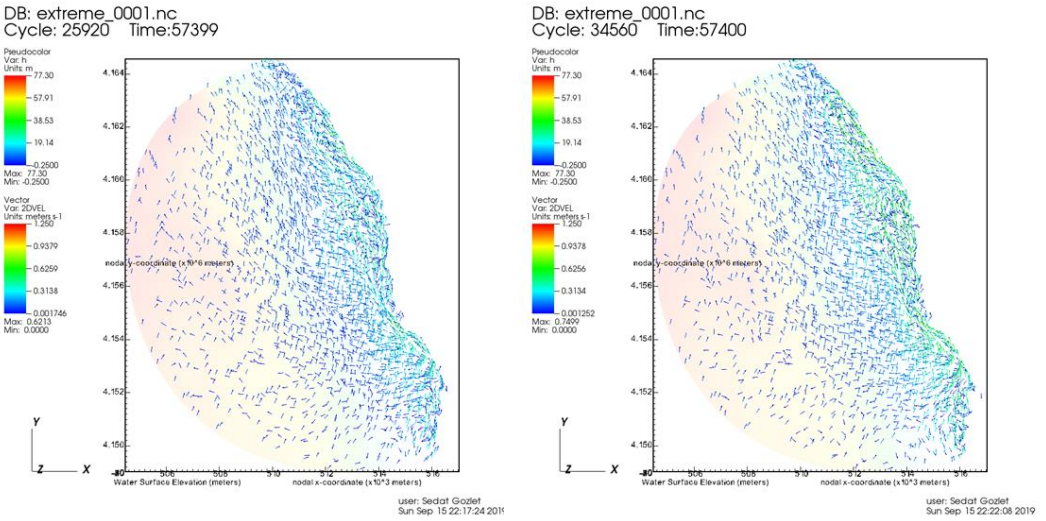

Figure 5.99. Circulation Pattern – The Extreme Case (Hour: 72 & 96)

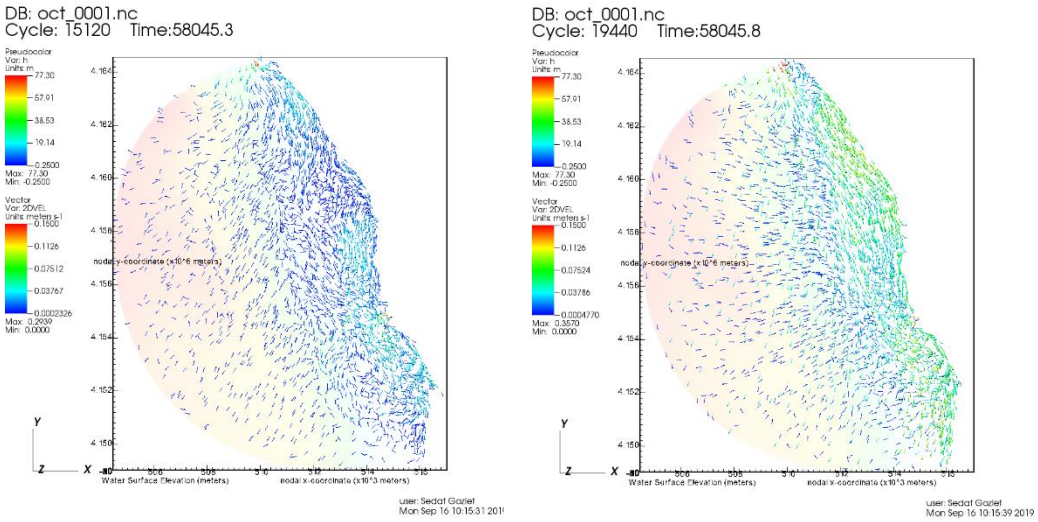

Figure 5.100. Circulation Pattern – The Extreme Case (Hour: 120 & 144)

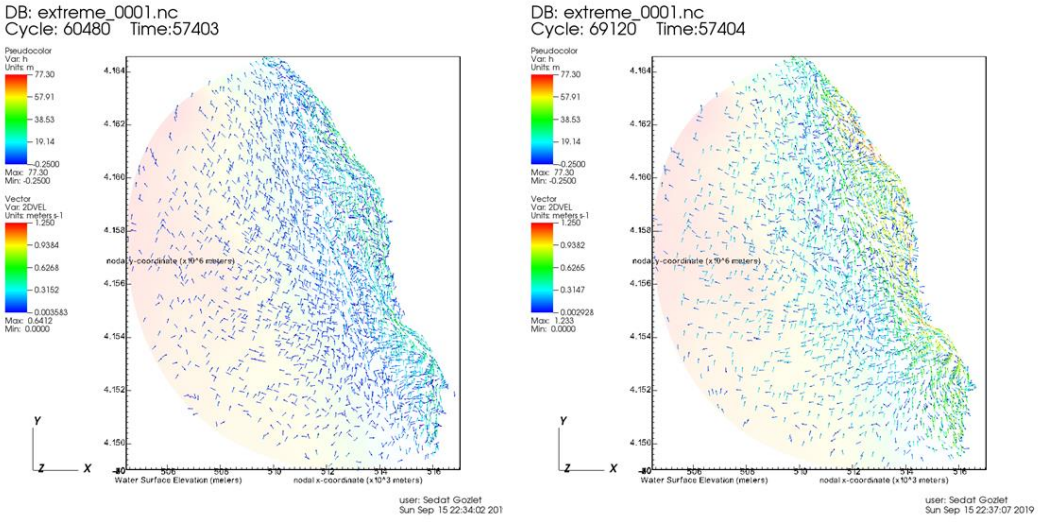

Figure 5.101. Circulation Pattern – The Extreme Case (Hour: 168 & 192)

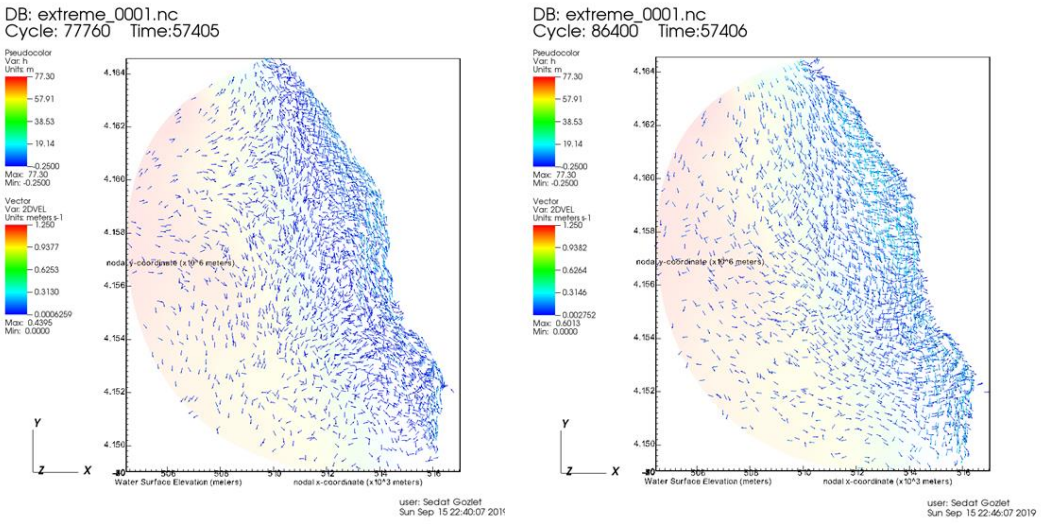

Figure 5.102. Circulation Pattern – The Extreme Case (Hour: 216 & 240)

For the extreme case analysis, as it was stated above, a research was conducted to find out if the event had a place on media, in both local and national scale. For that, the search span has been narrowed down to the day -January 9th, 2016- where the maximum wind speed of 40 years was measured. Furthermore, for spatial constraints, the proximity of computational domain was investigated.

For local media/press Söke, Didim and Kuşadası newspapers checked. On the 18th of January, Söke Express had a headline: "The storm and precipitation blew off the roofs, knocked down the trees: 50-ton roof blew up 2.5 meters, and fell to the other street". On the Figure 5.103 the newspaper clipping can be seen that describes the storm on the 17th of January.

Other than Söke, media agents from Aydın and Kuşadası had news about the storm which can be seen on the Figures below 5.104 and 5.105.

FIRTINA VE YAĞIŞ ÇATILARI UÇURDU, AĞAÇLARI DEVİRDİ

2.5 TONLUK ÇATI 50 METRE HAVALANDI BİR SOKAK ÖTEYE UÇTU

Söke Ekspres
Levent Tuncer

Söke'de yağış ve aynı zamanda fırtına etkili oldu. Bazı evlerin çatıları uçtu, ağaçlar devrildi. Can kaybının yaşanmaması sevindirdi.

2.5 TONLUK ÇATI 50 METRE HAVALANDI

Söke'nin Konak Mahallesi Abalaki Mevkii'nde Balaban Sokak'ta bulunan Enver Kıvılcım'a ait bir evin çatısı, yaklaşık 30 metre mesafedeki bir diğer Boğaziçi sokağa uçtu.

Devamı sayfa 4'de >>>

Figure 5.103. A Headline from Söke Express (18.01.2016) for the Storm of January 17th, 2016

Figure 5.104. Aydın Denge Newspaper (18.01.2016) : "Huge waves hit the shore at Didim"

Figure 5.105. Aydın Post (17.01.2016 – 13:58) : "Heavy Rain and Severe Storm At Kuşadası"

Moreover, on the national scale news agencies, the storm event was reported, like: Hürriyet, Milliyet, Habertürk and etc.

It can be concluded from the extreme case analysis and the news reports, the region, starting from the south – Didim to the north – Kuşadası, was subjected to an event that worth modelling both in the manners of magnitude and covering area.

CHAPTER 6

CONCLUSION AND DISCUSSIONS

In this thesis, the area of Büyük Menderes River Mouth and adjacent coastal field subjected to a modelling study to understand the flow dynamics inside the Balat Bay, under the effects of wind, river, tide, and Coriolis. Current and circulation patterns, salinity and temperature are the parameters discussed. An unstructured triangular mesh was created and optimized for the study area and FVCOM model results are validated with field data that have been taken during the expeditions held on the months March, May and October 2017. The parameters used for this assessment; temperature, salinity and mainly current.

Furthermore, for the extreme event on the date (09-19 January 2016), the consistency of the results is coherent in terms of intensity and the movement direction of flow when the blockage formation in front of the lagoon structure is taken into account.

Model setups performed satisfactorily for the validation cases for current and salinity observations. For temperature changed along the water column initial assumptions used in the model setup might have more effect. The tide is the least important component in the circulation system. River and wind forcings are more prominent for the basin. River has much impact for the river mouth as expected but the influence increases when the river discharge rates are higher. When river discharge rates are low, salinity intrusion into the river can be observed. Wind has the most dominant effect of the whole domain. However, the effect of the wind is observed with a lag in time which is actually expected and therefore modeled accurately by FVCOM.

An extreme historical event is also modeled to analyze the performance of model setup under extreme forcings.

As the possible failure sources: bathymetric data, in terms of merging process; using external data -like data set from State Hydraulic Works (DSI)- instead of in-situ measurements (due to lack or inconsistency); and above all, exclusion of wave parameter can be taken into account.

The recommendations for further studies can be listed as:

- In order to understand and replicate the circulation phenomena in the bay, waves are, also, need to be included by enabling SWAN couple of FVCOM. This parameter is important for conditions where wind speeds are high enough to generate significant waves.
- Current measurements should be performed for longer durations so that a calibration study can be performed. A good calibration study would also need wave, wind and river discharge measurements for a longer period as well.
- Salinity and temperature parameters can be defined in model in a way that varying spatially and in time.

REFERENCES

Akbaşoğlu, S., (2011), "Wind-Induced Circulation and Sediment Transport in Semi-Enclosed Basins, Case Study for Fethiye Bay", Ph.D. Dissertation, METU, Ankara, METU Press.

Balas, L., and Yilmaz, N. (2018). "NUMERICAL MODELING OF NEAR AND FAR FIELD DILUTION :" (3), 41–54.

Bekdemir, L. F. (2010). "Kültürel Peyzaj Değerlendirmesi: Dilek Yarımadası Büyük Menderes Deltası Milli Parkı Örneği."

Chen, C., and Beardsley, R. C. et al. (2011). "An Unstructured-Grid, Finite-Volume Community Ocean Model FVCOM User Manual (3rd Edition)." *Sea Grant College Program Massachusetts Institute of Technology Cambridge, Massachusetts 02139*, C.

Chen, C., and Beardsley, R. C. et al. (2011). "An Unstructured-Grid, Finite-Volume Community Ocean Model FVCOM User Manual (3rd Edition)." *Sea Grant College Program Massachusetts Institute of Technology Cambridge, Massachusetts 02139*, C.

Chen, C., Qi, J., Li, C., Beardsley, R. C., Lin, H., Walker, R., and Gates, K. (2008). "Complexity of the flooding/drying process in an estuarine tidal-creek salt-marsh system: An application of FVCOM." *Journal of Geophysical Research: Oceans*, 113(7).

Cihan, D., and Akdağ, T. (2018). "Nehir- Deniz Etkileşiminde Kısa Süreli Sediment Form Oluşumlarının Değerlendirilmesi : Gediz ve Büyük Menderes Örnekleri", TUBITAK Program Code: 3501, TUBITAK Project No: 115Y722, Ankara.

Crossland, C. J., Baird, D., Ducrotoy, J.-P., Lindeboom, H., Buddemeier, R. W., Dennison, W. C., Maxwell, B. A., Smith, S. V., and Swaney, D. P. (2005). "The Coastal Zone — a Domain of Global Interactions." 1–37.

Davies, A. M., Kwong, S. C. M., and Flather, R. A. (1998). "A three-dimensional model of wind-driven circulation on the shelf: Application to the storm of January 1993." *Continental Shelf Research*, 18(2–4), 289–340.

De Serio F., Malcangio D., Mossa M., (2007), “Circulation in a Southern Italy coastal basin: Modelling and field measurements”, Continental Shelf Research, Vol. 27, pg. 779–797.

DeCastro, M., Gómez-Gesteira, M., Prego, R., Taboada, J. J., Montero, P., Herbello, P., and Pérez-Villar, V. (2000). “Wind and tidal influence on water circulation in a galician ria (NW Spain).” *Estuarine, Coastal and Shelf Science*, 51(2), 161–176.

Ding, Y., Bao, X., Yao, Z., Zhang, C., Wan, K., Bao, M., Li, R., and Shi, M. (2017). “A modeling study of the characteristics and mechanism of the westward coastal current during summer in the northwestern South China Sea.” *Ocean Science Journal*, 52(1), 11–30.

Dzabic M. (2012), “Water Circulation and Yacht Carrying Capacity of Fethiye Bay”, MSc Thesis, METU, Ankara. METU Press.

Georgiou, I. Y., McCorquodale, J. A., Schindler, J., Retana, A. G., FitzGerald, D. M., Hughes, Z., and Howes, N. (2009). “Impact of Multiple Freshwater Diversions on the Salinity Distribution in the Pontchartrain Estuary under Tidal Forcing.” *Journal of Coastal Research*, 10054(10054), 59–70.

Hassid, S., and Galperin, B., (1983), “A turbulent energy model for geophysical flows.” *Boundary-Layer Meteorology*.

Huang, W., and Li, C. (2019). “Spatial variation of cold front wind-driven circulation and quasi-steady state balance in Lake Pontchartrain Estuary.” *Estuarine, Coastal and Shelf Science*, Elsevier, 224(April 2018), 154–170.

Koçyiğit M.B., Koçyiğit Ö. (2004). “Numerical Study of Wind-Induced Currents in Enclosed Homogeneous Water Bodies” Turkish J. Eng. Env. Sci., vol. 28, pg. 207-221.

Legović, T. (1991). “Exchange of water in a stratified estuary with an application to Krka (Adriatic Sea).” *Marine Chemistry*, 32(2–4), 121–135.

Levasseur A., Shi L., Wells N.C., Purdie D.A., Kelly-Gerreyn B.A., (2007), “A three-dimensional hydrodynamic model of estuarine circulation with an application to Southampton Water, UK”, Estuarine, Coastal and Shelf Science, Vol. pg. 753-767.

Lin, Y., Jiang, J., Fissel, D. B., Foreman, M. G., and Willis, P. G. (2012). “Application of finite-volume coastal ocean model in studying strong tidal

currents in discovery passage, British Columbia, Canada." *Proceedings of the International Conference on Estuarine and Coastal Modeling*.

Liu W-C., Chen W-B., Kuo J-T., (2008), "Modeling residence time response to freshwater discharge in a mesotidal estuary, Taiwan", Journal of Marine Systems Vol. 74, pg. 295–314.

Marinov D., Norro A., Zaldivar J-M., (2006), "Application of COHERENS model for hydrodynamic investigation of Sacca di Goro coastal lagoon (Italian Adriatic Sea shore)", Ecological Modelling, pg. 52–68.

Mellor, G. L., and Blumberg, A. F., (1985), "Modeling Vertical and Horizontal Diffusivities with the Sigma Coordinate System." *Monthly Weather Review*.

Mellor, G. L., and Yamada, T., (1982). "Development of a turbulence closure model for geophysical fluid problems." *Reviews of Geophysics*.

Moriasi, D. N., Arnold, J. G., Liew, M. W. Van, Bingner, R. L., Harmel, R. D., and Veith, T. L. (2007). "Model Evaluation Guidelines for Systematic Quantification of Accuracy in Watershed Simulations." 50(3), 885–900.

Pietrzak, J., Jakobson, J. B., Burchard, H., Jacob Vested, H., and Petersen, O. (2002). "A three-dimensional hydrostatic model for coastal and ocean modelling using a generalised topography following co-ordinate system." *Ocean Modelling*, 4(2), 173–205.

Pitcher, G. C. and al. (2014). "Journal of Geophysical Research : Oceans." *Journal of Geophysical Research: Oceans*, 119, 2183–2200.

Sankaranarayanan S., (2007), "Modeling the tide and wind-induced circulation in Buzzards Bay", Estuarine, Coastal and Shelf Science, Vol. 73, pg. 467-480.

Shore J.A., (2009), "Modelling the circulation and exchange of Kingston Basin and Lake Ontario with FVCOM", Ocean Modelling, Vol. 30, pg. 106–114.

Sirisup, S., Tomkratoke, S., and Lertapisit, W. (2016). "Simulation and EOF analysis of ocean circulation in the gulf of Thailand." *OCEANS 2016 - Shanghai*.

Smagorinsky, J., (1963), General Circulation Experiments with the Primitive Equation I the Basic Experiment. Monthly Weather Review, 91, 99-164.

T.R. - Ministry of Environment and Urban Planning (2016). "Büyük Menderes Nehir Havzası Taslak Yönetim Planı S.Ç.D. Pilot Projesi Stratejik Çevresel Değerlendirme Raporu."

Tsanis, I. K., and Boyle, S. (2001). “A 2D hydrodynamic/pollutant transport GIS model.” *Advances in Engineering Software*, 32(5), 353–361.

Ulses, C., Grenz, C., Marsaleix, P., Schaaff, E., Estournel, C., Meulé, S., and Pinazo, C. (2005). “Circulation in a semi-enclosed bay under influence of strong freshwater input.” *Journal of Marine Systems*, 56(1–2), 113–132.

Versteeg, H.K. and Malalasekera, W. (2007) An Introduction to Computational Fluid Dynamics: The Finite Volume Method. Pearson Education, Harlow.

Walter E. F., Tarang K., Anne C. S., Zhaoqing Y., (2007), “Estuarine-ocean exchange in a North Pacific estuary: Comparison of steady state and dynamic models.”, Estuarine, Coastal and Shelf Science, Vol. 74, pg.1-11.

WWF-Turkey, (2013), “Büyük Menderes Havza Atlası”, Ankara.

Zhao L., Chen C., Cowles G., (2006), “Tidal flushing and eddy shedding in Mount Hope Bay and Narragansett Bay: An application of FVCOM”, Journal of Geophysıcal Research, Vol. 111, pg. 1-16.

Zheng, L., Chen, C., and Liu, H. (2003). “A modeling study of the Satilla River estuary, Georgia. I: Flooding-drying process and water exchange over the salt marsh-estuary-shelf complex.” *Estuaries*, 26(3), 651–669.

APPENDICES

A. Monthly Wind Roses

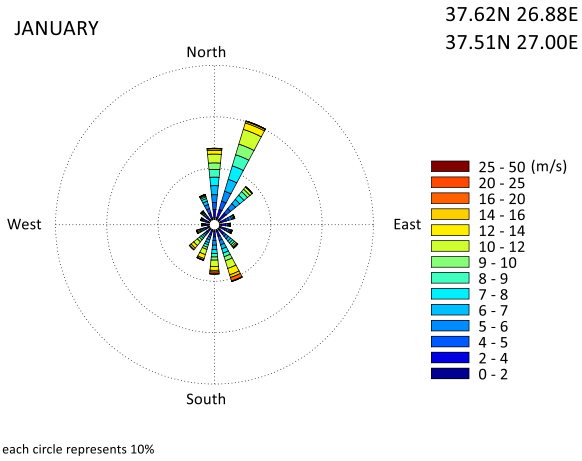

Figure A.1. Wind Rose for January

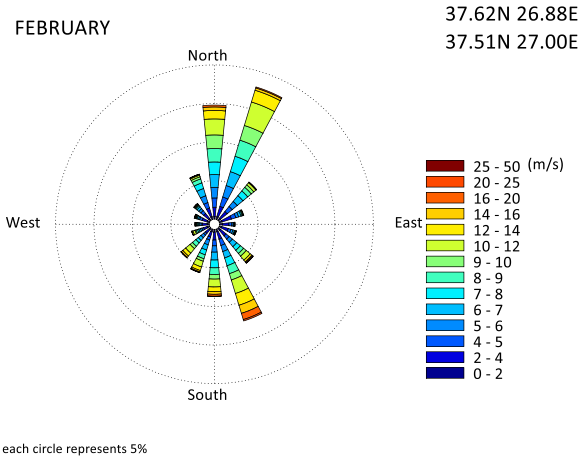

Figure A.2. Wind Rose for February

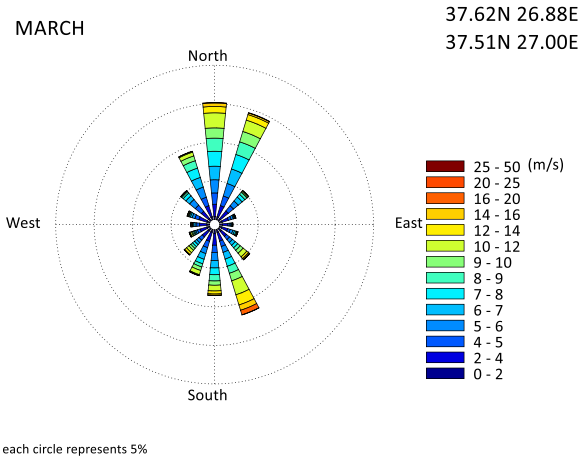

Figure A.3. Wind Rose for March

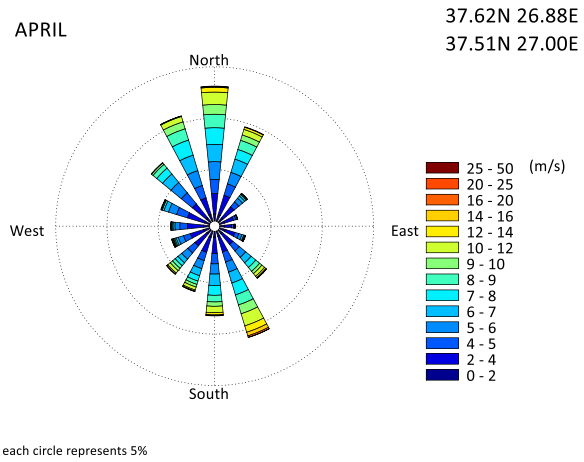

Figure A.4. Wind Rose for April

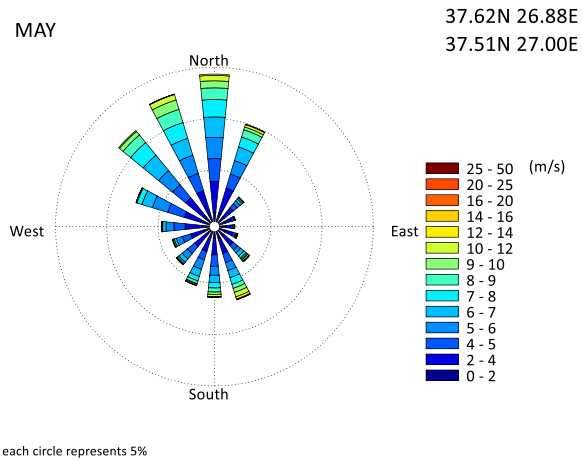

Figure A.5. Wind Rose for May

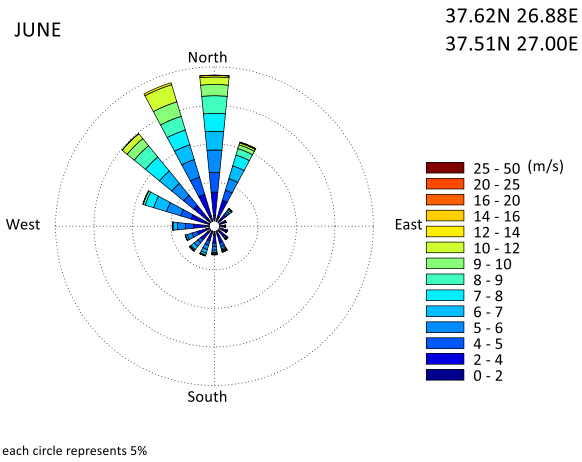

Figure A.6. Wind Rose for June

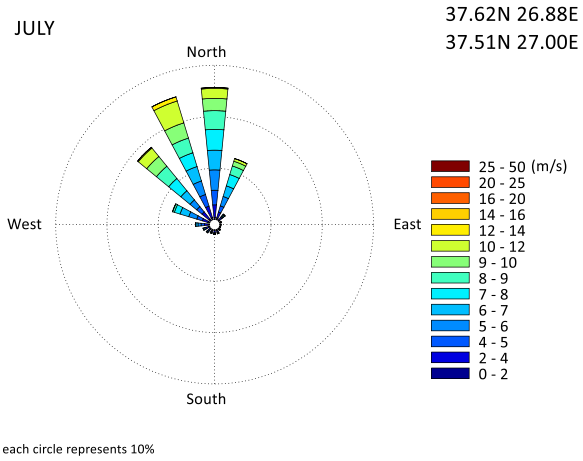

Figure A.7. Wind Rose for July

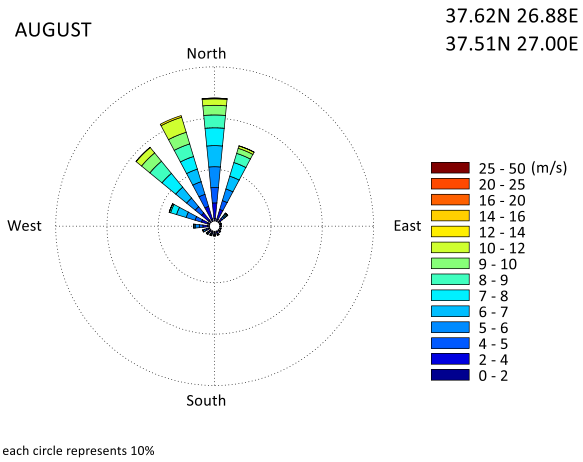

Figure A.8. Wind Rose for August

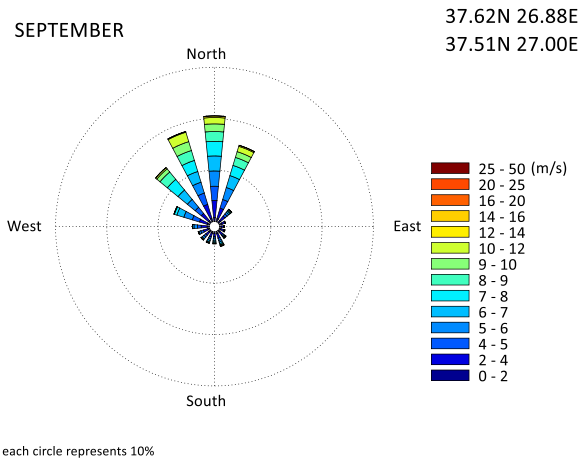

Figure A.9. Wind Rose for September

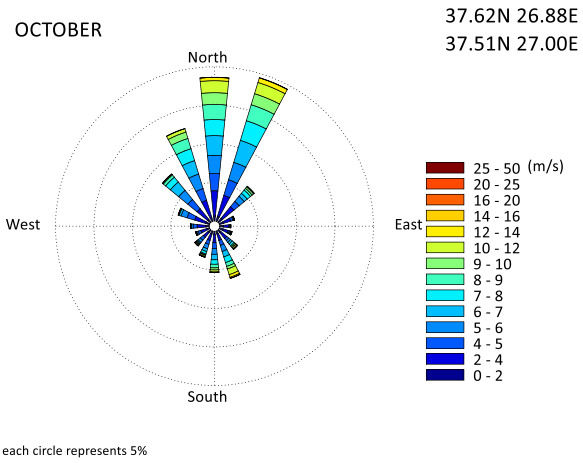

Figure A.10. Wind Rose for October

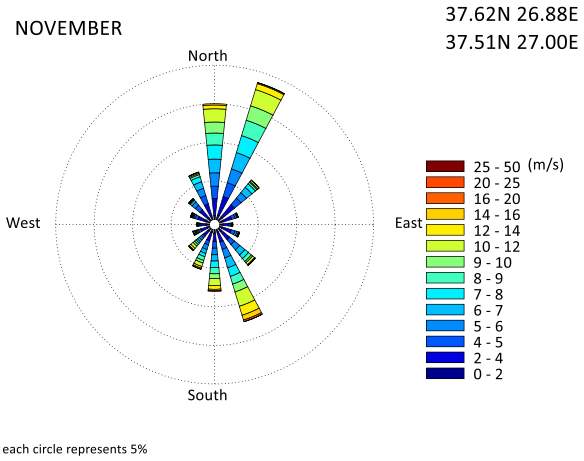

Figure A.11. Wind Rose for November

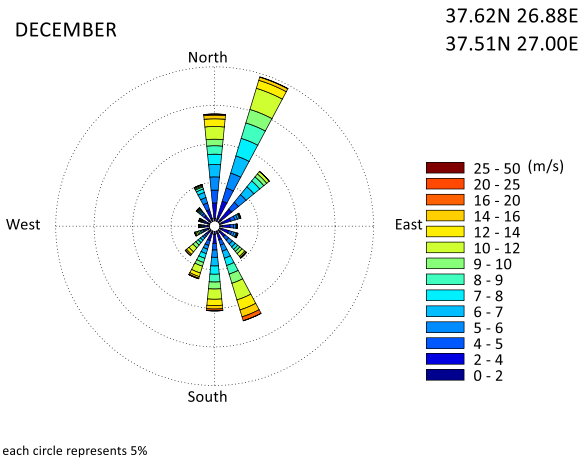

Figure A.12. Wind Rose for December

B. Yearly River Analysis (2011-2016)

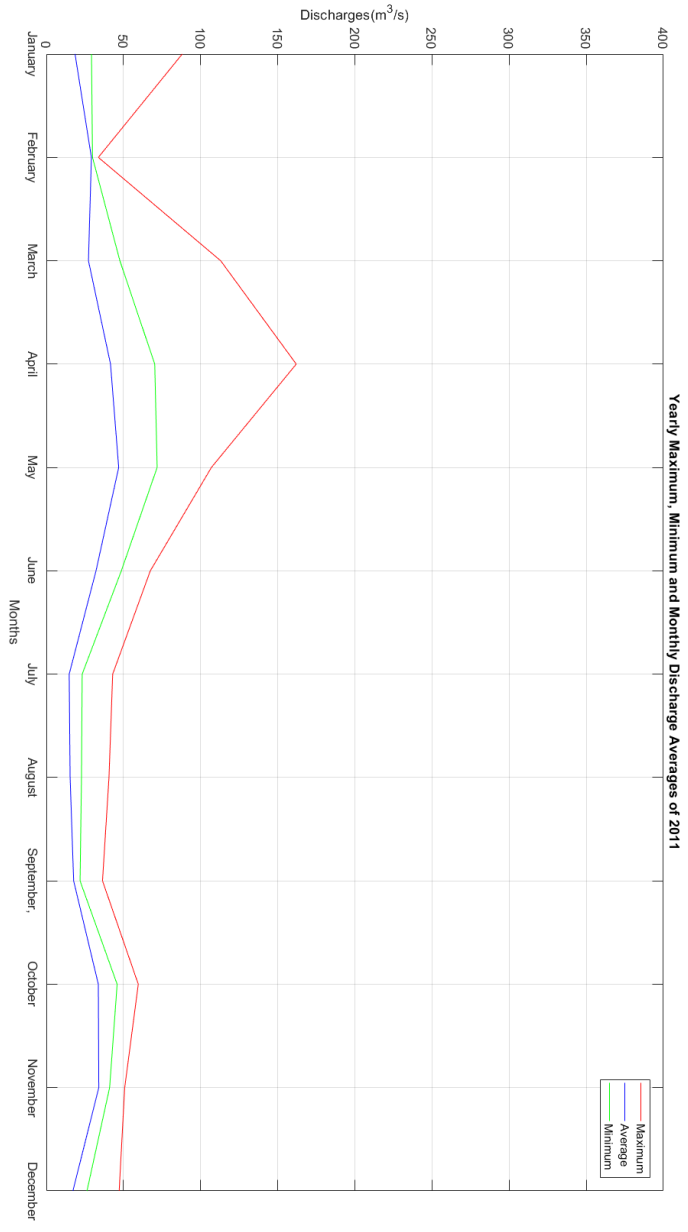

Figure B.13. Yearly River Discharge Analysis - 2011

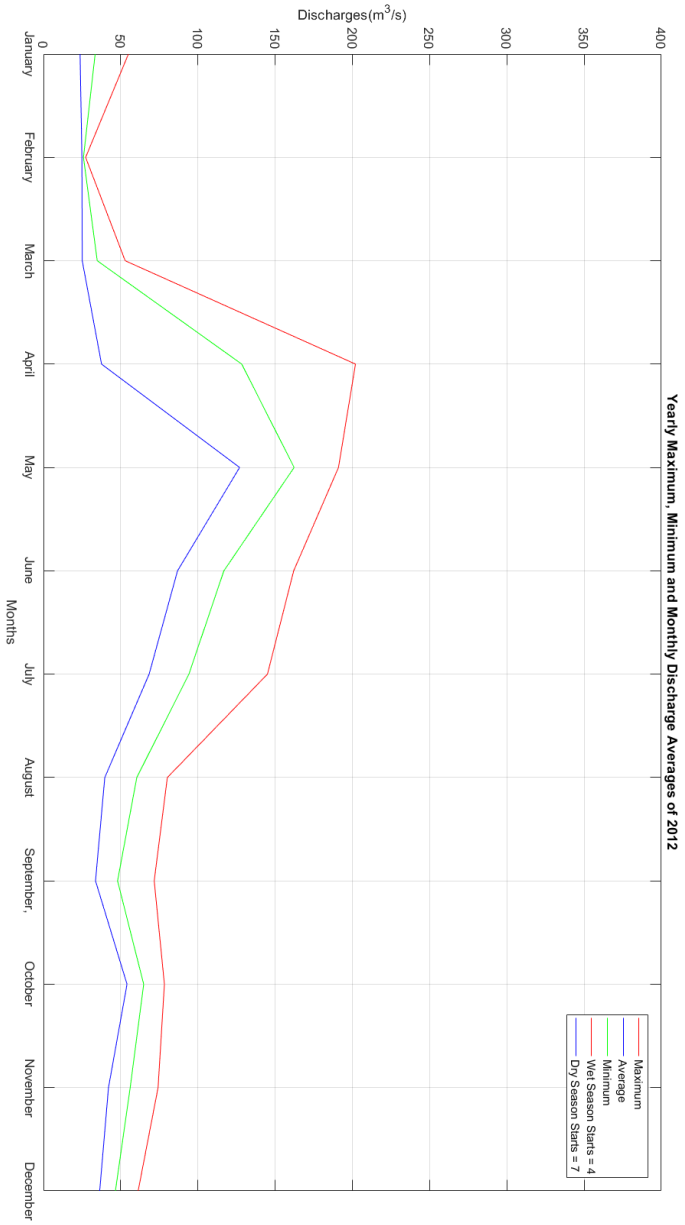

Figure B.14. Yearly River Discharge Analysis - 2012

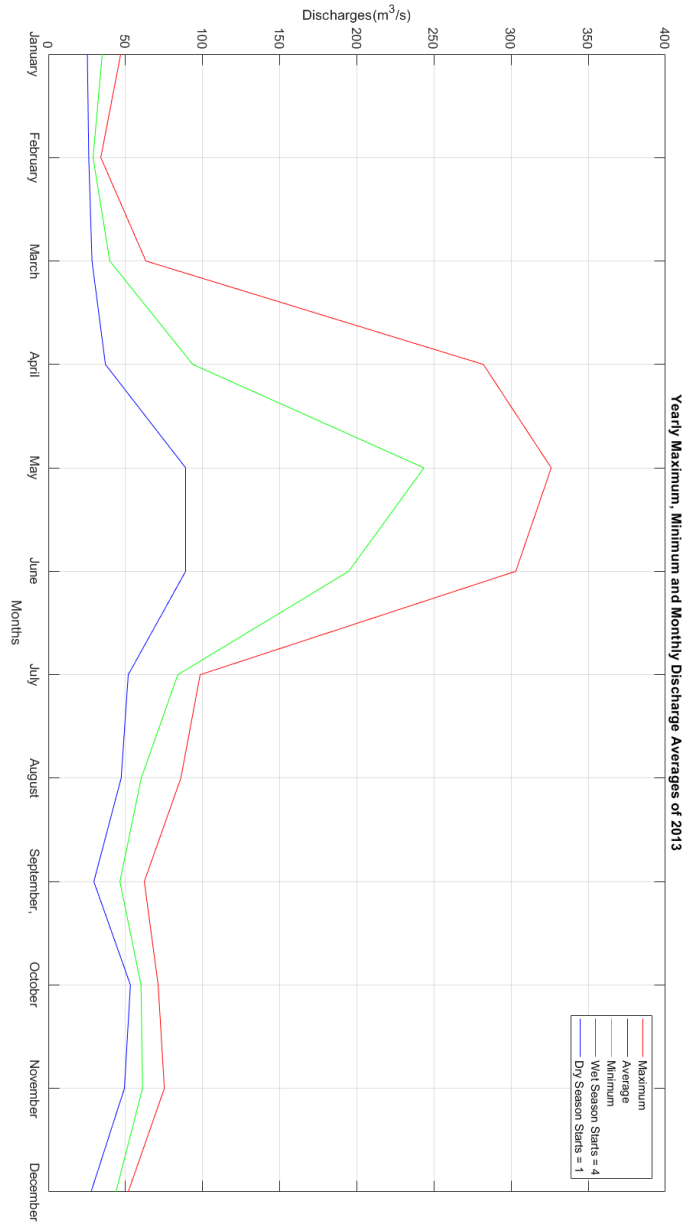

Figure B.15. Yearly River Discharge Analysis - 2013

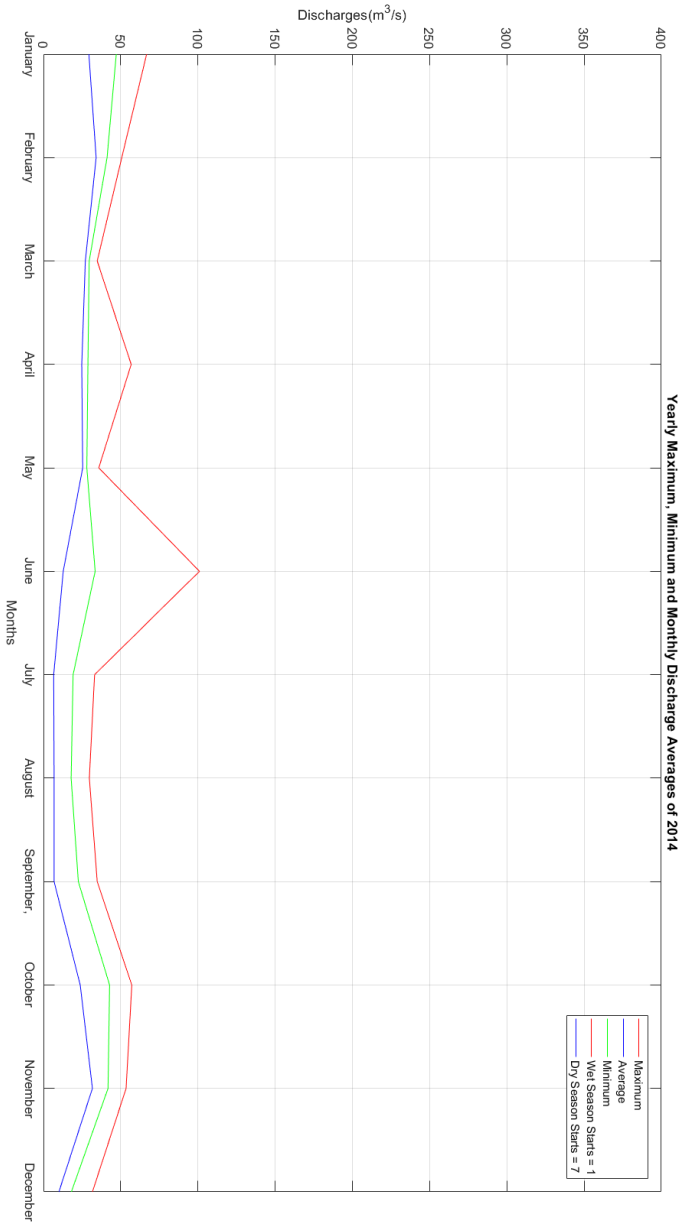

Figure B.16. Yearly River Discharge Analysis - 2014

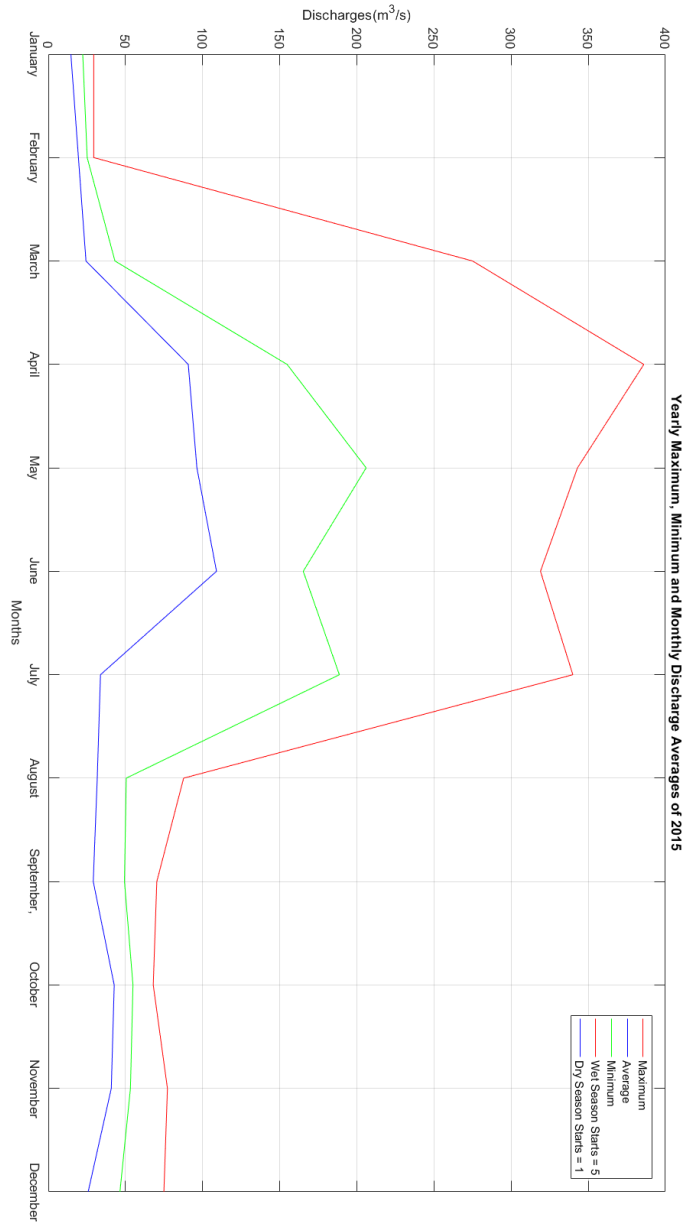

Figure B.17. Yearly River Discharge Analysis - 2015

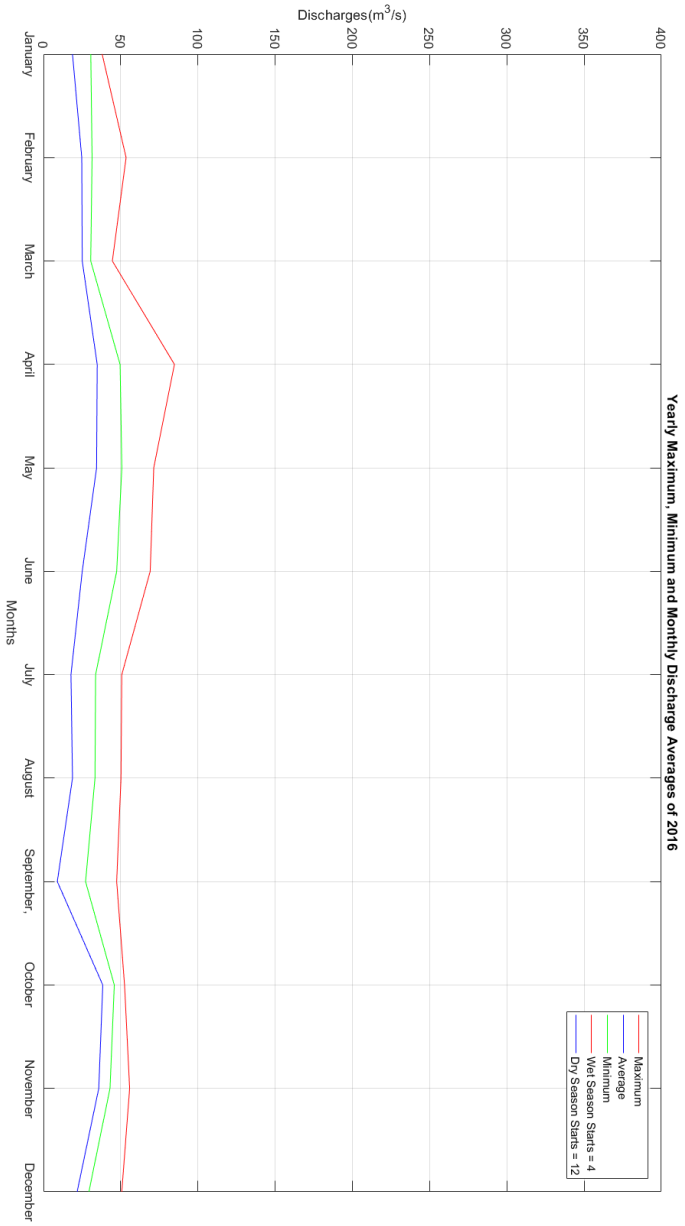

Figure B.18. Yearly River Discharge Analysis - 2016